Aspects of 18F-PSMA-1007 PET/CT in prostate cancer

Biokinetics, dosimetry, protocol and diagnostic accuracy

Hvittfeldt, Erland

2025

Aspects of ^{18}F-PSMA-1007 PET/CT in prostate cancer

Biokinetics, dosimetry, protocol and diagnostic accuracy

ERLAND HVITTFELDT
DEPARTMENT OF TRANSLATIONAL MEDICINE | FACULTY OF MEDICINE | LUND UNIVERSITY

FACULTY OF
MEDICINE

LUND
UNIVERSITY

Aspects of ^{18}F-PSMA-1007 PET/CT in prostate cancer

Biokinetics, dosimetry, protocol and diagnostic accuracy

Erland Hvittfeldt

LUNDS UNIVERSITET

DOCTORAL DISSERTATION

Doctoral dissertation for the degree of Doctor of Philosophy (PhD) at the Faculty of Medicine at Lund University.

To be publicly defended on 15th of May at 13.00 in Hall 2007, Department of Clinical Physiology and Nuclear Medicine, Inga Marie Nilssons gata 47, Malmö.

Faculty opponent
Professor Helle D Zacho, Aalborg University Hospital

Organization: LUND UNIVERSITY

Document name: Doctoral dissertation

Author(s): Erland Hvittfeldt

Date of issue: 2025-05-15

Title and subtitle: Aspects of ^{18}F-PSMA-1007 PET/CT in prostate cancer — biokinetics, dosimetry, protocol and diagnostic accuracy.

Abstract

Overview: Prostate cancer (PC) is the most common cancer in Sweden, and the leading cause of cancer death. Positron emission tomography with x-ray computed tomography (PET/CT) is an important imaging method for many cancers. A group of PET radiopharmaceuticals known as PSMA (prostate specific membrane antigen) ligands has been introduced for imaging of PC. This thesis investigates aspects of the ligand ^{18}F-PSMA-1007.

Paper I focuses on biokinetics and population level dosimetry, paper II on optimal timing of imaging, paper III on diagnostic accuracy for local lymph node metastases, paper IV on diagnostic accuracy of locally advanced tumor growth. All subjects were patients referred to our department for a PSMA PET/CT.

Methods: Paper I enrolled 12 patients to undergo eight PET/CT scans up to six hours after injection of ^{18}F-PSMA-1007. We measured time-activity data in 22 organs and created a biokinetic compartment model which we then used for dosimetry calculations. Paper II enrolled 195 patients to undergo PSMA PET/CT one and two hours after injection of ^{18}F-PSMA-1007. Three readers evaluated images at both time points, mainly looking for metastases. Paper III retrospectively included 104 patients who had performed a PSMA PET/CT for staging of PC, followed by prostatectomy with lymph node dissection. We compared PSMA PET/CT evaluations of local lymph node metastases to the histopathology results and calculated the diagnostic accuracy. Paper IV retrospectively included 124 patients who had undergone both magnetic resonance imaging (MRI) and a PSMA PET/CT before a prostatectomy. We evaluated local tumor growth with both MRI (one reader) and PSMA PET/CT (two readers). We used a novel semi-standardized method for the PSMA PET/CT and evaluated the interrater reliability.

Results: The effective dose coefficient for ^{18}F-PSMA-1007 was 25 µSv/MBq, comparable to similar radiopharmaceuticals. More metastases were found in images obtained after two hours as compared to one hour, which may affect PC staging and treatment planning. PSMA PET/CT had low sensitivity both for local lymph node metastases (26%) and for identifying locally advanced tumor growth (54%), but moderate to high specificity (98% and 76%) respectively. Intrarater reliability was weak to moderate (0.53–0.68) for the local tumor growth evaluation.

Summary: This work has contributed to the current body of knowledge of basic dosimetry, protocol optimization and diagnostic accuracy concerning the relatively new PET radiotracer ^{18}F-PSMA-1007.

Key words:

Classification system and/or index terms (if any)

Supplementary bibliographical information

Language: English

Number of pages:
67

Signature

Date 2025-05-15

Aspects of ^{18}F-PSMA-1007 PET/CT in prostate cancer

Biokinetics, dosimetry, protocol and diagnostic accuracy

Erland Hvittfeldt

LUNDS UNIVERSITET

Table of Contents

List of papers

Paper I

Biokinetics and dosimetry of ^{18}F-PSMA-1007 in patients with prostate cancer. Hvittfeldt E, Bjöersdorff M, Brolin G, Minarik D, Svegborn S L, Oddstig J, Trägårdh E.

Clin Physiol Funct Imaging. 2022 Nov;42(6):443-452

Paper II

PET/CT imaging 2 h after injection of [^{18}F]PSMA-1007 can lead to higher staging of prostate cancer than imaging after 1 h. Hvittfeldt E, Bitzén U, Minarik D, Oddstig J, Olsson B, Trägårdh E.

Eur J Hybrid Imaging. 2023 May 1;7(1):9

Paper III

Assessing the accuracy of [^{18}F]PSMA-1007 PET/CT for primary staging of lymph node metastases in intermediate- and high-risk prostate cancer patients. Ingvar J, Hvittfeldt E, Trägårdh E, Simoulis A, Bjartell A.

EJNMMI Research 2022 Aug 9;12(1):48

Paper IV

Semi-standardized evaluation of extraprostatic extension and seminal vesicle invasion with [^{18}F]PSMA-1007 PET/CT: a comparison to MRI using histopathology as reference. Hvittfeldt E, Hedeer F, Thimansson E, Sandeman K, Minarik D, Ingvar J, Bjartell A, Trägårdh E.

EJNMMI Reports 2025 Jan 3;9(1):1

Introduction and acknowledgments

In 2019 I was nearing the end of my specialist training in clinical physiology at the department of Clinical Physiology and Nuclear Medicine at Skåne University Hospital in Malmö. In many places in Sweden clinical physiology and nuclear medicine are closely integrated and as part of my training I had worked on positron emission tomography (PET) with the radiotracers ^{18}F-FDG (for general oncology and inflammation) and ^{18}F-fluorocholine (for prostate cancer). I was considering further specialization in nuclear medicine and was also interested in pursuing a PhD.

Around the same time, our department had decided to replace ^{18}F-fluorocholine with a PSMA-tracer (prostate-specific membrane antigen) for prostate cancer, as PET imaging with PSMA-tracers had been established as superior to choline-based imaging. Several PSMA-options were available, but the choice fell on ^{18}F-PSMA-1007 due to its low excretion in urine and capacity for high-volume production.

At that time, only a handful of clinical studies of ^{18}F-PSMA-1007 had been published. After the decision to use the tracer my supervisor to-be, associate professor (now professor) Elin Trägårdh had outlined several potential studies involving ^{18}F-PSMA-1007. So, when I approached her about the possibility of pursuing a PhD much of the plan for what became this thesis was already in place. There has been some changes and slight bumps along the way, but thanks to a supportive work and home environment my PhD journey has been a mostly smooth cruise.

I am very grateful to have been able to complete this journey with a supervisor who has shown great faith and trust in me. Thank you Elin for your support and for always keeping your door open.

I also want to acknowledge:

My co-supervisors Anders and Jenny — thank you both for your availability and generosity with your time, especially when preparing for my half-time and thesis seminars.

The physicists. David for many large and small contributions to my research and even more answers and explanations about physics both in research and in the clinic. Gustav who contributed greatly to Paper I and helped me understand dosimetry, at least a little,

when I was in over my head without realizing it. Sigrid for insightful input on Paper I and for answering many questions along the way. Martin, who wrote the software for dose calculations used in Paper I and who seems to be at every nuclear medicine meeting I attend, always ready to answer a few questions.

All the technologists at my department who made this thesis possible by recruiting patients, handling logistics and performing the actual PET/CT scans. A special thanks to Berit, Mimmi and Camilla for their contributions to the research.

My co-authors — Atanasios, Erik, Fredrik, Jacob, Kevin, Ulrika. Thank you for your contributions in planning and performing the research. A special thanks to Erik, Jacob and Kevin for expertise and guidance in their respective fields.

Thank you to everyone else in Elin's research group who has contributed to and commented on my work, and helped me grow by allowing me to comment on theirs. Elin's other PhD students — Anni, Johan, John, Kristian, Maria, Ragna, Sarah (so many!) — and all other participants — Hanna, Hanna, Irma, Jing, Malin, Olof, Sophia (and probably someone I forgot).

My boss Jonas for letting research be a natural part of our clinic.

My family — Sigrid, Harry and Laura — for your unwavering support. I would dedicate this thesis to you, but you are worth so much more. I love you❤️.

§ Glandulofum corpus uefic\u00e6 ceruicis initio adnatum, & femen deferentium uaforum infertio-
nem excipiens.
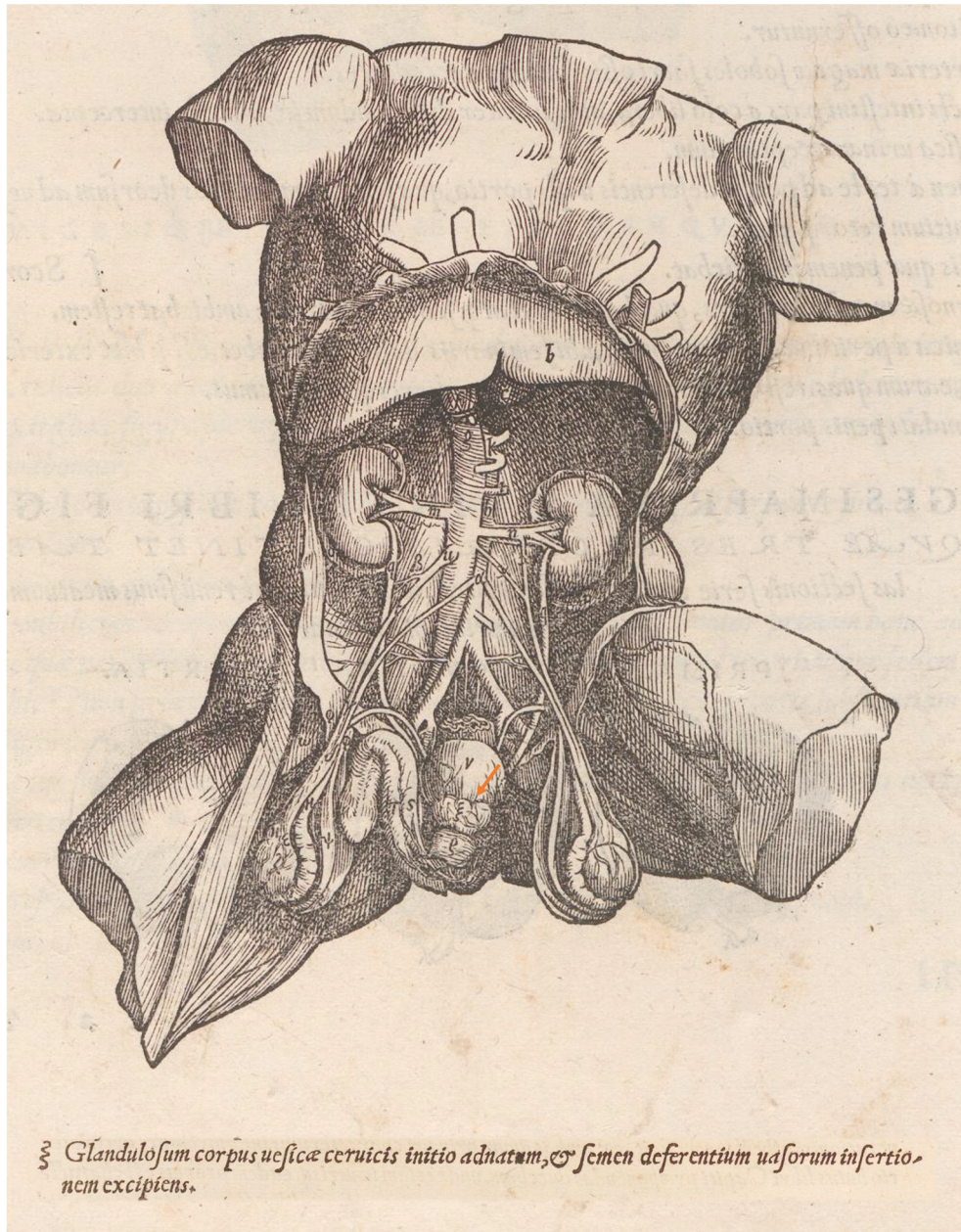
Figure 1
Illustration from Vesalius *De humanis corporis fabrica*. The prostate (arrow, labelled ξ) is located under the urinary bladder with the description " ξ A glandular body attached at the beginning of the neck of the bladder, receiving the insertion of the vessels that carry semen". Public domain, digitalized by Universitäts-bibliothek Basel [1].

Background

The prostate

The prostate is a gland of the male reproductive system. Classically described as the size and shape of a walnut, it is located below the urinary bladder against which it has a broad base where the urethra enters. It has dual functions: as an accessory sex gland contributing part of the ejaculate and as a mechanical switch between urination and ejaculation. The prostate extends downward from the base, between the pubic symphysis anteriorly and the rectum dorsally, towards the urogenital diaphragm where the urethra exits from a narrow apex. The two seminal vesicles (which store semen) enter each lobe in the dorsal base of the prostate and empty into the urethra mid-prostate.

Etymology and brief history

The Greek noun *prostates* (approximately "one who stands first") was used in antiquity to designate a leader or protector, but had no anatomical or medical meaning. The word *parastates* ("one who stands beside", companion) was however used to designate paired organs of the male reproductive system such as the testicles, spermatic cords, and seminal vesicles. It is unclear if antique anatomists like Galen recognized the prostate as an unpaired organ or even as an entity of its own. One source of confusion is the variability in different animals; in many mammals the prostate looks paired due to prominent left and right lobes. The presence of seminal vesicles is also variable.

Little progress was made in medieval times, due both to limited dissection on human bodies and to the veneration of antique knowledge, which was rarely challenged. In the early renaissance, Leonardo da Vinci clearly depicts the seminal ducts and vesicles in his anatomic drawings but not the prostate. [2, 3]

Clear descriptions of the prostate did not appear until the later renaissance, notably by the preeminent anatomist Andreas Vesalius in his seminal 1543 work *De humanis corporis fabrica*, which depicts and describes the organ without naming it (Figure 1) [1]. In 1600 the term *prostatae*, an incorrect pluralization of the malapropism *prostates,* was

applied to the organ by French anatomist André du Laurens. By the early 19th century much of modern terminology and physiological understanding of the prostate gland was established, as exemplified in "Practical observations on the treatment of the diseases of the prostate gland" (1811) by British surgeon sir Everard Home [2, 3]. The first references to prostate cancer date also date to this period, with the first histopathological description after autopsy by London surgeon John Adams in 1844. The first radical prostatectomy was performed by American urologist Hugh H. Young in 1904 [4].
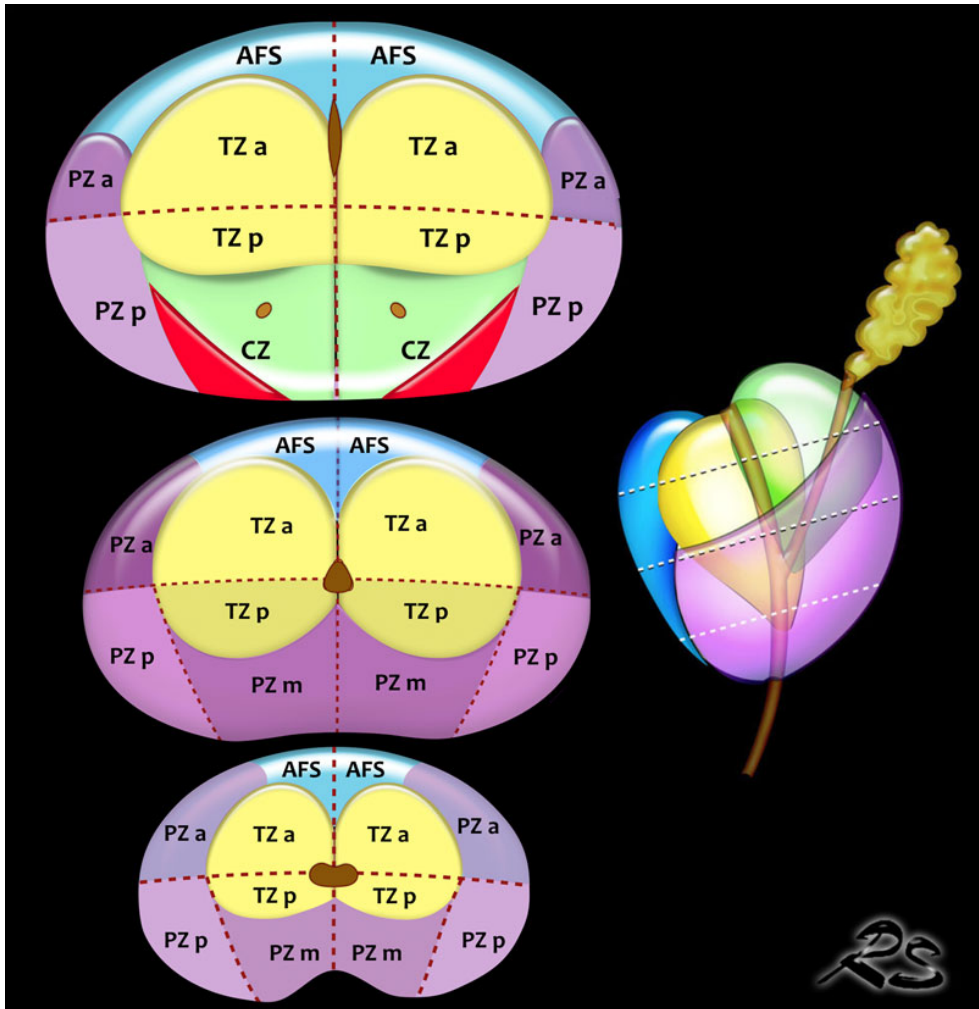
Current understanding of prostate anatomy

In modern terminology based on histopathological studies, the prostate is often divided into four zones (the McNeal prostate, Figure 2). Three zones are glandular — the peripheral, central and transition zones with about 65%, 30% and 5% of the glandular mass respectively in a young man. About 70% of prostate cancers arise in the peripheral zone. The transition zone enlarges with age and is the location of benign prostatic hyperplasia. About 25% of cancers arise in the transition zone. Cancer in the central zone is unusual. The fourth zone is the non-glandular anterior fibromuscular stroma.

Surrounding the prostate is a variable sheath of condensed fibromuscular tissue referred to as the capsule or pseudocapsule, which is removed with the prostate in prostatectomy. Prostatic surgery is challenging due to the anatomical location of the prostate and the close relation of the capsule to surrounding structures including nerves, blood vessels and muscles. [5-7]

Prostate cancer

Prostate cancer is the second most common form of cancer worldwide after lung cancer. In Sweden it is the most common cancer form and the leading cause of male cancer death [8, 9]. The main risk factor for prostate cancer is age. Family history is another important risk factor with a relative risk of 7.7 for a man with two brothers with prostate cancer [10]. Genetic risk factors also include ethnicity (for example African origin) and some germline mutations such as BRCA2. Although lifestyle factors such as diet and smoking are believed to be linked to prostate cancer, causal relations have not been established. There are no lifestyle interventions known to prevent prostate cancer [11].
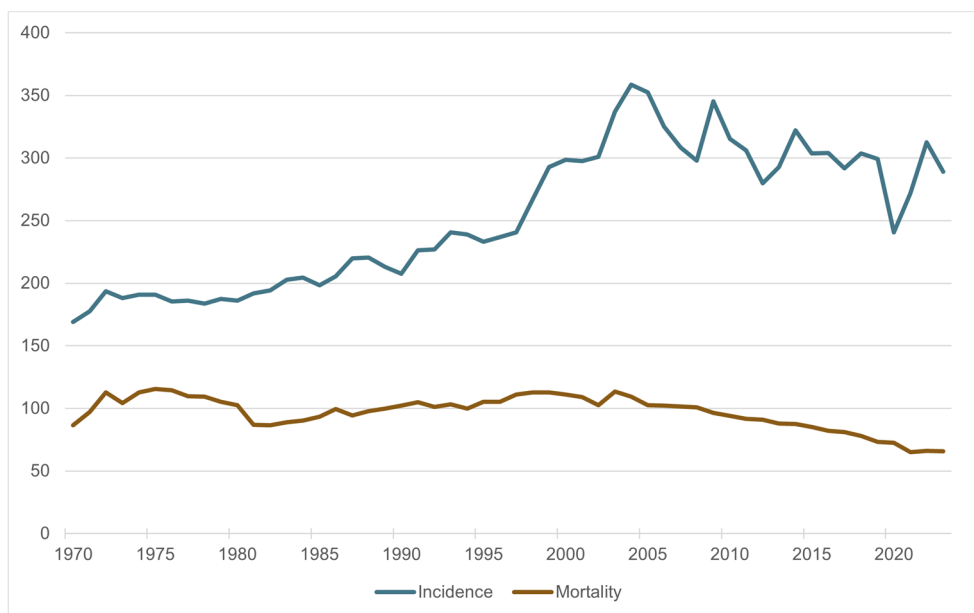
Figure 3
Age-standardized incidence and mortality of prostate cancer in Sweden from 1970–2023. Data from Socialstyrelsen.

Yearly incidence of prostate cancer has been increasing since the 1970s, largely due to widespread testing for prostate specific antigen (PSA). At the same time mortality has come down due to earlier diagnosis and more effective treatments (Figure 3). Worldwide incidence is expected to have more than doubled in 2040 compared to 2020, mainly due to changing age demographics [12].

An elevated PSA-level is a sensitive marker for prostate cancer but can also be caused by benign conditions such as prostatic hyperplasia and urinary infections. Prostate cancers are often slow-growing, meaning that even when an elevated PSA is caused by cancer it might not benefit the patient to have it diagnosed. In autopsy materials, undiagnosed prostate cancers are found in around 10% of men aged 30–35 years and in 50% of men aged 70–79 years [13]. Prostate cancers can be classified (mainly through histopathology, see below) as clinically significant or insignificant, based on whether they are likely to impact a patient's health in his lifetime [14]. The overdiagnosis and subsequent overtreatment of prostate cancer incur both health economic costs and social and psychological costs to the patient [15].

The following overview is centered around Swedish guidelines (2024) with occasional references to European guidelines (2024) [11, 16, 17].

Diagnosis

The chain of events leading to a diagnosis of prostate cancer usually starts with a PSA test.

Indications for PSA testing

In men over 40, rapidly progressing lower urinary tract symptoms, hematuria, skeletal pain and pathological digital rectal exam (DRE) are indications for a PSA test.

Reference values

Age-specific normal values are used; in men >70 years a PSA-value ≥ 3 µg/l is suspicious for cancer, in men 70–80 years ≥ 5 µg/l and above 80 years ≥ 7 µg/l. In asymptomatic patients with a normal DRE and an elevated PSA < 10 µg/l, repeat testing can performed to verify the elevation and avoid further diagnostics if the PSA normalizes. If the prostate volume is known (from imaging) the PSA-density can be calculated. PSA-density < 0.1 µg/l/cm^3 suggests prostatic hyperplasia as the cause of PSA-elevation, while a density > 0.2 µg/l/cm^3 is indicative of cancer.

Asymptomatic PSA testing

Due to the risk of overdiagnosis and overtreatment of clinically insignificant prostate cancer asymptomatic testing is not recommended in men with a life expectancy of less than 10–15 years, meaning most men older than 75 should not take a test. Men aged 50–75 should be informed of the benefits and drawbacks of testing before proceeding. Men younger than 50 with no significant family history are unlikely to benefit from a PSA test due to the low prevalence of clinically significant cancer.

Population-based screening with PSA

There have been large randomized controlled trials evaluating population-based screening for prostate cancer with PSA tests. A 2018 Cochrane review was based on five RCTs including more than 700 000 men. It found an increase in cancer diagnosis (IRR 1.23) in a screened population, more localized disease (RR 1.39) in those who were diagnosed, but no prostate cancer specific reduction in mortality (IRR 0.96). However, the review singled out the European Randomized study of Screening for Prostate Cancer (ERSPC) as the trial with the lowest risk for bias. In a 16-year follow-up this

study found, among 162 389 randomized men aged 55–69, a lower incidence of prostate cancer mortality (IRR 0.80) in the screened group. The greatest effect of screening was found in the Swedish group (IRR 0.63, 11 852 men) [18, 19].

The latest (2018) recommendation from the Swedish National Board of Health and Welfare concludes that a screening program would reduce prostate cancer mortality. It nevertheless recommends against population-based screening mainly due to the risk of overdiagnosis of clinically insignificant cancer [20]. The same report is positive to "organized testing" in a research context, to offer more structured and equal testing. In Region Skåne (the administrative body responsible for health care Skåne county) a project for organized testing has been expanding since 2020, aiming to offer PSA tests to all men 50–74 years of age. The offer of organized testing is accompanied by information about the pros and cons of the test so that the individual can make an informed decision on whether to participate. Population-based screening on the other hand implies a recommendation to take part in the program [21].

Magnetic resonance imaging (MRI)

MRI scanners use magnets and radio waves to affect hydrogen atoms in the body. Differences in hydrogen signal characteristics between tissues can then be detected and used to create tomographic images. If an elevated PSA is established in a patient, Swedish guidelines recommend MRI as a next step in most cases. A normal scan can be used to reevaluate the need for further diagnostics while a pathological scan can be used to assist targeted biopsies of the prostate [16].

Prostate Imaging – Reporting and Data System (PI-RADS)

PI-RADS is an international standard for performing and evaluating MRI of the prostate, currently in version 2.1 [22]. Prostate lesions detected on MRI are classified as PIRADS grade 1–5 ranging from "very low" to "very high" probability of clinically significant prostate cancer. MRI images included T2 and diffusion weighted images (T2w and DWI), and optionally dynamic contrast enhanced T1 weighted images (DCE).

Diagnostic accuracy and role in diagnosis.

A 2019 Cochrane meta-analysis found a sensitivity of 0.91 and a specificity of 0.37 for MRI to identify clinically significant prostate cancer, using PI-RADS ≥3 as cut-off. For

MRI-targeted biopsy the sensitivity and specificity were 0.80 and 0.94 respectively, compared to 0.63 and 1.0 for systematic biopsies with a relative cancer detection rate of 1.05 for the targeted biopsy. The high sensitivity for MRI means that, depending on the level of suspicion of cancer, a biopsy may be avoided in about one third of patients if the MRI is negative. If there had been a previous negative biopsy the detection rate was 1.44 meaning that there is a strong indication for MRI after negative systematic biopsies if there is still suspicion of cancer [23].

Prostate biopsy and staging

The histopathologic diagnosis of prostate cancer is made through ultrasound guided transperineal (recommended due to lower infection rates) or transrectal needle core biopsies. Biopsies can be systematic (normally 10–12 cores) or targeted to MRI lesions (2–4 cores). In Sweden, where access to MRI is high, targeted biopsies are the norm. Systemic biopsies can be performed as a complement to targeted biopsies (Table 1) or when an MRI is not possible [16].

Table 1
Guide for biopsy decision from Swedish guidelines, adapted from Schoots et al [24]. S=systematic, T=targeted.

	PSA density (μg/l/cm^3)		
	< 0.10	0.10–0.19	≥ 0.20
PI-RADS 1–2	No biopsy	No biopsy	Biopsy (S)
PI-RADS 3	No biopsy	Biopsy (T)	Biopsy (T+S)
PI-RADS 4–5	Biopsy (T)	Biopsy (T)	Biopsy (T)

More than 98% of prostate cancers are adenocarcinomas. Among other cancers small cell neuroendocrine cancer is the most common. The Gleason grading system is the standard for histopathological categorization of adenocarcinoma of the prostate. Donald F. Gleason described five increasingly dedifferentiated patterns of cancer, numbered 1–5, and the Gleason score was the sum of the two most common patterns ranging from 1+1=2 to 5+5=10 [25].

The definition and usage of patterns have changed over time. Currently, in needle core biopsies, the Gleason score is the sum of the primary (dominant) pattern and the secondary pattern (any grade higher than the primary or, if there is no higher grade, the second most common pattern comprising > 5% of the cancer). If there is no secondary pattern the primary pattern is doubled. In a prostate specimen after

prostatectomy a tertiary pattern can be described, which is a pattern of higher grade than the primary but comprising < 5% of the cancer. The presence of cribriform growth pattern (in Gleason pattern 4) or intraductal carcinoma (in any pattern) are negative prognostic markers usually reported alongside the Gleason score [26].

In modern practice patterns 1 and 2 are rarely described meaning that Gleason scores 2–5 have disappeared. To simplify classification the International Society of Urologic Pathology have introduced the ISUP grading based on Gleason scores (Table 2) [27]. Clinically significant cancer is often defined as ISUP grade ≥ 2.

Table 2
ISUP Grade Groups and Gleason scores

ISUP Grade Group	1	2	3	4	5
Gleason score	≤6	3+4=7	4+3=7	8	9–10

Risk classification

There are several algorithms for risk classification of prostate cancer. EAU risk groups are based on the long-standing D'Amico classification with three tiers (Table 3) [11, 28]. Risk classification in Swedish guidelines has changed between updates, and currently employs a six-tier system [16].

Table 3
EAU risk groups for biochemical recurrence of prostate cancer (based on systematic biopsies, no imaging for metastases)

	Low-risk — all of:	Intermediate-risk — any of:	High-risk — any of:
PSA	<10 µg/l	10–20 µg/l	>20 µg/l
ISUP grade	1	2–3	4–5
T stage	T1–2a	T2b	>T2b

Primary staging

The TNM (Tumor, Node, Metastasis) system is the international standard for cancer staging [29]. Table 4 gives an outline of TNM staging for prostate cancer.

Tumor (T stage)

The TNM manual states that the local tumor stage should be based on a digital rectal exam only and this is reflected in European and Swedish guidelines. However, all three sources acknowledge that MRI can provide additional information on the tumor stage [11, 16, 29].

Regional lymph node (N stage) and distant metastases (M stage)

The TNM manual classifies regional lymph node metastases as lymph node metastases in the pelvis below the iliac bifurcation. There is an ongoing debate whether the iliac or aortic bifurcation is the clinically relevant anatomical classifier, due to differences in surgical and radiotherapeutic approaches in the common iliac area [30, 31]. Distant metastases are all other metastases, most commonly in bone.

When the risk for metastatic disease is high enough to warrant imaging, European guidelines recommend PSMA PET/CT rather than conventional imaging with CT and bone scan. Swedish guidelines still recommend conventional imaging as first line imaging, due to uncertain clinical implications of the higher sensitivity of PSMA PET/CT [11, 16].

Table 4
Overview of TNM stages for prostate cancer [29]

T		N		M	
T1	Tumour not palpable	N0	No regional lymph node metastases	M1a	Distant lymph node metastases
T2	Palpable tumour	N1	Regional lymph node metastasis present	M1b	Bone metastases
T3	Tumor palpably extends outside prostate			M1c	Other distant metastases
T4	Tumor invades adjacent structures				

Treatment

Curative treatment

For patients with a life expectancy of at least 10–15 years (5 years in high-risk cancer) and no metastases or only limited lymph node metastases, curative treatment can be considered.

There is a lack of randomized trials comparing survival for the two curative treatment options of radical prostatectomy and radiotherapy [32]. In stage T1–T2 cancers the two options are considered equal on a group level. Patient-specific factors such as age, urinary symptoms and co-morbidities and personal preference guide the choice. In locally advanced (T3–T4) cancers radiotherapy is recommended due to high risk of non-radical surgery.

Active surveillance

When curative treatment is an option but not immediately necessary. It is the strategy for most low- and favorable intermediate-risk cancers. The aim is to avoid overtreatment in patients with cancer that might not be clinically significant (i.e. won't impact the patient's health before death of other causes). Active means a predefined strategy for patients in this category, e.g. PSA testing every six months, new MRI every two–three years. If the cancer progresses the need for curative treatment is re-appraised.

Radical prostatectomy

Radical prostatectomy can be performed with open surgery (radical retropubic prostatectomy, RRP) or as robot-assisted laparoscopic prostatectomy (RALP). In Sweden the more expensive RALP is the standard technique due to fewer intra- and perioperative complications [33]. There is no difference in long-term complications and mortality between the techniques [34]. Nerve-sparing surgery may reduce the risk of erectile dysfunction and incontinence but increase the risk of positive margins (cancer cells in the margin of the prostate specimen) [14]. PSA should be undetectable (<0.1 µg/l) six weeks post-surgery.

Pelvic lymph node dissection can be performed in high-risk cancers or when N1 disease is suspected. No therapeutic value of dissection has been shown but the confirmation of N1 disease can guide treatment planning [35, 36].

Adjuvant radiotherapy can be considered when there are extensive positive margins and N0 disease.

Radiotherapy

In Sweden usually performed as external beam therapy (EBT). Hypofractionation is used mainly in intermediate-risk tumors. Local irradiation techniques (brachytherapy) can be an alternative as monotherapy in intermediate-risk tumors or in combination with EBT in high-risk tumors.

Pelvic lymph node irradiation is often performed in high risk-cancers in Sweden, but the evidence of survival benefits is limited [37].

Radiotherapy is combined with hormonal therapy in high- and some intermediate-risk tumors, as neoadjuvant, concomitant or adjuvant therapy.

Local recurrence after curative treatment

A rising PSA-value after curative treatment is cause for concern. PSA > 0.1–0.2 µg/l after prostatectomy, or a PSA elevation > 2.0 µg/l above the lowest (nadir) value after radiotherapy is considered biochemical recurrence (BCR). If there is a high risk of

metastases, PSMA PET/CT should be considered. In non-metastatic BCR after prostatectomy salvage radiotherapy (SRT) of the prostate bed is usually performed, sometimes in combination with hormone therapy. After radiotherapy several treatment options are possible (e.g. salvage prostatectomy, brachytherapy). If PSA is rising slowly watchful waiting is an option. [16]

Palliative treatment

Watchful waiting

Like in active surveillance treatment is postponed until there is disease progress, but curative treatment is not an option due to low life expectancy (< 10–15 years or < 5 years in high-risk tumors). The follow-up strategy can be individualized to the patient and hormonal treatment is considered in case of disease progress.

Hormonal therapy

Prostate cancer is a testosterone-dependent disease. Hormonal therapy has been a cornerstone in the treatment of advanced prostate cancer since the 1940's when treatment with estrogen or surgical castration was introduced. Surgical castration is still a viable treatment, but estrogen is rarely used. The following is a brief overview of current medical hormonal therapy presented in chronological order (of market introduction) [4].

Androgen deprivation therapy (ADT, medical castration)

GnRH agonists (e.g. leuprolide), introduced in the 1980s, suppress testosterone production by causing downregulation of GnRH receptors in the pituitary. There is an initial flare of testosterone production which is treated with androgen receptor blockade. GnRH antagonists (degarelix, relugolix) avoid this flare reaction.

First generation androgen receptor inhibitors/antiandrogens

Introduced later in the 1980s, these pharmaceuticals suppress the effect of testosterone by blocking the androgen receptor. Bicalutamide is still in use.

Androgen receptor pathway inhibitors (ARPIs)

Introduced in the 2010s these include second generation antiandrogens such as enzalutamide and apalutamide, that both block the androgen receptor with high affinity and prevents the receptor's transfer to the cell nucleus. Also in this group is abiraterone, a blocker of the enzyme CYP17 which is important for androgen production.

Chemotherapy

The main chemotherapies in use are docetaxel and cabazitaxel.

PARP-inhibitors

Olaparib inhibits the DNA repair enzyme PARP. It can be used in patients with a genetic or tumor-specific BRCA mutation.

Radium-223

Symptomatic bone metastases can be treated with radium-223, an alpha-emitter which is taken up in bone tissue. [16]

Hormone-sensitive prostate cancer (HSPC)

Hormonal therapy is first-line treatment in most palliative situations.

Primary hormonal treatment of non-metastasized cancer

Bicalutamide and GnRH agonists, separately or in combination, can be used in high-risk tumors when curative treatment or watchful waiting is not an option.

Primary treatment of metastasized cancer (mHSPC)

In metastatic disease ADT is the cornerstone. With a maximum of four skeletal metastases or only regional lymph node metastases Swedish guidelines also recommend radiotherapy of the prostate (if life expectancy > 5 years). In more widespread metastases, addition of chemotherapy (docetaxel) is recommended instead. Addition of ARPI treatment is indicated in patients with limited co-morbidity. [16]

Castration resistant prostate cancer (CRPC)

When a patient on ADT progresses (either locally, with metastases, or rising PSA) the cancer has become castration resistant.

Without metastases (nmCRPC)

First-line treatment is addition of a second-generation antiandrogen.

With metastases (mCRPC)

First line treatment is addition of docetaxel or abiraterone. Other hormone- or chemotherapies as well as radium-223 can be used as second- or third-line treatment. [16]

Positron emission tomography (PET)

PET is a nuclear medicine imaging method developed in the 1970´s. The development of the PET scanner was tightly coupled with the synthesis of ^{18}F-fluoro-2-deoxyglucose (FDG) at the University of Pennsylvania. Initially a research tool for measuring and visualizing the distribution of glucose metabolism, FDG PET gained massive ground as a clinical tool for cancer detection in the early 2000's.

The basis of nuclear medicine imaging is the radiotracer, a radionuclide combined with a tracer molecule. A radionuclide is an unstable element that spontaneously emits radiation at a predictable rate. PET technology is based on the labelling of tracers with positron emitting radionuclides such as ^{18}F, ^{68}Ga, ^{11}C and [64]Cu. The tracer is designed to visualize (without disturbing) a physiological process, such as glucose metabolism or the excretion of urine though the kidneys.

A positron antiparticle of the electron. When a positron is emitted in tissue it will quickly interact with an electron in an annihilation reaction. Both particles' mass is converted into energy in the form of two 511 keV gamma rays (photons) which are released in opposite directions from the site of annihilation.
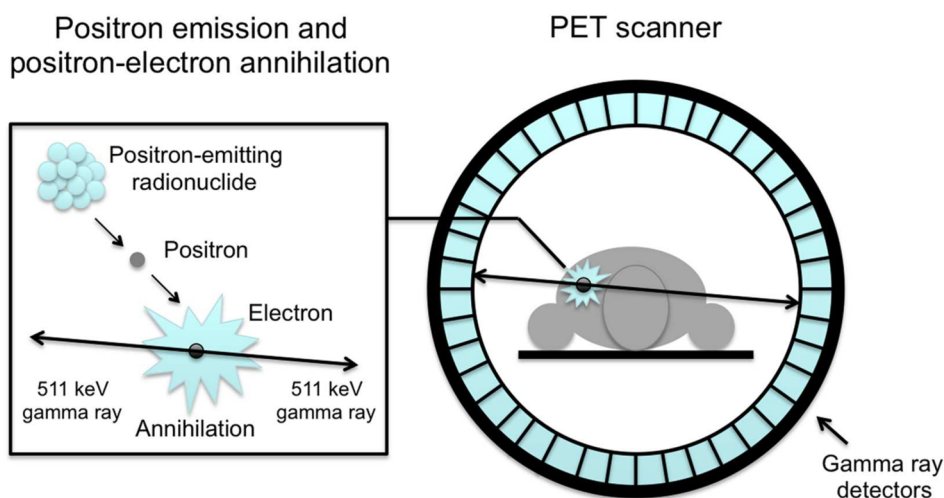
Figure 4
Schematic representation of a PET scanner. Image from Veldt et al [38] (CC-BY).

A PET scanner is a cylindrical array of elements that detect the 511 keV photons. When two such photons are detected simultaneously this is called a coincidence detection (Figure 4). The geometry of the scanner allows the system to calculate the line along

which the annihilation took place, called the line of response. Modern scanners can also detect minute time differences in the coincidence detections allowing more precise localization of the annihilation along the line of response, a technique called time of flight.

The radiotracer can be visualized either dynamically over a time period (e. g. from injection, moving through the circulatory system to a target organ) or statically at a fixed time point (e. g. an hour after injection, when uptake organs has stabilized).

The standardized uptake value (SUV) is a commonly used semi-quantitative, dimensionless measure of tracer uptake in PET imaging. If the PET scanner is properly calibrated, the number of detected photons from a given region can be converted into an estimate of the radioactivity (decay events) in that region. This activity is corrected for decay and normalized to the injected activity and, usually, the patient's weight to obtain the SUV.

The main advantage of PET scanners over the older nuclear medicine technology of gamma cameras (which detect single photons directly emitted from a gamma ray emitting isotope) is higher sensitivity and spatial resolution mainly due to coincidence detection. A PET scan is usually combined with a computed tomography (CT) x-ray scan to form PET/CT images (Figure 5) [39].
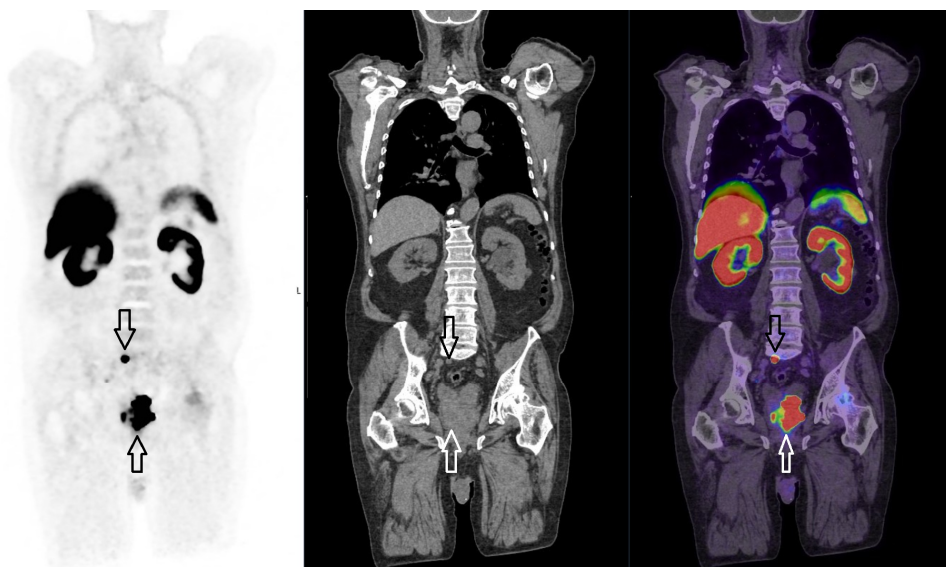
Figure 5
PET images, CT images, and fused PET/CT from an ^{18}F-PSMA-1007 PET/CT scan. Besides physiological uptake (mainly in liver, kidneys and spleen), there is uptake in a prostate cancer (upwards arrows) and a lymph node metastasis (downward arrows)

Prostate Specific Membrane Antigen (PSMA)

PSMA is an enzyme located in the cell membrane of prostate epithelial cells and in other tissues such as kidneys, small intestines and salivary glands. It is also known as glutamate carboxypeptidase II due to its function in glutamate metabolism. Its function in the prostate is not fully understood. It is highly upregulated in most prostate cancer adenocarcinomas and, to a lesser degree, in the neovasculature of most solid tumors. Due to inadequate diagnostic performance of ^{18}F-FDG PET in prostate cancer, development of a PSMA radiotracer for use in PET imaging was explored after the clinical breakthrough of ^{18}F-FDG PET in the early 2000's. [40, 41]

In 2012 the first in-human images of prostate cancer visualized with the PET radiotracer ^{68}Ga-PSMA-HEBD-CC (now known as ^{68}Ga-PSMA-11) were published [42]. PSMA-11 is a PSMA ligand that binds to the external portion of the PSMA enzyme, which is then internalized into the cell, allowing for imaging of PSMA-expressing tissues. Soon after PSMA-617 — a modification of PSMA-11 — was introduced, which can be labelled with ^{68}Ga for imaging or ^{177}Lu for therapy [43]. ^{177}Lu has been used for radioligand therapy since the 2000's [44]. The principle is the same as for a radiotracer — a pharmaceutical is labelled with a radionuclide, administered to the patient and distributed in the body. ^{177}Lu is a beta emitter like ^{18}F or ^{68}Ga but emits an electron instead of a positron, inducing localized tissue damaged in the area of uptake. ^{177}Lu also emits photons, enabling gamma camera imaging. Table 5 lists some available ligands for imaging and therapy. PSMA ligands have largely replaced earlier PET radiotracers for prostate cancer such as ^{18}F- or ^{11}C-choline and ^{18}F-fluciclovine [45].

Table 5
List of some of the available PSMA-ligands. FDA=Food & Drug Administration (US), EMA = European Medicines agency (EU)

Name	Radionuclide	Main use	FDA/EMA approval
PSMA-11 (gozetotide, Locametz)	^{68}Ga	Imaging	FDA, EMA
DCFPyL (piflufolastat, Pylclari)	^{18}F	Imaging	FDA, EMA
rhPSMA-7.3 (flotufolastat, Posluma)	^{18}F	Imaging	FDA
PSMA-1007 (Radelumin)	^{18}F	Imaging	
JK-PSMA-7	^{18}F	Imaging	
AIF-PSMA-11	^{18}F	Imaging	
PSMA-617 (vipivotide tetraxetan, Pluvicto)	^{177}Lu (^{68}Ga, ^{225}Ac)	Therapy	FDA, EMA (^{177}Lu)
PSMA-I&T	^{177}Lu (^{68}Ga, ^{225}Ac)	Therapy, imaging	

^{68}Ga-PSMA-11 is generally considered the reference standard for imaging radiotracers due to having the largest body of research available. ^{18}F-PSMA-1007 is unique due to its mainly hepatobiliary excretion, an advantage over the renal excretion of the other tracers since the prostate is close to the urinary bladder. There is no research proving the superiority of one tracer over another [46-48].

[18]F-labelled tracers offer the logistical advantage of large-scale production in cyclotrons, with a half-life of 110 minutes enabling transport to several clinical sites. On the other hand, for sites without easy cyclotron access a ^{68}Ga-generator (producing enough activity for 3–4 patients/day) might be the only option.

Research on PSMA PET imaging

Biochemical recurrence (BCR)

Early PSMA PET imaging research focused on the BCR setting with promising results in retrospective trials [49, 50]. Table 6 summarizes four phase III trials on patients with BCR. An American phase III trial of ^{18}F-PSMA-1007 (NCT04742361) in BCR has finished recruiting (n=136).

Table 6
Phase III trials of PSMA PET in the setting of BCR PPV/CLR = positive predictive value
DR = detection rate (overall | PSA<0.5 µg/l | PSA>5 µg/l)

Trial	PSMA-BCR [51]			CONDOR [52]			Olivier et al [53]			SPOTLIGHT [54]		
Year	2019			2021			2022			2023		
Radiotracer	^{68}Ga-PSMA-11			^{18}F-DCFPyL			^{18}F-PSMA-1007			^{18}F-rhPSMA-7.3		
n	635			208			190			389		
PPV	84–92%			86%			96%			65–82%		
DR (%)	75	38	97	63	36	97	82	57	–	82	63	97

In a follow-up to the PSMA-BCR trial, intended major changes in management due to PSMA PET findings occurred in 68% of patients [55]. In the CONDOR trial this number was 64%.

The randomized PSMA-SRT trial has enrolled 193 patients and will compare the 5-year success rate of salvage radiotherapy (SRT) after PSMA PET compared to standard of care imaging. A Swedish randomized trial will enroll an estimated 450 patients to compare standard SRT to individualized SRT based on PSMA PET results [56, 57].

N- and M- staging

The landmark proPSMA trial included 302 patients with newly diagnosed high-risk prostate cancer. They were randomized to conventional imaging (CT and bone scan) or ^{68}Ga-PSMA-11 PET. For any metastases, the sensitivity and specificity of PSMA PET was 85% and 98% compared to 38% and 91% for conventional imaging. The reference standard was a composite of histopathology, imaging and clinical follow-up. [58]

Three prospective trials phase III with ^{68}Ga-PSMA-11 (Hope et al, n=277), ^{18}F-DCFPyL (OSPREY, n=252) and ^{18}F-rhPSMA-7.3 (LIGHTHOUSE, n=296) examined PSMA PET before prostatectomy in patients with intermediate- to high-risk cancer. With post-operative histopathology as reference standard, the sensitivity for detection of pelvic lymph node metastasis was 27% to 40% and specificity was 94% to 98% in the three trials. [59-61] A phase III trial of primary staging with ^{18}F-PSMA-1007 (NCT04742361) is currently recruiting with an estimated n=380.

The randomized PSMA dRT trial will enroll 312 patients to compare success rates of radiotherapy with or without PSMA PET/CT to control for metastases prior to treatment [62].

T-staging

A 2021 meta-analysis of seven studies (n=389) found pooled sensitivity and specificity of 97% and 66% for the correct diagnosis of prostate cancer with ^{68}Ga-PSMA PET [63].

A 2023 meta-analysis of head-to-head comparisons of PSMA PET/CT and MRI staging found sensitivity and specificity of 52% and 81% for PET vs 61% and 86% for MRI in detection of T3a disease (EPE). For T3b (SVI) the numbers were 45% and 93% vs 62% and 96%. [64]

Comparison and meta-analysis of staging trials with PSMA PET/CT is complicated by a lack of standardization for reporting [65]. For detection of clinically significant prostate cancer (csPCa) the PRIMARY score is an attempt to standardize reporting and improve diagnostic performance. It is a 5-point scale which takes into account the localization, pattern and intensity of uptake in the prostate (Table 7). A randomized phase III trial (PRIMARY2) will recruit 660 patients with PI-RADS 3 findings to investigate if biopsy can be safely postponed with a negative PSMA PET using PRIMARY score cut-offs.

Table 7
Sensitivity and specificity for detection of psPCa for PET and MRI from the PRIMARY trials.
*Original PRIMARY study with fixed SUV for PET and PI-RADS for MRI (n=291) [66]
**Post hoc analysis on same population with PRIMARY score [67]
*** "Real world"- assessment of PRIMARY and PI-RADS (n=242) [68]

	PET*	MRI*	PET**	PET***	MRI***
Sensitivity	90%	83%	88%	86%	89%
Specificity	50%	53%	64%	76%	74%

Research on PSMA radioligand therapy

Early retrospective trials of ^{177}Lu-PSMA-617 showed promise for the treatment to be safe and efficacious in advanced prostate cancer [69]. Two open-label randomized trials published in 2021 TheraP (phase 2) and VISION (phase 3) established ^{177}Lu-PSMA-617 as a treatment option in certain patients with metastatic castration-resistant prostate cancer (mCRPC) [70, 71]. The VISION trial included 831 patients with mCRPC and disease progression despite both ARPI treatment and chemotherapy. Patients were randomized (ratio 1:2) to standard care or standard care plus ^{177}Lu-PSMA-617 (4–6 cycles of 7.4 GBq every four weeks). With a median follow-up of 21 months, overall survival was 11.3 months in the control group and 15.3 months in the ^{177}Lu-PSMA-617 group (hazard ratio 0.62).

Another phase 3 trial (PSMAfore) randomized 468 patients with mCRPC and progression on ARPI treatment (no chemotherapy) to ^{177}Lu-PSMA-617 (6 x 7.4 GBq) or change to another ARPI. After a median follow-up of 24 months, median radiographic progression-free survival was 11.6 months in the ^{177}Lu-PSMA-617 group vs 5.6 months in the ARPI group (HR 0.49) [72].

Other trials have shown promising results in earlier stages of disease. ENZA-p (phase 2, n=162) compared ARPI (enzalutamide) with ARPI plus ^{177}Lu-PSMA-617 as a first-line treatment in mCRPC. HR for progression-free survival was 0.43 after a median follow-up of 20 months. [73] UpFrontPSMA (phase 2, n=130) compared ADT+docetaxel with ADT+docetaxel plus ^{177}Lu-PSMA-617 in patients with recently diagnosed metastatic hormone sensitive prostate cancer (mHSPC). OR for undetectable PSA at 48 weeks was 3.9. [74]

An ongoing phase 3 trial (PSMAddition) will recruit about 1100 patients with mHSPC to receive either ADT+ARPI or ADT+ARPI plus ^{177}Lu-PSMA-617 with radiographic progression-free survival as primary endpoint [75].

Internal radiation dosimetry

Internal dosimetry deals with the estimation of the radiation doses delivered to tissues in the body. In diagnostic nuclear medicine the purpose of dosimetry is to quantify the radiation dose from a diagnostic procedure on a population level. The dose should be acceptable from a risk perspective and be kept as low as possible without compromising the diagnostic performance of the procedure (the ALARA principle — as low as reasonably achievable).

In therapeutic nuclear medicine the aim is to deliver therapeutic radiation doses to the target lesions (usually cancer) while minimizing toxicity in healthy tissues. Here, personalized (patient-level) dosimetry is usually the aim.

Two types of effects of radiation exposure are relevant.

- *Stochastic* effects are the long-term risks of for example cancer after exposure to low doses of radiation. These effects are random and can only be described in terms of probability of an effect, which increases with the dose.

- *Deterministic* effects involve predictable tissue damage from higher doses of exposure to tumors or healthy organs. There is a direct causal relationship between the exposure and the effect.

Definitions

Administered activity

The administered activity is the amount of radioactive material given to a patient, measured in becquerels (Bq, decays per second). The administered activity is decided beforehand and depends on the radiotracer, purpose of the procedure and often patient-specific factors such as weight. It is measured with a dose calibrator before administration.

Absorbed dose

The absorbed dose D is the mean energy deposited in a tissue of a specific mass (e.g. a tumor or an organ) and is measured in Gray (Gy, joules/kilogram). It depends on the administered activity, the energy and type of radiation emitted from the radionuclide and the patient-specific distribution of the radiotracer.

Equivalent dose

The equivalent dose H accounts for the biological effects of the radiation. It is obtained by multiplying the absorbed dose with a radiation-specific weighting factor (W_R). W_R is determined mainly by the linear energy transfer — the mean energy deposited from the radiation while traversing a specific distance in tissue. For example, alpha radiation (W_R=20) will deposit more energy per mm — and travel a shorter distance for a given amount of energy — than gamma radiation (W_R=1). The energy deposition is more concentrated and so causes more damage for a given absorbed dose. The unit of H is Sievert (Sv). Like Gy, 1 Sv is defined as 1 J/kg but weighted for biological effect.

Effective dose

The effective dose E is an attempt to express the total risk of cancer and genetic defects to a person from an exposure to radiation. In nuclear medicine it is often calculated on a whole-body basis. In such a case it is the sum of the equivalent doses to each organ weighted by a tissue-specific weighting factor (W_T, Table 8). It is also expressed in Sv. For reference, the average annual background radiation is about 1–3 mSv while a chest X-ray gives an E of 0.1 mSv, and a whole-body CT 10–20 mSv. [76, 77]

Table 8
Tissue weighting factors from ICRP publication 103 [78].

Tissue	W_T	ΣW_T
Red bone-marrow, colon, lung, stomach, breast, remainder tissues	0.12	0.72
Gonads	0.08	0.08
Bladder, oesophagus, liver, thyroid	0.04	0.16
Bone surface, brain, salivary glands, skin	0.01	0.04
	Total	1.00

Dose calculations

The most commonly used framework for dose calculations is the MIRD schema, developed by the Medical internal radiation dose committee of the Society of nuclear medicine and molecular imaging [77].

An administered radiotracer is distributed in the body and any organ that contains the tracer will be a source region of radiation (r_S). All organs can also be the target regions of radiation (r_T). A simplified equation for the calculation of absorbed dose D from any r_S to any r_T is:

$$D = \tilde{A} \times S(r_T \leftarrow r_S)$$

where Á is the cumulated activity (i.e. the number of decays) in r_S in a defined time and $S(r_T \leftarrow r_S)$ is called the S value.

Á can be estimated from measurements in animals or humans, or through simulations. It is affected by the biokinetics of the radiotracer and the physical decay of the radionuclide. For in vivo measurements, repeated scans (for example in a PET-scanner) are obtained and the activity in a defined r_S (e.g. the liver) is measured at each time point. A time-activity curve (TAC) can be plotted and Á is the area under that curve. Mathematical curve-fitting or biokinetic models can be used to obtain time-activity curves that approximates the TAC beyond the obtained point measurements (Figure 6).
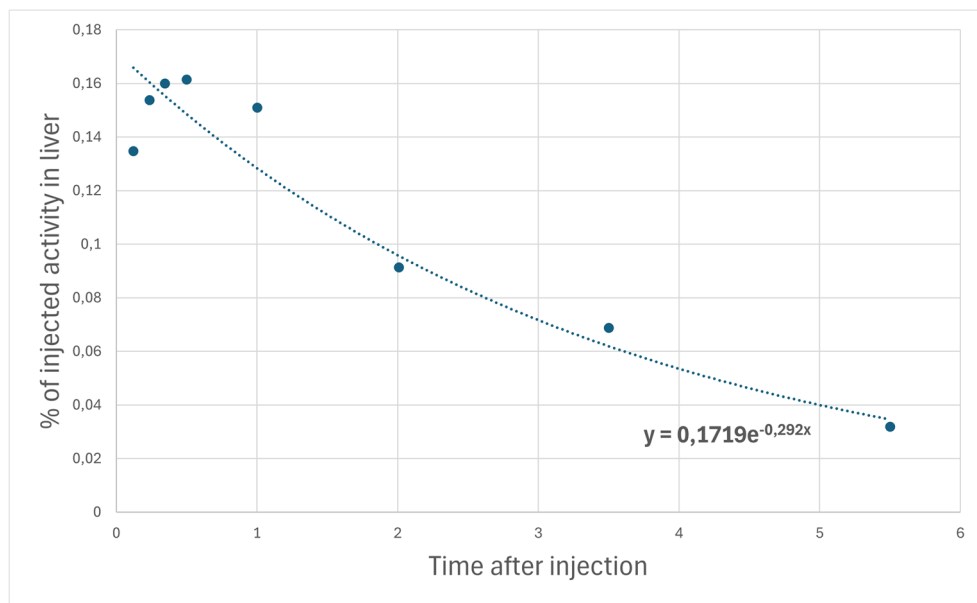
Figure 6
Simple exponential curve fitting in Microsoft Excel of point measurements of activity in the liver. The obtained function can be integrated to calculate the area under the curve beyond the measured time period.

The S value represents the total energy absorbed in r_T for every decay in r_S, divided by the mass of r_T (to give the unit Gy=J/Bq). It depends on the particular radionuclide since all radionuclides emit different spectra of radiation. It also depends on an anatomical model to calculate what fraction of radiation from r_S that will affect r_T. Since r_S and r_T usually represent organs, in whole-body dosimetry there will be an S-value specific for each combination of organs, including how each organ irradiates itself. The International Commission on Radiological Protection publishes age- and sex-specific

anatomical models (phantoms) which are used to calculate S values (Figure 7). It should be noted that even if activity is measured on a patient level, the dose calculations will still depend on such generalized models.
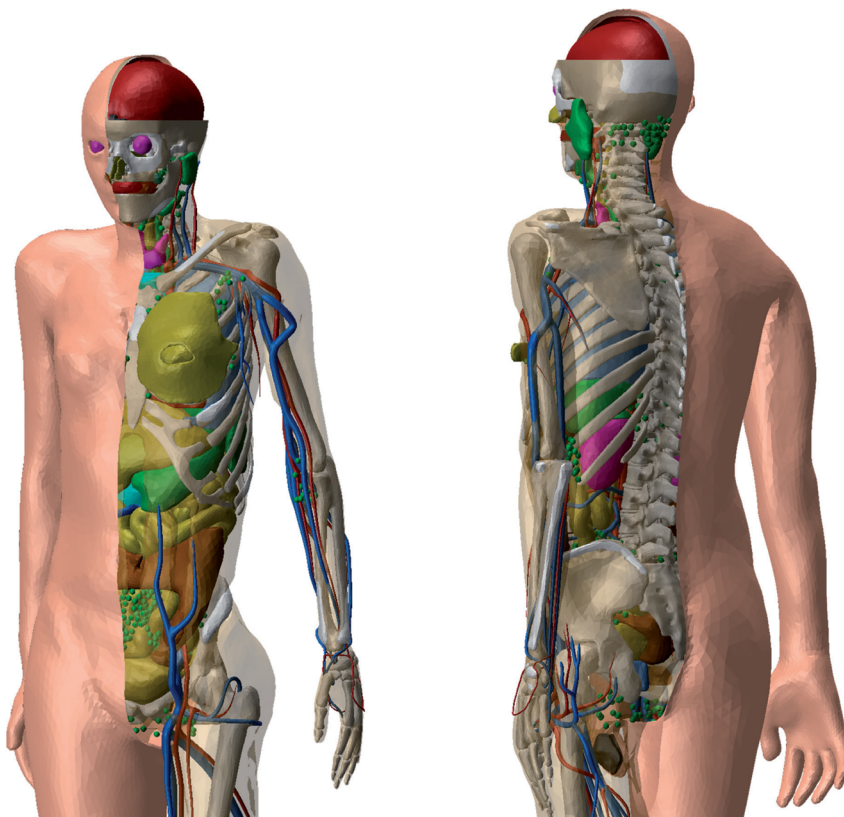
Figure 7
Renderings of female and male reference computational phantoms, © ICRP, reprinted with permission from [79].

When D has been calculated for all relevant organs the equivalent and effective doses can be calculated using the appropriate weighting factors. [76, 77]

Thesis

Rationale for thesis

The unique advantage of ^{18}F-PSMA-1007 is its mainly hepatobiliary excretion whereas other PSMA-tracers are excreted in urine [46]. This may lead to better visualization of uptakes close to the urinary bladder [80]. A possible disadvantage noted early was a high frequency of unspecific uptakes compared to ^{68}Ga-PSMA-11, especially in bone [81].

As I mentioned in the introduction, when our clinic started using ^{18}F-PSMA-1007 in 2019, little clinical research had been published on this specific tracer.

The first in-human research was published in 2017, imaging three healthy volunteers for dosimetry and ten patients with prostate cancer. It reported an effective dose 0f 0.022mSv/MBq and diagnostic performance at least comparable to ^{68}Ga-PSMA-11 [82].

Another study imaged patients (n=40) after 60 and 120 minutes and found higher uptake in cancer lesions and possibly more lesions found after 120 minutes [83].

Other early research was mainly in the setting of biochemical recurrence showing performance similar to that of ^{68}Ga-PSMA-11 [84, 85]. In other clinical settings, only small (n<20) studies had been performed [86, 87].

With this background we planned four papers, detailed below, with the aim of adding to the body of knowledge of ^{18}F-PSMA-1007 PET/CT.

My contributions

I was active in planning and designing all four papers with an increasingly active role. Paper IV was chiefly designed, planned and coordinated by me. I wrote the main manuscript for papers I, II and IV and submitted them to journals.

I performed most of the organ segmentation in the PET images in Paper I. In papers II–IV I reviewed all PET images.

In paper I, I collaborated with medical physicist Gustav Brolin in creating the compartment model and I performed the dose calculations. I compiled data from all readers and performed the statistics in Papers III and IV. In Paper II statistics were performed by the main author Jacob Ingvar but double-checked by me.

Aims

Paper I — biokinetics and dosimetry

This paper was a collaboration with our radiophysics department. The aim was to provide more robust data than previously available on the biokinetics of ^{18}F-PSMA-1007, with the purpose of performing population-based dosimetry calculations.

Paper II — optimal uptake time

The aim was to examine whether imaging one and two hours after injection of ^{18}F-PSMA-1007 leads to a different number of suspected metastases found. We focused especially on metastases that would change the TNM-classification, as this might lead to a change in treatment.

Paper III — N1 staging

This paper was a collaboration with our urology department. The first author was urologist and PhD student Jacob Ingvar. The aim was to evaluate the performance of ^{18}F-PSMA-1007 PET/CT in lymph node staging in intermediate- and high-risk prostate cancer, using histopathology after extended pelvic lymph node dissection as reference.

Paper IV — T3 staging

This paper was a multidisciplinary collaboration involving specialists in nuclear medicine, radiology, pathology and urology. The aim was to evaluate the performance of ^{18}F-PSMA-1007 PET/CT in T3 staging of prostate cancer using a semi-standardized assessment method with histopathology after prostatectomy as reference.

Methods and materials

Ethics

All projects were performed in accordance with the 1964 Helsinki Declaration and its later amendments. All subjects signed an informed consent form. Papers I and II were approved by the Swedish Ethical Review Authority (2020-00689) under the following conditions:

- For paper I, all subjects must be >50 years of age, effective dose limit 50 mSv.

- For Paper II, all subjects must be >18 years of age, effective dose limit 10 mSv.

Papers III and IV were both covered by approvals 2016/417 and 2018/753 (Lund Regional Ethical Review Board) which approve retrospective inclusion of patients referred for a clinical PET/CT scan, if they signed a consent form at the time of the scan.

Subjects

All subjects were patients with needle-core verified prostate cancer who had been referred to our department for an ^{18}F-PSMA-1007 PET/CT.

Paper I — biokinetics and dosimetry

We enrolled 12 patients at least 50 years of age who agreed to perform repeated PET scans for 6 hours after injection of ^{18}F-PSMA-1007.

Paper II — optimal uptake time

We enrolled 195 patients with BCR or newly diagnosed prostate cancer. In addition to our clinical PET/CT scan two hours after injection of ^{18}F-PSMA-1007, they performed an extra scan one hour after injection.

Paper III — N1 staging

We retrospectively included 104 patients with intermediate- or high-risk cancer who had undergone primary staging with an ^{18}F-PSMA-1007 PET/CT followed by robotic-assisted laparoscopic prostatectomy (RALP) with extended pelvic lymph node dissection (ePLND).

Paper IV — T3 staging

We retrospectively included 124 patients who had undergone and MRI of the prostate and primary staging with an ^{18}F-PSMA-1007 PET/CT followed by robotic-assisted laparoscopic prostatectomy (RALP).

Study design

Paper I — biokinetics and dosimetry

After injection of ^{18}F-PSMA-1007, the 12 patients underwent eight knee-to-head PET/CT scans from 3 to 330 minutes post-injection, with blood samples drawn at the same time points (Figure 8). Urine was collected until the morning after injection. In the PET images volumes of interest (VOIs) were created for 22 organs, with assistance from an AI.
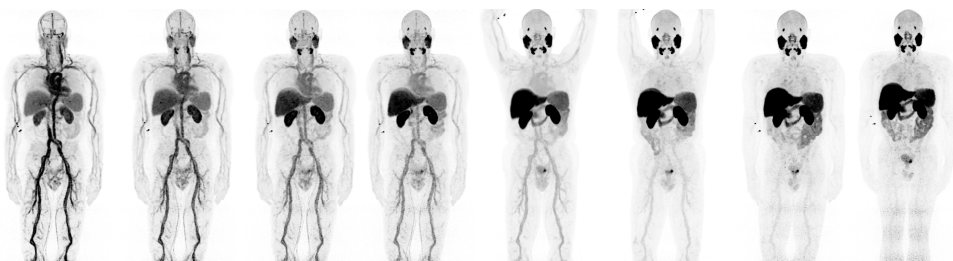
Figure 8
Eight scans at different time points up to 330 minutes after injection of ^{18}F-PSMA-1007. Early images show uptake mainly in vasculatur structures, and later images distribution in organs.

Activity data for each organ, urine and blood were entered into a compartment model created by medical physicist Gustav Brolin. The model was used to create time-activity-curves (TACs) visualizing the biokinetic behavior of ^{18}F-PSMA-1007, and to calculate cumulated activity (Ã) for the organs. We used Ã to calculate absorbed and effective dose coefficients with the software IDAC-Dose 2.1.

Paper II — optimal uptake time

Three nuclear medicine physicians (me, Elin Trägårdh and collaborator Ulrika Bitzén) did a complete clinical evaluation of the two ^{18}F-PSMA-1007 PET/CT PECT/CT scans performed on 195 patients (at one and two hours post-injection). We noted tumor visibility in the prostate and lesions suspicious for metastases, and measured SUV at both time points. Patients were then TNM classified at both time points.

Paper III — N1 staging

For all 197 patients I evaluated ^{18}F-PSMA-1007 PET/CT scans looking for pelvic lymph node metastases. I did this blinded to the clinical evaluation done at the time of the scan. Afterwards I compared my results to the clinical evaluation. Any discrepancies were discussed with an experienced nuclear medicine specialist (my supervisor Elin Trägårdh).

We compared these data with the clinical histopathologic evaluation of lymph nodes removed at surgery and did statistical analyses of the diagnostic performance of ^{18}F-PSMA-1007 PET/CT with regards to pelvic lymph node metastases. For both PET and histopathology, the side of pathology was noted (left or right iliac).

Paper IV — T3 staging

Two nuclear medicine physicians (me and collaborator Fredrik Hedeer) evaluated all 124 ^{18}F-PSMA-1007 PET/CT scans looking for signs of stage T3 cancer, i.e. signs of extra prostatic extension (EPE, T3a) or seminal vesicle invasion (SVI, T3b). EPE was evaluated both quantitatively (by measuring length of the tumor's capsule contact, LCC, as an indirect marker of risk for EPE) and visually. We built on a previously described method for standardizing the SUV window levels used when viewing images [88]. This is important since different SUV levels can strongly affect both the LCC and the visual appearance of the fused PET/CT images (Figure 9). We also developed a 1–5 Likert scale to standardize reporting.
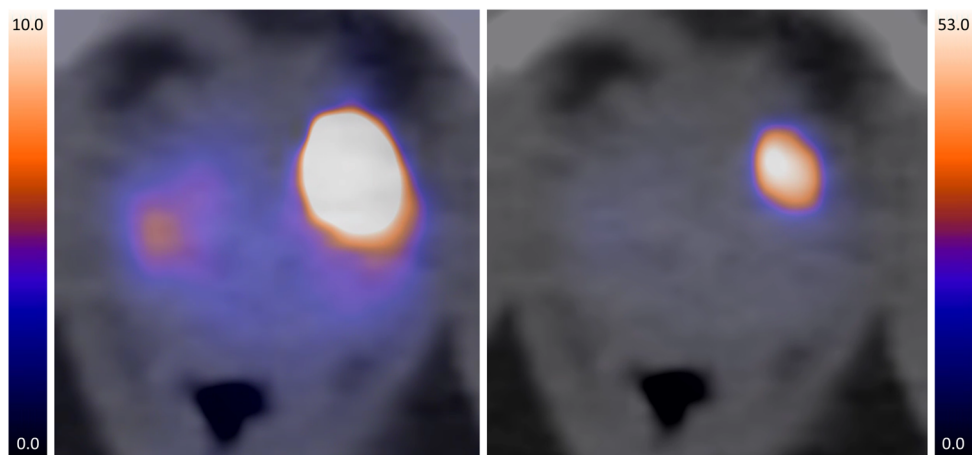
Figure 9
A prostate cancer lesion shown with different SUV window level settings. On the left, all SUV:s above 10 are seen as white (a common clinical setting). In our study, we set the maximum window level to the maximum SUV measured in the lesion, which will usually make the lesion appear smaller.

MRI images were evaluated for EPE and SVI by radiologist Erik Thimansson using PI-RADS. All prostatectomy specimens were evaluated by pathologist Kevin Sandeman. We did statistical analyses of the diagnostic performance of ^{18}F-PSMA-1007 PET/CT with regards to T3 stage, and of the interrater reliability of the methods using for PET evaluation.

Statistics

I performed statistic calculations in IBM SPSS Statistics v 29.0 and Microsoft Excel 365.

Diagnostic performance

The diagnostic performance of ^{18}F-PSMA-1007 PET/CT was evaluated in Papers III and IV. Table 9 shows a so-called contingency table outlining the calculations of the most common diagnostic indices for a test.

Table 9
Calculations of diagnostic indices. In this example the performance of a PET scan is evaluated against a reference standard of histopathology. PPV = positive predictive vaule, NPV = negative predictive value, FNR = false negative rate, FPR = false positive rate

	Histopathology positive	Histopathology negative	
PET positive	True positive (TP)	False positive (FP)	PPV = TP/(TP+FP)
PET negative	False negative (FN)	True negative (TN)	NPV = TN/(TN+FN)
	Sensitivity = TP/(TP+FN)	Specificity = TN/(TN+FP)	
	FNR = FN/(TP+FN)	FPR = FP/(TN+FP)	

Sensitivity (also called true positive rate) and specificity (true negative rate) answer the question "If a patient has (or doesn't have) a condition, how often does the test get it right?". They are properties of test performance and less informative when looking at a single test result.

Sensitivity is inversely correlated to the false negative rate (1-sensitivity) which answers the question "If a patient has the condition, how often does the test miss it?". The same holds for specificity and false positive rate.

Positive and negative predictive value (PPV and NPV) answer the question "Given this patient's test result, what is the probability they actually have (or don't have) a condition?". They are dependent on the prevalence of the condition in the population being tested and are therefore less generalizable than sensitivity and specificity.

Accuracy is usually calculated as (TP+TN)/(TP+FP+TN+FN), i.e. the proportion of correct tests in the whole population. It can be useful as an overall marker of test performance but there is no clear interpretation of its clinical meaning. Like PPV and NPV, accuracy depends on prevalence.

A ROC (Receiver Operating Characteristic) curve is a plot of sensitivity (true positive rate) as a function of 1-specificity (false positive rate) (Figure 10). The area under the ROC curve summarizes the performance of continuous variable across different thresholds and can vary from 0.5 (random chance) to 1.0 (perfect test). The optimal threshold will depend on whether sensitivity or specificity is more important. The Youden index (sensitivity+specificity-1) can be calculated for different thresholds and the maximum index is an indicator of the optimal threshold if sensitivity and specificity are equally important [89].
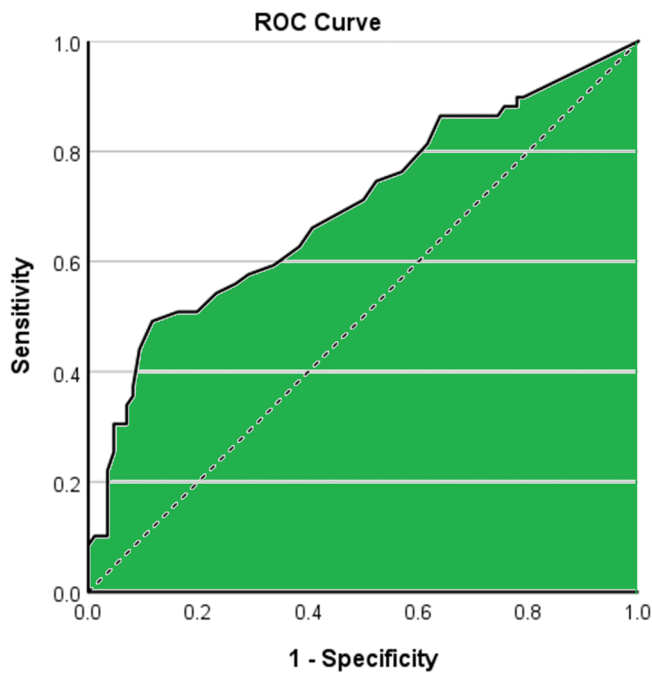
Figure 10
ROC curve for the LCC variable from paper III. The green area under the curve is 0.70.

Inter-rater reliability (IRR)

In paper IV we evaluated IRR between two readers of PET scans. IRR statistics are designed to evaluate the consistency of ratings or observations between different readers. The formula on which these statistics are based is:

$$X = T + E$$

Where X = the observed score from a reader, T = the "true score" and E = measurement error. Since there are no perfect measurements, T can never be observed directly. The variances of the variables are related in the correlate equation:

$$Var(X) = Var(T) + Var(E)$$

The reliability measures how much of the variance in the observed score is due to the variance in the true scores.

$$IRR = \frac{Var(T)}{Var(X)}$$

An IRR of 0.80 would indicate that 80% of the variance in the observed scores are due to true variance and 20% is due to measurement imperfections, including inter-rater disagreement. [90]

The most common methods for calculating IRR are Cohen's kappa (for nominal and ordinal variables) and Intra-class correlation coefficients (ICC, for ordinal, interval and continuous variables). We used Cohen's weighted kappa for our Likert scale and ICC for the LCC measurement.

In IRR research, agreement is often considered poor for values < 0.20, fair for 0.21–0.40, moderate for 0.41–0.60, substantial for 0.61–0.80 and near perfect for > 0.80, based on suggestions from Landis and Koch in 1977 [91]. These cut-offs have been criticized for being arbitrary and too lax. An alternative approach suggests levels of agreement as according to Table 10 [92]. These are based on the fact that IRR measurements are a form of correlation. Similar to Pearsons r in correlation statistics they can be squared to estimate the amount of the variance in the observed data explained by agreement among raters, an estimate of the percentage of correct scores.

Table 10
Level of agreement for IRR statistics suggested

Level of agreement	None	Minimal	Weak	Moderate	Strong	Near perfect
IRR coefficient	≤0.2	0.2–0.4	0.4–0.6	0.6–0.8	0.8–0.9	>0.9
% "Correct scores"	<4%	4–15%	15–35%	35–63%	64–81%	>81%

Comparisons

In paper II various outcomes were compared when measured one and two hours after injection of ^{18}F-PSMA-1007 (dependent groups) using Wilcoxon signed-rank test or McNemar's test (for binary variables). In Paper III SUVs in different patients (independent groups) were compared using the Mann-Whitney U-test.

Results and discussion

Paper I — biokinetics and dosimetry

Figure 11 shows decay-corrected time-activity-curves derived from the compartment model to visualize the biokinetics of ^{18}F-PSMA-1007. Measured urinary excretion was 5-10% (mean 8%) after 20 hours, excretion through bile was estimated at 15% by the compartment model.

The highest absorbed doses were in lacrimal glands, kidneys, salivary glands, liver and spleen (Table 11).

Table 11
Absorbed doses for the organs with the highest doses, and for red marrow.

Organ	Absorbed dose coefficient (μGy/MBq)	Absorbed dose/300 MBq activity (mGy)
Lacrimal glands	98	29
Kidneys	85	25
Salivary glands	83	25
Liver	70	21
Spleen	66	20
Red bone-marrow	22	6

The effective dose coefficient was 25 μSv/MBq of injected activity. This translates to an effective dose of 5-10 mSv in most patients. Table 12 shows effective dose coefficients from other studies of PSMA PET tracers, and for ^{18}F-FDG PET.

Table 12
Effective dose coefficients (μGy/MBq)

^{18}F-PSMA-1007 [82]	^{68}Ga-PSMA-11 [93]	^{68}Ga-PSMA-11 [94]	^{68}Ga-PSMA-617 [43]	^{18}F-DCFPyl [95]	^{18}F-FDG [96]
22	22	16	21	14	19

The effective dose is in line with similar tracers and very close to the previous study of ^{18}F-PSMA-1007 by Giesel et al (25 vs 22 μSv/MBq) [82]. The absorbed dose coefficients for organs from our data compared to Giesel et al were more varied, (from 2.0–0.5), with a mean of 1.4 (higher in our study). Compared to that study we included more subjects for scanning (12 vs 3) and segmented more organs (19 vs 7), while Giesel et al collected more PET scans (10 vs 8). We developed a compartment model while Giesel et al used a combination of trapezoidal approximations and curve fitting. Compartment models have theoretical advantages over simpler biokinetic models, and
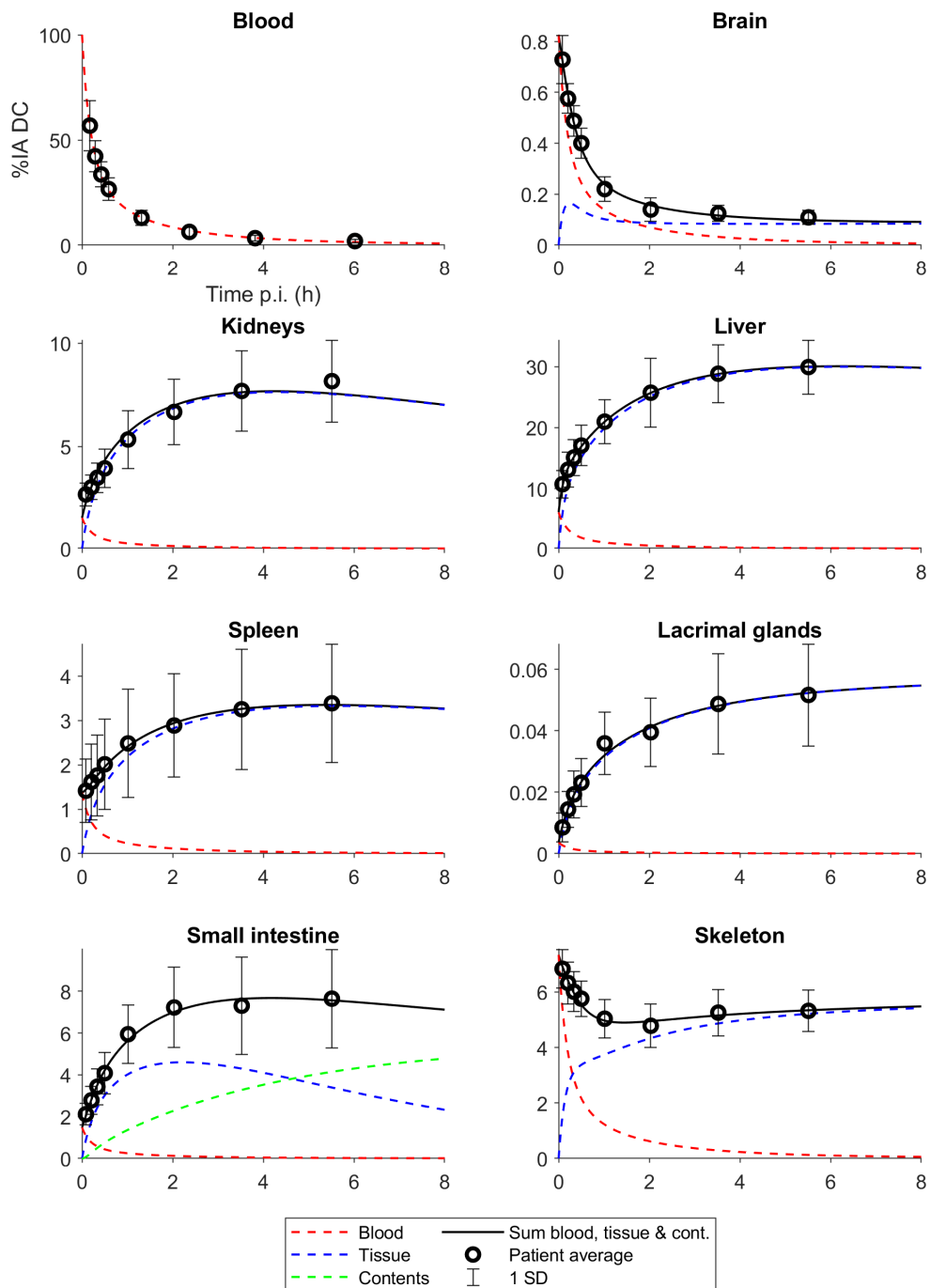
Figure 11
Decay-corrected TACs and patient-averaged activities for some organs in the compartment model.

are often the basis for dose estimates from organizations like ICRP and MIRD [97, 98]. However, without validation we cannot assume the superiority of our model.

Paper II — optimal uptake time

SUV was higher in malignant lesions and reference organs, and lower in the blood pool (aorta) and in urine, two hours after injection of ^{18}F-PSMA-1007 as compared to after one hour (Table 13).

Table 13
Median SUV at one and two hours after injection. P<0.001 for all comparisons.

Malignant lesions	SUVmax at one hour	SUVmax at two hours
Prostate (n=118)	13.3	17.2
Lymph nodes (n=116)	5.7	9.5
Bone (n=177)	5.1	7.5
Reference organs (n=195)	**SUVmean at one hour**	**SUVmean at two hours**
Aorta	2.1	1.0
Urine	3.2	1.2
Liver	10.5	12.9

More suspected lymph node and bone metastases were found after two hours with higher N- and M-stages as a result, on a per PET/CT scan basis (Table 14).

Table 14
Differences in readings 1 and 2 hours after injection of ^{18}F-PSMA-1007. Each PET reading (3 readers and 195 PET scans) was evaluated so that n=585. N1=regional lymph node metastases, M1a = non-regional lymph node metastases, M1b = bone metastases

	Readings with at least one metastases		Change in number of metastases	
	At 1 hour	At 2 hours	More at 1 hour	More at 2 hours
Pelvic LN:s	110	130	7	51
Abdominal LN:s	23	29	1	10
Bone	66	84	10	30
	Number of readings with at least stage N1			
	At 1 hour	At 2 hours	At 1 hour	At 2 hours
N1 disease	110	130	4	24
M1a disease	31	41	0	10
M1b disease	66	84	4	22

On a patient level, in two patients all three readers agreed on a higher N- or M-stage after two hours (Table 15, Figure 12).

Table 15
Patients where two or three readers agreed at a higher stage 1 or 2 hours after injection.

	Higher stage at 1 hour		Higher stage at 2 hours	
	2 readers	3 readers	2 readers	3 readers
N1 disease	1	0	7	1
M1a disease	0	0	1	1
M1b disease	1	0	1	0
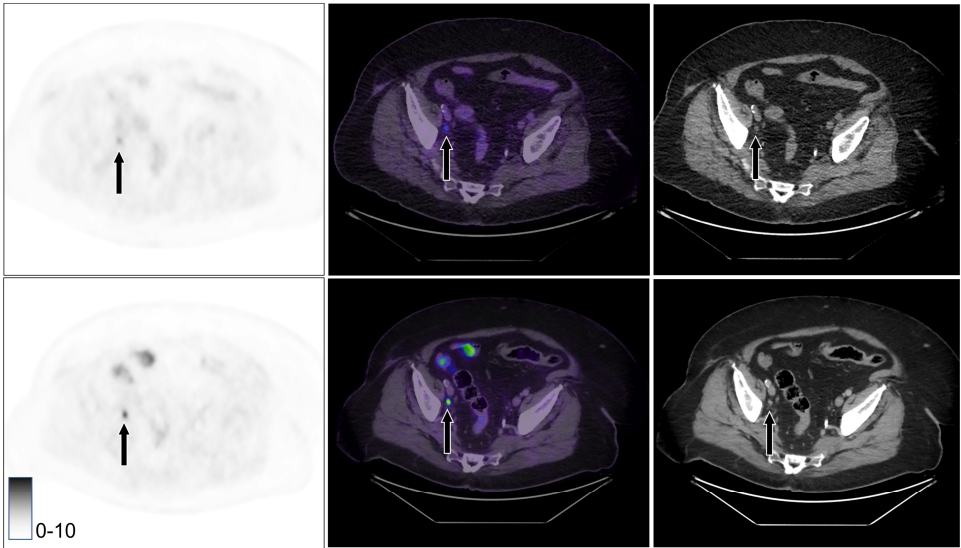
Figure 12
A lymph node suspect for metastasis, not flagged by any reader at one hour (top row) but by all three readers after two hours (bottom row).

Our motivation for this paper was uncertainty with regards to optimal timing of imaging after injection of ^{18}F-PSMA-1007. Guidelines recommend imaging after 1.5–2 hours and at our clinic we image after two hours [46]. While higher SUVs after two hours has been established, the largest available study (n=40) evaluating clinical findings reported only one additional lymph node after two hours [82, 83]. Also, this study was performed shortly after the introduction of ^{18}F-PSMA-1007 and the additional lymph node found seems to have been physiological uptake in a sacral ganglion misclassified due to inexperience (Figure 13).
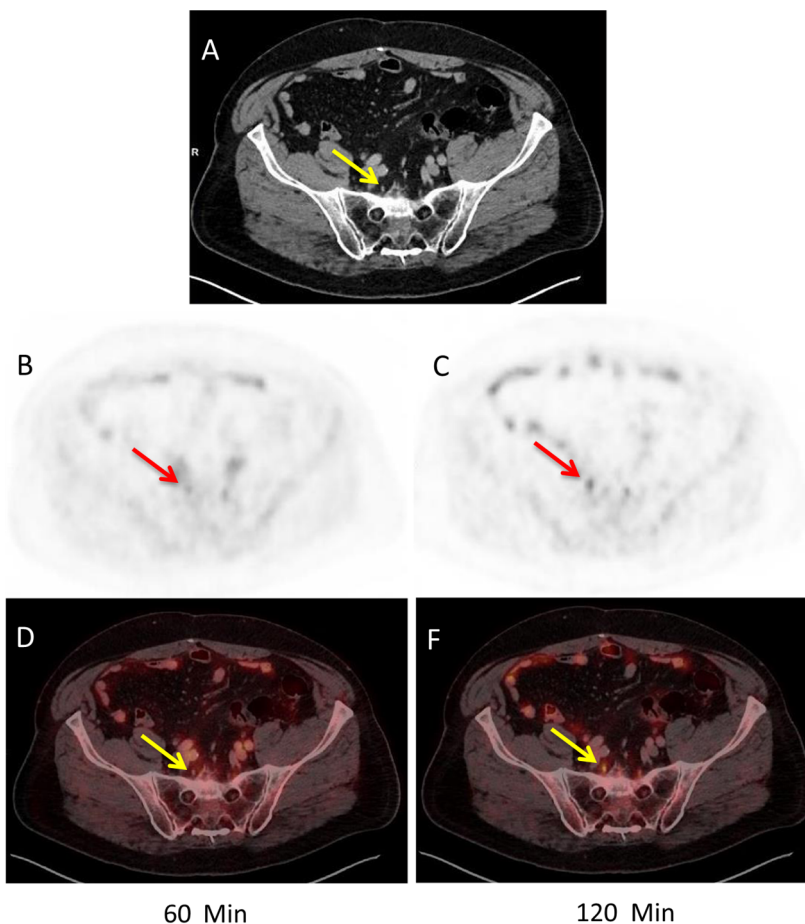
Figure 13
Uptake likely in sacral ganglion misclassified as lymph node uptake in Rahbal et al [83]. © Springer-Verlag GmbH Germany, reprinted with permission.

Our study demonstrates that more pathological lesions are found after two hours. The lack of histopathological verification is a limitation but the generally high specificity of PSMA PET/CT, as referenced in the background and previous discussions, supports the reliability of our findings. Even so, the limited sensitivity means that after two hours the disease burden may still be underestimated.

Another limitation is the use of a "soft end point" — change in N- or M-stage as assessed by nuclear medicine physicians. We speculate that this could influence the treatment of patients, but our methodology does not allow us to confirm this. Clinical decision-making in prostate cancer is a complex process where PSMA PET/CT is one of several important tools.

While imaging two hours after injection of ^{18}F-PSMA-1007 leads to more malignant findings, other factors such as scan indication, and the logistical constraints of the nuclear medicine facility will also guide the choice of uptake time.

Paper III — N1 staging

Table 16 is a contingency table with diagnostic indices based on left and right pelvic lymph node dissection in 104 patients. The prevalence of metastases was 15% (31/208).

Table 16
Diagnostic indices for ^{18}F-PSMA-1007 PET/CT to detect pelvic lymph node metastases with histopathology after ePLND as reference.

	Histopathology pos	Histopathology neg	
PET positive	8	3	PPV 73% (8/11)
PET negative	23	174	NPV 88% (174/197)
	Sensitivity 26% (8/31)	Specificity 98 % (174/177)	

On a patient basis, sensitivity and specificity were 27% and 96%. In high-risk patients only (n=80), sensitivity and specificity were 35% and 97% on a patient basis. On PET images, all false positives had the same uptake pattern of ^{18}F-PSMA-1007, faint uptake in normal size lymph node along the external iliac vessels. No true positive showed this pattern of uptake.

The main limitation of our trial is its retrospective design, which introduces a selection bias likely to decrease sensitivity.

Our results are similar to those of the three phase III trials — all with histopathology after ePLND as reference — referenced in the background section on PSMA, where sensitivity was 27-40% and specificity 94–98% [59-61]. These trials were — together with BCR trials from the same research groups — the basis for FDA approval of ^{68}F-PSMA-11, ^{18}F-DCFPyl and ^{18}F-PSMA-rh-7.3. Two prospective trials (n=99 and 134) of ^{18}F-PSMA-1007 with histopathology as reference, published after our paper, found patient-based sensitivity of 50–53% and specificity of 90–98% [99, 100].

The proPSMA trial published 2020 was the first large prospective randomized trial to confirm the superiority of PSMA PET/CT over conventional imaging (CT and bone scan) 302 men with newly diagnosed high risk prostate cancer were randomized to perform either ^{68}Ga-PSMA-11 PET/CT or conventional imaging. At six months follow-up, imaging results were evaluated against a composite reference standard which included histopathology, further imaging and biochemistry. The sensitivity and specificity for pelvic lymph node metastases were 83% and 99%. A prospective trial of

^{18}F-PSMA-1007 (n=79) published in 2021 used a similar composite endpoint with a median follow-up of 21 months and found a sensitivity of 87% and a specificity of 98%.

The composite reference will likely underestimate the number of false negatives in lymph nodes. For example, a small pelvic lymph node metastasis that would be found after ePLND may not be detectable by PSA testing or on imaging 6 months after curative radiotherapy. On the other hand, while histopathology is considered a gold standard for cancer, sampling error can led to true positives being classified as false positives (since a surgeon cannot be guaranteed to remove all lymph nodes visible on imaging).

In summary, while PSMA PET/CT is established as the most accurate modality for lymph node staging, it is not sensitive enough to avoid the need for a planned ePLND in prostatectomy patients, at least in high-risk patients [14, 101]. The addition of PSMA PET/CT to nomograms that are used to determine the risk of N1 disease increases their performance [102]. Ongoing research may determine the optimal use of PSMA PET/CT for risk stratification and surgical planning [103-106].

Paper IV — T3 staging

The diagnostic performance of ^{18}F-PSMA-1007 PET/CT and MRI is given in Table 17. AUC for the ROC-curve of the LCC parameter vas 0.70. Based on a Youden index of 0.37 a cut-off of 14 mm was chosen for EPE.

Table 17

Diagnostic performance of ^{18}F-PSMA-1007 PET/CT and MRI in detection of extraprostatic extension (EPE) seminal vesicular invasion (SVI). The prevalence of EPE was 40% and SVI 11%. LCC — length of capsular contact, cut-off 14 mm.

		Sensitivity	Specificity	PPV	NPV	Accuracy
EPE	PET combined	54%	76%	60%	71%	67%
	PET visual	28%	82%	52%	63%	60%
	PET LCC	46%	91%	77%	71%	73%
	MRI	80%	64%	60%	83%	70%
SVI	PET	14%	100%	100%	90%	90%
	MRI	50%	92%	44%	94%	87%

For EPE ^{18}F-PSMA-1007 PET/CT had superior specificity while MRI had higher sensitivity. The visual PET evaluation had poor sensitivity and performed worse than the LCC value, with no clear value in combining the two. This may partly be explained by selection bias which will likely affect the visual evaluation more. Both tests had high specificity for SVI, but PET had very low sensitivity.

Correct T3-staging is most important in the context of curative therapy — helping decide between surgery and radiotherapy, as well as guiding pre-operative planning of surgery. Highly sensitive imaging will identify most T3 patients, who may be more suitable for radiotherapy. In surgical planning, suspicion of T3 disease will discourage nerve-sparing surgery and lead to a wider excision, increasing the risk of post-operative complications. Here, specificity may be more important as discovery of T3 disease in histopathology after surgery can often be managed with adjuvant radiotherapy.

The inter-reader reliability (IRR) measurements for ^{18}F-PSMA-1007 PET/CT were 0.53 (kappa for visual EPE), 0.63 (kappa for SVI) and 0.68 (ICC for the LCC measurement), indicating weak to moderate agreement (Table 10). The reliability should be possible to improve by training, especially the quantitative LCC where several MRI studies have found ICCs >0.80 [107, 108].

As referenced earlier, results for studies of T3-staging have been varied for both PSMA PET/CT and MRI. In PSMA PET studies, criteria for T3 disease have often been insufficiently specified, with few attempts at standardization. A large (n=600) retrospective multicenter published shortly before ours is — due to its size — probably the most significant work on PSMA PET/CT [109]. Criteria were both PET and CT based and used a 3-point Likert scale. Sensitivity and specificity were 58% and 59% for EPE and 30% and 97% for SVI. Four different PSMA tracers (including ^{18}F-PSMA-1007) were used with no significant differences between them. Kappa values were 0.47 for overall T3 disease and 0.41 for T3b (SVI), indicating weak agreement (no kappa value for T3a/EPE was reported).

As in paper III, the retrospective methodology introduces a selection bias since patients with clear T3-tumors are more likely to receive radiotherapy rather than surgery.

Conclusion and future perspectives

Summary of thesis

This thesis has contributed to the research field of PSMA PET/CT, especially concerning the tracer ^{18}F-PSMA-1007.

We have calculated more robust dosimetry data for the tracer than was previously available. We have (at their request) shared the transfer coefficients from our compartment model with the International Commission on Radiological Protection for possible use in future reference publications.

The recommendation of uptake time of ^{18}F-PSMA-1007 before imaging in current guidelines if informed by rather weak data. Our paper on this topic allows nuclear medicine sites to make an informed choice on which uptake time is optimal for them, and can be the basis for future guidelines.

For N1-staging there is still limited data available for ^{18}F-PSMA-1007, but the tracer is used in this setting. Trials like ours, which indicate performance on par with more well-studied tracers, are important despite the moderate number of included patients.

T3-staging with PSMA PET is an area of uncertainty, regardless of the tracer used. The specificity for SVI has been consistently high in studies, with weak to moderate sensitivity. For EPE the performance has been more variable. We have contributed additional data on accuracy, and a method of standardization of quantitative and qualitative aspects of T3-staging with better reliability than previous methods.

^{18}F-PSMA-1007 research

^{18}F-PSMA-1007 currently holds a marketing authorization under the name Radelumin in nine European countries, based on a French phase III trial [53]. There is no marketing authorization in Sweden and ^{18}F-PSMA-1007 is currently unavailable for clinical examinations. In Region Skåne this has led to a switch to PSMA-11 labelled with ^{68}Ga from a generator, reducing the availability of the examination. There are two ongoing phase III trials (NCT06122584 for BCR, NCT04742361 for N-staging) which may lead to wider approval.

The unique advantage of ^{18}F-PSMA-1007 compared to other PSMA tracers is its low excretion in urine. This should improve detection of local recurrence after radical therapy — especially after prostatectomy — and possibly T3 disease. Although ^{18}F-PSMA-1007 has shown the highest detection rate and positive predictive value in phase III trials (Table 6), this does not prove superiority due to differences in methodology and patient selection. An upcoming head-to-head comparison of ^{18}F-PSMA-1007 (NCT05079828) in the recurrence setting after prostatectomy has finished enrolling 100 patients. If the results are positive for ^{18}F-PSMA-1007 a similar comparison regarding T3 stage could be the next step.

Several studies have reported a high number of unspecific bone uptakes with ^{18}F-PSMA-1007 compared to most other tracers [110]. Although this is considered a disadvantage, in practice these uptakes are often mild and can be disregarded by an experienced reader. Studies of moderate to intense bone uptakes without CT correlates could help clinical decision making, preferably with histopathological verification.

Levels of efficacy and future PSMA PET/CT research

An often-referenced model describes six levels of efficacy of diagnostic imaging, and how they can be measured through research [111]. The model says that for a procedure to show efficacy at a higher level, it must be efficacious at a lower level, while the reverse isn't true. For example, the low urinary excretion of ^{18}F-PSMA-1007 may increase tumor to background-ratio compared to other tracers (technical efficacy). This does not necessarily translate to higher accuracy and even if it does, the information might not be important enough to influence treatment, and so on (Figure 14).
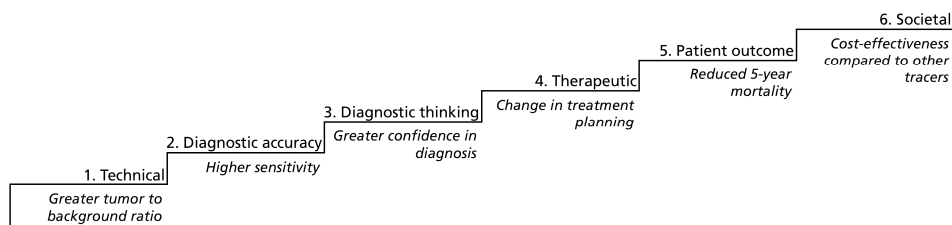
Figure 14
Six hierarchical levels of efficacy of diagnostic imaging, and possible ways to measure each level.

My research, and most research on PSMA PET/CT, is largely in the second tier. The proPSMA trial can be argued to have established level 2, 3, 4 and 6 efficacy of PSMA PET/CT in one trial. It established greater diagnostic accuracy of PSMA PET/CT compared to conventional imaging. Through its cross-over design it could at the same time show greater diagnostic thinking efficacy (through fewer inconclusive scans) and therapeutic efficacy by influencing treatment decision-making [58]. A separate cost-effectiveness analysis showed lower costs compared to conventional imaging (under Australian conditions) [112].

While societal efficacy tops the hierarchy, patient outcome efficacy is for most clinicians — and for patients — the measure of success. It should preferably be established in a randomized controlled trial (RCT). In prostate cancer, a clinically relevant patient outcome (e.g. overall survival rather than progression-free survival on imaging) requires a long follow-up. An alternative is the decision-analytic approach, which uses available information, for example on imaging efficacy and expected treatment outcomes, to calculate relevant outcomes. One such analysis found that PSMA PET/CT instead of bone scan and CT would reduce the number of deaths from prostate cancer with 13% [113].

RCTs will however remain the gold standard. An example could be an intervention arm receiving a PSMA PET/CT and a control arm receiving conventional imaging

before planning of salvage radiotherapy for BCR. While waiting for the results of such trials, some of which are underway, clinicians will have to make decisions based on imperfect information.

Undoubtedly, PSMA imaging and therapy will continue to be a dynamic area of research in nuclear medicine for years to come, with patient and health economic benefits as the ultimate markers of success.

Popular scientific summary

Nuclear medicine is a medical specialty that involves the use of radioactive substances — materials that spontaneously emit electromagnetic radiation. Different substances emit different types of radiation, making them suitable for various applications. In nuclear medicine diagnostics, which is the focus of this thesis, substances that emit radiation detectable by imaging or measurement are used to diagnose diseases or assess bodily functions.

The cornerstone of nuclear medicine is radiopharmaceuticals — compounds in which a radioactive substance is bound to a tracer. A tracer is a substance that behaves in a predictable manner after being introduced into the body, typically via intravenous injection. There are radiopharmaceuticals designed to accumulate in specific organs, such as the heart, bones, and lungs, or to be excreted by the kidneys. One of the most common nuclear medicine imaging techniques is FDG-PET (Positron Emission Tomography with FluoroDeoxyGlucose). FDG is a radioactive glucose molecule that is taken up in tissues that utilize glucose. Since cancer cells often have a high glucose metabolism, FDG-PET can detect many different types of cancer with high sensitivity — often identifying tumors too small to be seen with other imaging techniques like x-ray CT scans. However, prostate cancer cells often have a lower glucose metabolism, making FDG-PET less effective in detecting prostate cancer.

PET imaging with Prostate-Specific Membrane Antigen (PSMA) is a relatively new technique for visualizing prostate cancer. This method uses radiopharmaceuticals that bind to PSMA, a protein highly expressed in prostate cancer cells. Several different PSMA-targeting radiopharmaceuticals exist, and at Skåne University Hospital, we have used ^{18}F-PSMA-1007 since 2019. Compared to other PSMA radiopharmaceuticals, relatively little research has been conducted on this specific variant. The goal of my thesis is to improve our understanding of ^{18}F-PSMA-1007 through four studies.

Paper 1 — distribution and radiation dose
The aim of this study was to map how ^{18}F-PSMA-1007 distributes throughout the body after injection. We performed repeated PET scans on 12 patients and measured uptake in different organs to create curves showing uptake over time. These curves allowed us

to calculate the radiation dose delivered to each organ, which is used for radiation safety assessments. The radiation dose was comparable to that of other similar PET scans, roughly 3–4 times the background radiation we are all exposed to in one year.

Paper 2 — optimal imaging time

We investigated how accurate ^{18}F-PSMA-1007 PET imaging performed one hour after injection was as compared to imaging two hours after injection. In 195 patients, we acquired PET images at both time points and assessed them for metastases (spread cancer).

We found more metastases and reclassified several patients to higher disease stages when imaging was performed after two hours. While detecting every metastasis is not always necessary, a two-hour imaging delay is recommended when accurate disease staging is desired.

Paper 3 — lymph node metastases

This study aimed to determine how accurate ^{18}F-PSMA-1007 PET is at detecting metastases in lymph nodes near the prostate. We analyzed PET scans from 104 patients who later underwent prostate cancer surgery, during which lymph nodes were removed and examined to confirm whether they contained cancer.

We found that ^{18}F-PSMA-1007 PET had low sensitivity, meaning it often failed to detect lymph node metastases. As a result, lymph node removal during surgery may be needed even if they appear normal on PET scans. However, the test showed high specificity, meaning that when PET imaging did detect metastases, the findings were reliable.

Paper 4 — tumor growth outside the prostate

Unlike the previous two studies that focused on metastases, this study examined the primary tumor in the prostate. The goal was to assess how well ^{18}F-PSMA-1007 PET can determine whether the tumor has grown beyond the prostate. This is important for treatment decisions, particularly in choosing between radiation therapy and surgery.

Although prior studies with PSMA PET have explored this topic, they usually haven't described in much detail how they determine where the cancer grows. We tried to standardize and describe our method so that it can be repeated by others. We also evaluated how well different reviewers agreed when using this method.

Like in paper 3, PSMA PET had low sensitivity but high specificity, meaning it was better at confirming tumor spread outside of the prostate than at ruling it out. Agreement between reviewers was moderate.

Populärvetenskaplig sammanfattning

Nuklearmedicin är en medicinsk specialitet där vi arbetar med radioaktiva ämnen, det vill säga ämnen som spontant avger elektromagnetisk strålning. Olika ämnen avger olika typer av strålning som lämpar sig för olika sammanhang. I nuklearmedicinsk diagnostik, som är ämnet för denna avhandling, används ämnen som avger strålning som kan avbildas eller mätas för att ställa olika diagnoser eller värdera kroppens funktioner.

Grundstenen i nuklearmedicin är olika typer av radiofarmaka. Det är ämnen där ett radioaktivt ämne binds till ett spårämne — ett ämne som beter sig på ett förutsägbart sätt efter att man tillfört det till kroppen (oftast med en intravenös injektion). Det finns bland annat radiofarmaka som tas upp i hjärtat, skelettet, lungorna och som utsöndras i njurarna. En vanlig nuklearmedicinsk undersökning är FDG-PET (Positron Emissions-Tomografi med FluoroDeoxyGlukos). FDG är en radioaktiv sockermolekyl som tas upp i alla vävnader som använder socker. Cancerceller har ofta en hög sockerförbrukning och undersökningen kan med hög känslighet hitta många olika typer av cancer — ofta förändringar som är för små för att se med andra undersökningar som till exempel skiktröntgen. Prostatacancerceller använder oftast inte så mycket socker och därför har FDG-PET fungerat sämre där.

PET med Prostata-Specifikt Membran-Antigen (PSMA) är en ganska ny metod för att avbilda prostatacancer. Den utförs med radiofarmaka som binder till ämnet PSMA som finns i stor mängd i prostatacancerceller. Det finns flera olika radiofarmaka som binder till PSMA. På Skånes universitetssjukhus använder vi varianten ^{18}F-PSMA-1007 sedan 2019. Jämfört med andra PSMA-radiofarmaka finns det relativt lite forskning på just denna variant och syftet med min avhandling är att förbättra kunskapsläget med fyra studier.

Studie 1 — distribution i kroppen och stråldoser

Syftet var att noggrant kartlägga hur ^{18}F-PSMA-1007 fördelar sig i kroppen efter injektion. Vi gjorde upprepade PET-undersökningar hos 12 patienter och gjorde mätningar i bilderna för att kunna skapa kurvor över hur ^{18}F-PSMA-1007 togs upp i olika organ. Med hjälp av de kurvorna kunde vi också beräkna vilken stråldos alla organ

får. Det är viktigt att veta för att kunna göra strålsäkerhetsbedömningar. Stråldosen var i nivå med andra liknande undersökningar (motsvarande ungefär 3-4 gånger den normala bakgrundsstrålningen vi alla exponeras för under ett år).

Studie 2 — bildtagningsprotokoll

Syftet var att se om det går lika bra att ta bilder en timme efter injektion av ^{18}F-PSMA-1007 som efter två timmar. På 195 patienter tog vi bilder både en och två timmar efter injektion av ^{18}F-PSMA-1007 och granskade sedan bilderna för att hitta metastaser (spridd cancer).

Vi hittade fler metastaser och flera patienter placerades också i högre sjukdomsstadier efter två timmar. Det är inte alltid viktigt att hitta alla metastaser men vill man ha en noggrann stadieindelning bör man vänta två timmar innan bildtagning.

Studie 3 — lymfkörtelmetastaser

Syftet var att avgöra hur bra ^{18}F-PSMA-1007 PET är på att hitta metastaser i lymfkörtlar nära prostata. Vi gick igenom PET-undersökningar av 104 patienter som sedan hade opererats för sin cancer. Hos alla patienterna hade man tagit ut lymfkörtlar vid operationen så vi kunde bekräfta om det verkligen fanns cancer eller inte.

^{18}F-PSMA-1007 PET hade en låg känslighet för dessa metastaser, vilket betyder att vi inte kan lita på att undersökningen hittar metastaserna. Därför kan det vara bra att ta bort lymfkörtlarna vid operationen även om de ser normala ut med PET. Däremot var specificiteten hög vilket innebär att om ^{18}F-PSMA-1007 PET visar metastaser så kan vi lita på det.

Studie 4 — lokal tumörväxt

Här tittade vi inte på metastaser utan på tumören i prostatan. Syftet var att se hur bra ^{18}F-PSMA-1007 PET är på att se om tumören växer utanför prostatan. Det påverkar vilken behandling som är lämplig, framför allt valet mellan strålning och operation. Det finns flera studier på det här området sedan tidigare men de har ofta inte beskrivit hur de bedömt bilderna. Vi var därför noggranna med att granska bilderna på ett standardiserat sätt och testade hur väl två granskare var överens om sina bedömningar. Även i denna studie hade PSMA PET låg sensitivitet men hög specificitet. Överensstämmelsen mellan de två granskarna var måttligt bra.

Abbreviations

ADC Apparent diffusion coefficient

ADT Androgen deprivation therapy

AI Artificial intelligence

ALARA As low as reasonably achievable

AUC Area under the curve

ARPI Androgen receptor pathway inhibitor

BCR Biochemical recurrence

BRCA Breast cancer gene

CRPC Castration resistant prostate cancer

mCRPC Metastatic castration-resistant prostate cancer

csPCa clinically significant prostate cancer

CT Computed tomography

DRE Digital rectal exam

ePLND extended pelvic lymph node dissection

EBT External beam therapy

EMA European Medical Authority

EPE Extraprostatic extension

FDA Food and Drug Administration

FDG Fluorodeoxyglucose

GnRH Gonadotropin-releasing hormone

HSPC Hormone-sensitive prostate cancer

ICC Intraclass correlation coefficient

IRCP International Commission on Radiological Protection

IRR Interrater reliability

LCC Length of capsular contact

LN Lymph node

LUT Look up table

MIRD Medical internal radiation dose committee

MRI Magnetic resonance imaging

NEMA National Electrical Manufacturers Association

NPV Negative predictive value

PET Positron emission tomography

PhD Philosophiae doctor

PI-RADS Prostate Imaging–Reporting and Data System

PPV Positive predictive value

PS Primary staging

PSA Prostate specific antigen

PSMA Prostate specific membrane antigen

RRP Radical retropubic prostatectomy

RALP Robot-assisted laparoscopic prostatectomy

RCT Randomized controlled trial

ROC Receiver operating characteristic

SUV Standardized uptake value

SV Seminal vesicles

TAC Time-activity curve

TNM Tumor node metastasis

VOI Volume of interest

References

1. Vesalius, A., *Andreae Vesalii Bruxellensis, scholae medicorum Patavinae professoris, de Humani corporis fabrica Libri septem.* Universitätsbibliothek Basel doi.org/10.3931/e-rara-20094 1543.
2. Goddard, J.C., *The history of the prostate, part one: say what you see.* Trends in Urology & Mens Health, 2019. **10**(1): p. 28-30.
3. Marx, F.J. and A. Karenberg, *History of the Term Prostate.* Prostate, 2009. **69**(2): p. 208-213.
4. Lehtonen, M. and P.L. Kellokumpu-Lehtinen, *The past and present of prostate cancer and its treatment and diagnostics: A historical review.* SAGE Open Med, 2023. **11**: p. 20503121231216837.
5. Coakley, F.V. and H. Hricak, *Radiologic anatomy of the prostate gland: a clinical approach.* Radiol Clin North Am, 2000. **38**(1): p. 15-30.
6. Fine, S.W. and V.E. Reuter, *Anatomy of the prostate revisited: implications for prostate biopsy and zonal origins of prostate cancer.* Histopathology, 2012. **60**(1): p. 142-52.
7. McNeal, J.E., *The zonal anatomy of the prostate.* Prostate, 1981. **2**(1): p. 35-49.
8. Bray, F., et al., *Global cancer statistics 2022: GLOBOCAN estimates of incidence and mortality worldwide for 36 cancers in 185 countries.* CA Cancer J Clin, 2024. **74**(3): p. 229-263.
9. Socialstyrelsen, *Statistik om nyupptäckta cancerfall 2023.* 2024.
10. Hemminki, K., *Familial risk and familial survival in prostate cancer.* World J Urol, 2012. **30**(2): p. 143-8.
11. Cornford, P., et al., *EAU-EANM-ESTRO-ESUR-ISUP-SIOG Guidelines on Prostate Cancer-2024 Update. Part I: Screening, Diagnosis, and Local Treatment with Curative Intent.* European Urology, 2024. **86**(2): p. 148-163.
12. James, N.D., et al., *The Lancet Commission on prostate cancer: planning for the surge in cases.* Lancet, 2024. **403**(10437): p. 1683-1722.
13. Bell, K.J., et al., *Prevalence of incidental prostate cancer: A systematic review of autopsy studies.* Int J Cancer, 2015. **137**(7): p. 1749-57.
14. EAU, *EAU Guidelines. Edn presented at the EAU Annual Congress April 2024. ISBN 978-94-92671-23-3.*
15. Klotz, L., *Prostate cancer overdiagnosis and overtreatment.* Curr Opin Endocrinol Diabetes Obes, 2013. **20**(3): p. 204-9.
16. Regionala cancercentrum, *Nationellt vårdprogram prostatacancer 9.0* 2024.

17. Tilki, D., et al., *EAU-EANM-ESTRO-ESUR-ISUP-SIOG Guidelines on Prostate Cancer. Part II-2024 Update: Treatment of Relapsing and Metastatic Prostate Cancer.* European Urology, 2024. **86**(2): p. 164-182.

18. Hugosson, J., et al., *A 16-yr Follow-up of the European Randomized study of Screening for Prostate Cancer.* Eur Urol, 2019. **76**(1): p. 43-51.

19. Ilic, D., et al., *Prostate cancer screening with prostate-specific antigen (PSA) test: a systematic review and meta-analysis.* BMJ, 2018. **362**: p. k3519.

20. Socialstyrelsen, *Screening för prostatacancer – Rekommendation och bedömningsunderlag.* 2018.

21. Regionala Cancercentrum., *Organiserad prostatacancertestning.* 2024.

22. ACR – ESUR – AdMeTech, *PI-RADS version 2.1.* 2019.

23. Drost, F.H., et al., *Prostate MRI, with or without MRI-targeted biopsy, and systematic biopsy for detecting prostate cancer.* Cochrane Database Syst Rev, 2019. 4(4): p. CD012663.

24. Schoots, I.G. and A.R. Padhani, *Risk-adapted biopsy decision based on prostate magnetic resonance imaging and prostate-specific antigen density for enhanced biopsy avoidance in first prostate cancer diagnostic evaluation.* BJU Int, 2021. **127**(2): p. 175-178.

25. Gleason, D.F., *Classification of prostatic carcinomas.* Cancer Chemother Rep, 1966. **50**(3): p. 125-8.

26. van Leenders, G., et al., *The 2019 International Society of Urological Pathology (ISUP) Consensus Conference on Grading of Prostatic Carcinoma.* Am J Surg Pathol, 2020. **44**(8): p. e87-e99.

27. Epstein, J.I., et al., *The 2014 International Society of Urological Pathology (ISUP) Consensus Conference on Gleason Grading of Prostatic Carcinoma: Definition of Grading Patterns and Proposal for a New Grading System.* Am J Surg Pathol, 2016. **40**(2): p. 244-52.

28. D'Amico, A.V., et al., *Biochemical outcome after radical prostatectomy, external beam radiation therapy, or interstitial radiation therapy for clinically localized prostate cancer.* JAMA, 1998. **280**(11): p. 969-74.

29. Brierley, J., M.K. Gospodarowicz, and C. Wittekind, *TNM classification of malignant tumours.* Eighth edition. ed. 2017, Chichester, West Sussex, UK ; Hoboken, NJ: John Wiley & Sons, Inc. p.

30. Aluwini, S., et al., *M1a prostate cancer: Results of a Dutch multidisciplinary consensus meeting.* BJUI Compass, 2021. **2**(3): p. 159-168.

31. Oprea-Lager, D.E., et al., *Lymph node classification in E-PSMA reporting guidelines for PSMA-PET.* Eur J Nucl Med Mol Imaging, 2022. **50**(1): p. 10-11.

32. Hamdy, F.C., et al., *Fifteen-Year Outcomes after Monitoring, Surgery, or Radiotherapy for Prostate Cancer.* N Engl J Med, 2023. **388**(17): p. 1547-1558.

33. Ramsay, C., et al., *Systematic review and economic modelling of the relative clinical benefit and cost-effectiveness of laparoscopic surgery and robotic surgery for removal of the prostate in men with localised prostate cancer.* Health Technol Assess, 2012. **16**(41): p. 1-313.

34. Ilic, D., et al., *Laparoscopic and robotic-assisted versus open radical prostatectomy for the treatment of localised prostate cancer.* Cochrane Database Syst Rev, 2017. **9**(9): p. CD009625.

35. Preisser, F., et al., *Effect of Extended Pelvic Lymph Node Dissection on Oncologic Outcomes in Patients with D'Amico Intermediate and High Risk Prostate Cancer Treated with Radical Prostatectomy: A Multi-Institutional Study.* J Urol, 2020. **203**(2): p. 338-343.

36. Andruska, N., et al., *Survival Outcomes in Men with Unfavorable Intermediate-Risk and High-Risk Prostate Cancer Treated with Prostate-Only versus Whole Pelvic Radiation Therapy.* J Urol, 2022. **207**(6): p. 1227-1235.

37. Murthy, V., et al., *Prostate-Only Versus Whole-Pelvic Radiation Therapy in High-Risk and Very High-Risk Prostate Cancer (POP-RT): Outcomes From Phase III Randomized Controlled Trial.* J Clin Oncol, 2021. **39**(11): p. 1234-1242.

38. van der Veldt, A.A., E.F. Smit, and A.A. Lammertsma, *Positron Emission Tomography as a Method for Measuring Drug Delivery to Tumors in vivo: The Example of [(11)C]docetaxel.* Front Oncol, 2013. **3**: p. 208.

39. Jones, T. and D. Townsend, *History and future technical innovation in positron emission tomography.* J Med Imaging (Bellingham), 2017. **4**(1): p. 011013.

40. Ghosh, A. and W.D. Heston, *Tumor target prostate specific membrane antigen (PSMA) and its regulation in prostate cancer.* J Cell Biochem, 2004. **91**(3): p. 528-39.

41. Jadvar, H., *Is There Use for FDG-PET in Prostate Cancer?* Semin Nucl Med, 2016. **46**(6): p. 502-506.

42. Afshar-Oromieh, A., et al., *[68Ga]Gallium-labelled PSMA ligand as superior PET tracer for the diagnosis of prostate cancer: comparison with 18F-FECH.* Eur J Nucl Med Mol Imaging, 2012. **39**(6): p. 1085-6.

43. Afshar-Oromieh, A., et al., *The Theranostic PSMA Ligand PSMA-617 in the Diagnosis of Prostate Cancer by PET/CT: Biodistribution in Humans, Radiation Dosimetry, and First Evaluation of Tumor Lesions.* J Nucl Med, 2015. **56**(11): p. 1697-705.

44. Kwekkeboom, D.J., et al., *Radiolabeled somatostatin analog [177Lu-DOTA0,Tyr3]octreotate in patients with endocrine gastroenteropancreatic tumors.* J Clin Oncol, 2005. **23**(12): p. 2754-62.

45. Niaz, M.J., et al., *Review of commonly used prostate specific PET tracers used in prostate cancer imaging in current clinical practice.* Clin Imaging, 2021. **79**: p. 278-288.

46. Fendler, W.P., et al., *PSMA PET/CT: joint EANM procedure guideline/SNMMI procedure standard for prostate cancer imaging 2.0.* Eur J Nucl Med Mol Imaging, 2023. **50**(5): p. 1466-1486.

47. Hope, T.A. and H. Jadvar, *PSMA PET AUC Updates: Inclusion of rh-PSMA-7.3.* J Nucl Med, 2024. **65**(4): p. 540.

48. Huang, S., et al., *Comparison of (18)F-based PSMA radiotracers with [(68)Ga]Ga-PSMA-11 in PET/CT imaging of prostate cancer-a systematic*

49. Eiber, M., et al., *Evaluation of Hybrid (6)(8)Ga-PSMA Ligand PET/CT in 248 Patients with Biochemical Recurrence After Radical Prostatectomy.* J Nucl Med, 2015. **56**(5): p. 668-74.

50. Afshar-Oromieh, A., et al., *The diagnostic value of PET/CT imaging with the (68)Ga-labelled PSMA ligand HBED-CC in the diagnosis of recurrent prostate cancer.* Eur J Nucl Med Mol Imaging, 2015. **42**(2): p. 197-209.

51. Fendler, W.P., et al., *Assessment of 68Ga-PSMA-11 PET Accuracy in Localizing Recurrent Prostate Cancer: A Prospective Single-Arm Clinical Trial.* JAMA Oncol, 2019. **5**(6): p. 856-863.

52. Morris, M.J., et al., *Diagnostic Performance of (18)F-DCFPyL-PET/CT in Men with Biochemically Recurrent Prostate Cancer: Results from the CONDOR Phase III, Multicenter Study.* Clin Cancer Res, 2021. **27**(13): p. 3674-3682.

53. Olivier, P., et al., *Phase III Study of (18)F-PSMA-1007 Versus (18)F-Fluorocholine PET/CT for Localization of Prostate Cancer Biochemical Recurrence: A Prospective, Randomized, Crossover Multicenter Study.* J Nucl Med, 2023. **64**(4): p. 579-585.

54. Jani, A.B., et al., *Diagnostic Performance and Safety of (18)F-rhPSMA-7.3 Positron Emission Tomography in Men With Suspected Prostate Cancer Recurrence: Results From a Phase 3, Prospective, Multicenter Study (SPOTLIGHT).* J Urol, 2023. **210**(2): p. 299-311.

55. Fendler, W.P., et al., *Impact of (68)Ga-PSMA-11 PET on the Management of Recurrent Prostate Cancer in a Prospective Single-Arm Clinical Trial.* J Nucl Med, 2020. **61**(12): p. 1793-1799.

56. Calais, J., et al., *Update from PSMA-SRT Trial NCT03582774: A Randomized Phase 3 Imaging Trial of Prostate-specific Membrane Antigen Positron Emission Tomography for Salvage Radiation Therapy for Prostate Cancer Recurrence Powered for Clinical Outcome.* Eur Urol Focus, 2021. 7(2): p. 238-240.

57. Carlsson, S., *A randomized trial comparing conventional "salvage" radiotherapy and individualized 68Ga-PSMA-11 PET/CT targeted treatment in patients with biochemical recurrence after prostate cancer surgery.20.* 2023.

58. Hofman, M.S., et al., *Prostate-specific membrane antigen PET-CT in patients with high-risk prostate cancer before curative-intent surgery or radiotherapy (proPSMA): a prospective, randomised, multicentre study.* Lancet, 2020. **395**(10231): p. 1208-1216.

59. Hope, T.A., et al., *Diagnostic Accuracy of 68Ga-PSMA-11 PET for Pelvic Nodal Metastasis Detection Prior to Radical Prostatectomy and Pelvic Lymph Node Dissection: A Multicenter Prospective Phase 3 Imaging Trial.* JAMA Oncol, 2021. 7(11): p. 1635-1642.

60. Pienta, K.J., et al., *A Phase 2/3 Prospective Multicenter Study of the Diagnostic Accuracy of Prostate Specific Membrane Antigen PET/CT with (18)F-DCFPyL in Prostate Cancer Patients (OSPREY).* J Urol, 2021. **206**(1): p. 52-61.

61. Surasi, D.S., et al., *Diagnostic Performance and Safety of Positron Emission Tomography with (18)F-rhPSMA-7.3 in Patients with Newly Diagnosed Unfavourable Intermediate- to Very-high-risk Prostate Cancer: Results from a Phase 3, Prospective, Multicentre Study (LIGHTHOUSE).* Eur Urol, 2023. **84**(4): p. 361-370.

62. Calais, J., et al., *Phase 3 multicenter randomized trial of PSMA PET/CT prior to definitive radiation therapy for unfavorable intermediate-risk or high-risk prostate cancer [PSMA dRT]: study protocol.* BMC Cancer, 2021. **21**(1): p. 512.

63. Satapathy, S., et al., *Diagnostic Accuracy of (68)Ga-PSMA PET/CT for Initial Detection in Patients With Suspected Prostate Cancer: A Systematic Review and Meta-Analysis.* AJR Am J Roentgenol, 2021. **216**(3): p. 599-607.

64. Chow, K.M., et al., *Head-to-head Comparison of the Diagnostic Accuracy of Prostate-specific Membrane Antigen Positron Emission Tomography and Conventional Imaging Modalities for Initial Staging of Intermediate- to High-risk Prostate Cancer: A Systematic Review and Meta-analysis.* Eur Urol, 2023. **84**(1): p. 36-48.

65. Abrams-Pompe, R.S., et al., *The Role of Magnetic Resonance Imaging and Positron Emission Tomography/Computed Tomography in the Primary Staging of Newly Diagnosed Prostate Cancer: A Systematic Review of the Literature.* Eur Urol Oncol, 2021. **4**(3): p. 370-395.

66. Emmett, L., et al., *The Additive Diagnostic Value of Prostate-specific Membrane Antigen Positron Emission Tomography Computed Tomography to Multiparametric Magnetic Resonance Imaging Triage in the Diagnosis of Prostate Cancer (PRIMARY): A Prospective Multicentre Study.* Eur Urol, 2021. **80**(6): p. 682-689.

67. Emmett, L., et al., *The PRIMARY Score: Using Intraprostatic (68)Ga-PSMA PET/CT Patterns to Optimize Prostate Cancer Diagnosis.* J Nucl Med, 2022. **63**(11): p. 1644-1650.

68. Emmett, L., et al., *Reproducibility and Accuracy of the PRIMARY Score on PSMA PET and of PI-RADS on Multiparametric MRI for Prostate Cancer Diagnosis Within a Real-World Database.* J Nucl Med, 2024. **65**(1): p. 94-99.

69. Rahbar, K., et al., *German Multicenter Study Investigating 177Lu-PSMA-617 Radioligand Therapy in Advanced Prostate Cancer Patients.* J Nucl Med, 2017. **58**(1): p. 85-90.

70. Hofman, M.S., et al., *[(177)Lu]Lu-PSMA-617 versus cabazitaxel in patients with metastatic castration-resistant prostate cancer (TheraP): a randomised, open-label, phase 2 trial.* Lancet, 2021. **397**(10276): p. 797-804.

71. Sartor, O., M.J. Morris, and B.J. Kraus, *Lutetium-177-PSMA-617 for Prostate Cancer. Reply.* N Engl J Med, 2021. **385**(26): p. 2495-2496.

72. Morris, M.J., et al., *(177)Lu-PSMA-617 versus a change of androgen receptor pathway inhibitor therapy for taxane-naive patients with progressive metastatic castration-resistant prostate cancer (PSMAfore): a phase 3, randomised, controlled trial.* Lancet, 2024. **404**(10459): p. 1227-1239.

73.   Emmett, L., et al., *[(177)Lu]Lu-PSMA-617 plus enzalutamide in patients with metastatic castration-resistant prostate cancer (ENZA-p): an open-label, multicentre, randomised, phase 2 trial.* Lancet Oncol, 2024. **25**(5): p. 563-571.

74.   Azad, A.A., et al., *Sequential [(177)Lu]Lu-PSMA-617 and docetaxel versus docetaxel in patients with metastatic hormone-sensitive prostate cancer (UpFrontPSMA): a multicentre, open-label, randomised, phase 2 study.* Lancet Oncol, 2024. **25**(10): p. 1267-1276.

75.   Tagawa, S.T., et al., *PSMAddition: A phase III trial to compare treatment with ¹⁷⁷Lu-PSMA-617 plus standard of care (SOC) versus SOC alone in patients with metastatic hormone-sensitive prostate cancer.* Annals of Oncology, 2021. **32**: p. S673-S675.

76.   Zanzonico, P., *The MIRD Schema for Radiopharmaceutical Dosimetry: A Review.* J Nucl Med Technol, 2024. **52**(2): p. 74-85.

77.   Bolch, W.E., et al., *MIRD pamphlet No. 21: a generalized schema for radiopharmaceutical dosimetry--standardization of nomenclature.* J Nucl Med, 2009. **50**(3): p. 477-84.

78.   ICRP, *The 2007 Recommendations of the International Commission on Radiological Protection. ICRP publication 103.* Ann ICRP, 2007. **37**(2-4): p. 1-332.

79.   Kim, C.H., et al., *ICRP Publication 145: Adult Mesh-Type Reference Computational Phantoms.* Ann ICRP, 2020. **49**(3): p. 13-201.

80.   Rahbar, K., et al., *Advantage of (18)F-PSMA-1007 over (68)Ga-PSMA-11 PET imaging for differentiation of local recurrence vs. urinary tracer excretion.* Eur J Nucl Med Mol Imaging, 2018. **45**(6): p. 1076-1077.

81.   Rauscher, I., et al., *Matched-Pair Comparison of (68)Ga-PSMA-11 PET/CT and (18)F-PSMA-1007 PET/CT: Frequency of Pitfalls and Detection Efficacy in Biochemical Recurrence After Radical Prostatectomy.* J Nucl Med, 2020. **61**(1): p. 51-57.

82.   Giesel, F.L., et al., *F-18 labelled PSMA-1007: biodistribution, radiation dosimetry and histopathological validation of tumor lesions in prostate cancer patients.* Eur J Nucl Med Mol Imaging, 2017. **44**(4): p. 678-688.

83.   Rahbar, K., et al., *(18)F-PSMA-1007 PET/CT at 60 and 120 minutes in patients with prostate cancer: biodistribution, tumour detection and activity kinetics.* Eur J Nucl Med Mol Imaging, 2018. **45**(8): p. 1329-1334.

84.   Rahbar, K., et al., *Diagnostic performance of (18)F-PSMA-1007 PET/CT in patients with biochemical recurrent prostate cancer.* Eur J Nucl Med Mol Imaging, 2018. **45**(12): p. 2055-2061.

85.   Giesel, F.L., et al., *Detection Efficacy of (18)F-PSMA-1007 PET/CT in 251 Patients with Biochemical Recurrence of Prostate Cancer After Radical Prostatectomy.* J Nucl Med, 2019. **60**(3): p. 362-368.

86.   Kuten, J., et al., *Head-to-Head Comparison of (68)Ga-PSMA-11 with (18)F-PSMA-1007 PET/CT in Staging Prostate Cancer Using Histopathology and Immunohistochemical Analysis as a Reference Standard.* J Nucl Med, 2020. **61**(4): p. 527-532.

87. Kesch, C., et al., *Intraindividual Comparison of (18)F-PSMA-1007 PET/CT, Multiparametric MRI, and Radical Prostatectomy Specimens in Patients with Primary Prostate Cancer: A Retrospective, Proof-of-Concept Study.* J Nucl Med, 2017. **58**(11): p. 1805-1810.

88. Brauchli, D., et al., *Tumour-capsule interface measured on 18F-DCFPyL PSMA positron emission tomography/CT imaging comparable to multi-parametric MRI in predicting extra-prostatic extension of prostate cancer at initial staging.* J Med Imaging Radiat Oncol, 2020. **64**(6): p. 829-838.

89. Youden, W.J., *Index for rating diagnostic tests.* Cancer, 1950. **3**(1): p. 32-5.

90. Hallgren, K.A., *Computing Inter-Rater Reliability for Observational Data: An Overview and Tutorial.* Tutor Quant Methods Psychol, 2012. **8**(1): p. 23-34.

91. Landis, J.R. and G.G. Koch, *The measurement of observer agreement for categorical data.* Biometrics, 1977. **33**(1): p. 159-74.

92. McHugh, M.L., *Interrater reliability: the kappa statistic.* Biochem Med (Zagreb), 2012. **22**(3): p. 276-82.

93. Afshar-Oromieh, A., et al., *Radiation dosimetry of (68)Ga-PSMA-11 (HBED-CC) and preliminary evaluation of optimal imaging timing.* Eur J Nucl Med Mol Imaging, 2016. **43**(9): p. 1611-20.

94. Pfob, C.H., et al., *Biodistribution and radiation dosimetry of (68)Ga-PSMA HBED CC-a PSMA specific probe for PET imaging of prostate cancer.* Eur J Nucl Med Mol Imaging, 2016. **43**(11): p. 1962-70.

95. Szabo, Z., et al., *Initial Evaluation of [(18)F]DCFPyL for Prostate-Specific Membrane Antigen (PSMA)-Targeted PET Imaging of Prostate Cancer.* Mol Imaging Biol, 2015. **17**(4): p. 565-74.

96. Icrp, *Radiation dose to patients from radiopharmaceuticals. Addendum 3 to ICRP Publication 53. ICRP Publication 106. Approved by the Commission in October 2007.* Ann ICRP, 2008. **38**(1-2): p. 1-197.

97. Hays, M.T., et al., *MIRD dose estimate report no. 19: radiation absorbed dose estimates from (18)F-FDG.* J Nucl Med, 2002. **43**(2): p. 210-4.

98. Mattson, S. and L. Johansson, *Radiation Dose to Patients from Radiopharmaceuticals: A Compendium of Current Information Related to Frequently Used Substances ICRP Publication 128.* Ann ICRP, 2015. **44** (**2S**): p. 1-321.

99. Hermsen, R., et al., *Lymph node staging with fluorine-18 prostate specific membrane antigen 1007-positron emission tomography/computed tomography in newly diagnosed intermediate- to high-risk prostate cancer using histopathological evaluation of extended pelvic node dissection as reference.* Eur J Nucl Med Mol Imaging, 2022. **49**(11): p. 3929-3937.

100. Mookerji, N., et al., *Fluorine-18 Prostate-Specific Membrane Antigen-1007 PET/CT vs Multiparametric MRI for Locoregional Staging of Prostate Cancer.* JAMA Oncol, 2024. **10**(8): p. 1097-1103.

101. Stabile, A., et al., *Can Negative Prostate-specific Membrane Antigen Positron Emission Tomography/Computed Tomography Avoid the Need for Pelvic Lymph Node Dissection in Newly Diagnosed Prostate Cancer Patients? A Systematic*

Review and Meta-analysis with Backup Histology as Reference Standard. Eur Urol Oncol, 2022. **5**(1): p. 1-17.

102. Meijer, D., et al., *External Validation and Addition of Prostate-specific Membrane Antigen Positron Emission Tomography to the Most Frequently Used Nomograms for the Prediction of Pelvic Lymph-node Metastases: an International Multicenter Study.* Eur Urol, 2021. **80**(2): p. 234-242.

103. Vis, A.N., et al., *Development and External Validation of a Novel Nomogram to Predict the Probability of Pelvic Lymph-node Metastases in Prostate Cancer Patients Using Magnetic Resonance Imaging and Molecular Imaging with Prostate-specific Membrane Antigen Positron Emission Tomography.* Eur Urol Oncol, 2023. **6**(6): p. 553-563.

104. Gandaglia, G., et al., *External Validation of Nomograms for the Identification of Pelvic Nodal Dissection Candidates Among Prostate Cancer Patients with Negative Preoperative Prostate-specific Membrane Antigen Positron Emission Tomography.* Eur Urol Oncol, 2025.

105. Gandaglia, G., et al., *Identification of the Optimal Candidates for Nodal Staging with Extended Pelvic Lymph Node Dissection Among Prostate Cancer Patients Who Underwent Preoperative Prostate-specific Membrane Antigen Positron Emission Tomography. External Validation of the Memorial Sloan Kettering Cancer Center and Briganti Nomograms and Development of a Novel Tool.* Eur Urol Oncol, 2023. **6**(6): p. 543-552.

106. Incesu, R.B., et al., *Negative PSMA PET can be used to avoid unnecessary pelvic lymph node dissection in intermediate risk prostate cancer.* Prostate Cancer Prostatic Dis, 2025.

107. Ito, K., et al., *Combining the Tumor Contact Length and Apparent Diffusion Coefficient Better Predicts Extraprostatic Extension of Prostate Cancer with Capsular Abutment: A 3 Tesla MR Imaging Study.* Magn Reson Med Sci, 2022. **21**(3): p. 477-484.

108. Guerra, A., et al., *Early biomarkers of extracapsular extension of prostate cancer using MRI-derived semantic features.* Cancer Imaging, 2022. **22**(1): p. 74.

109. Donswijk, M.L., et al., *The accuracy and intra- and interobserver variability of PSMA PET/CT for the local staging of primary prostate cancer.* Eur J Nucl Med Mol Imaging, 2024. **51**(6): p. 1741-1752.

110. Rizzo, A., et al., *The Homunculus of unspecific bone uptakes associated with PSMA-targeted tracers: a systematic review-based definition.* Eur J Nucl Med Mol Imaging, 2024. **51**(12): p. 3753-3764.

111. Fryback, D.G. and J.R. Thornbury, *The efficacy of diagnostic imaging.* Med Decis Making, 1991. **11**(2): p. 88-94.

112. de Feria Cardet, R.E., et al., *Is Prostate-specific Membrane Antigen Positron Emission Tomography/Computed Tomography Imaging Cost-effective in Prostate Cancer: An Analysis Informed by the proPSMA Trial.* Eur Urol, 2021. **79**(3): p. 413-418.

113. Kunst, N., et al., *Long-Term Outcomes of Prostate-Specific Membrane Antigen-PET Imaging of Recurrent Prostate Cancer.* JAMA Netw Open, 2024. 7(10): p. e2440591.

Paper I

ORIGINAL ARTICLE

Biokinetics and dosimetry of ^{18}F-PSMA-1007 in patients with prostate cancer

Erland Hvittfeldt[1,2,3] | Mimmi Bjöersdorff[1,2,3] | Gustav Brolin[2,3,4] | David Minarik[2,3,4] | Sigrid L. Svegborn[3,4] | Jenny Oddstig[2,3,4] | Elin Trägårdh[1,2,3]

[1]Department of Clinical Physiology and Nuclear Medicine, Skåne University Hospital, Malmö, Sweden

[2]Wallenberg Centre for Molecular Medicine, Lund University, Lund, Sweden

[3]Department of Translational Medicine, Lund University, Lund, Sweden

[4]Department of Radiation Physics, Skåne University Hospital, Malmö and Lund, Sweden

Correspondence
Erland Hvittfeldt, Department of Clinical Physiology and Nuclear Medicine, Carl Bertil Laurells gata 9, 205 02 Malmö, Sweden.
Email: erland.hvittfeldt@med.lu.se

Funding information
The Cancer Research Foundation at the Department of Oncology, Malmö University Hospital; Medical Faculty at Lund University; Swedish Prostate Cancer federation; Knut och Alice Wallenbergs Stiftelse; Region Skåne

Abstract

Purpose: Positron emission tomography-computed tomography (PET-CT) using prostate-specific membrane antigen (PSMA) ligands is a method for imaging prostate cancer. A recent tracer, ^{18}F-PSMA-1007, offers advantages concerning production and biokinetics compared to the standard tracer (^{68}Ga-PSMA-11). Until now, radiation dosimetry data for this ligand was limited to the material of three healthy volunteers. The purpose of this study is to study the biokinetics and dosimetry of ^{18}F-PSMA-1007.

Methods: Twelve patients with prostate cancer were injected with 4 MBq/kg ^{18}F-PSMA-1007. Eight PET-CT scans with concomitant blood sampling were performed up to 330 min after injection. Urine was collected until the following morning. Volumes of interest for radiation-sensitive organs and organs with high uptake of ^{18}F-PSMA-1007 were drawn in the PET images. A biokinetic compartment model was developed using activity data from PET images and blood and urine samples. Time-activity curves and time-integrated activity coefficients for all delineated organs were calculated. The software IDAC-dose 2.1 was used to calculate the absorbed and effective doses.

Results: High concentrations of activity were noted in the liver, kidneys, parts of the small intestine, spleen, salivary glands, and lacrimal glands. The elimination through urine was 8% of injected activity in 20 h. The highest absorbed doses coefficients were in the lacrimal glands, kidneys, salivary glands, liver, and spleen (98–66 μGy/MBq). The effective dose coefficient was 25 μSv/MBq.

Conclusion: The effective dose of ^{18}F-PSMA-1007 is 6.0–8.0 mSv for a typical patient weighing 80 kg injected with 3–4 MBq/kg.

KEYWORDS
biodistribution, dosimetry, prostate cancer, PSMA, PSMA-1007

1 | INTRODUCTION

Prostate cancer is, together with lung cancer, the most common cancer form and the fifth leading cause of cancer death in men worldwide (Sung et al., 2021). Imaging is important for correct primary staging and for the detection of sites of biochemical recurrence. Recently, positron emission tomography (PET) radio-pharmaceuticals have been developed from ligands to the extra-cellular domain of the membrane-bound protein prostate-specific membrane antigen (PSMA), which is overexpressed in prostate cancer cells (Leek et al., 1995). The most commonly used radioligand is ^{68}Ga-PSMA-11 which has been validated against conventional imaging in the primary staging of prostate cancer and in the setting of biochemical recurrence after radical treatment (Fendler et al., 2019; Herlemann et al., 2016; Hofman et al., 2020; Maurer et al., 2016; Perera et al., 2016). Another PSMA ligand, PSMA-1007, offers possible advantages over PSMA-11. It can be labelled with ^{18}F enabling high-quantity production, a more convenient half-life, and potentially higher spatial image resolution compared with [68]Ga. In addition, its low excretion in urine facilitates visualization of pathological uptake in the pelvic region (Giesel et al., 2017). Clinical studies suggest performance similar to or better than ^{68}Ga-PSMA-11 (Giesel et al., 2019; Liu et al., 2020; Sprute et al., 2021; Trägårdh et al., 2021; Watabe et al., 2021).

The biodistribution and radiation dosimetry of ^{18}F-PSMA-1007 has been studied in three healthy volunteers (Giesel et al., 2017). The volunteers underwent multiple ^{18}F-PSMA-1007 PET-computed tomography (CT) scans up to 6 h postinjection, and blood- and urine samples were obtained. The effective dose coefficient was 22 μSv/ MBq, similar to other PSMA-targeting PET tracers. A comprehensive dosimetry study is needed as the tracer is increasingly being used in clinical practice. This study aimed to investigate the whole body distribution and radiation dosimetry of ^{18}F-PSMA-1007.

2 | MATERIALS AND METHODS

2.1 | Patients

Twelve patients referred for clinical ^{18}F-PSMA-1007 PET-CT at Skåne University Hospital in Malmö and Lund, Sweden, were included. They were all >50 years of age and deemed able to undergo repeated PET scans up to 6 h after injection of ^{18}F-PSMA-1007.

This study was conducted following the Helsinki declaration and approved by the Regional Ethical Review Board (#2020-00689). All patients provided written informed consent.

2.2 | ^{18}F-PSMA-1007

^{18}F-PSMA-1007 was produced at Skåne University Hospital, Lund, using precursor, reagents, and hardware kits supplied by ABX

advanced biochemical compounds. All methods followed good manufacturing practices according to the Eudralex vol. 4. The protocol activity was 4.0 MBq/kg ^{18}F-PSMA-1007 through intra-venous bolus injection. The mean administrated activity was 4.0 MBq/kg (range 3.8–4.2 MBq) as measured from the syringe pre-and postinjection.

2.3 | PET-CT system

Two GE Discovery MI PET-CT systems (Discovery MI; GE Healthcare) were used for the examinations. The axial field of view (FOV) of the PET camera is 20 cm. Multi-FOV acquisitions were performed with 24% axial overlap. The PET-CT systems are calibrated quarterly following the protocol recommended by GE Healthcare. The same dose calibrator (Capintec CRC-15R; Capintec Inc.) is used for measuring syringe ^{18}F-activity both for the calibration phantom and for the patient doses. The dose calibrator is cross calibrated to a Fidelis secondary standard dose calibrator (Southern Scientific). The scanner calibration is vali-dated monthly using a homogenous phantom with known activity concentration.

The Q.Clear (Ross, 2014) reconstruction algorithm was used, including time-of-flight, point spread function, and CT-based attenu-ation correction with a 256×256 matrix (pixel size 2.7×2.7 mm^2, slice thickness 2.8 mm). The noise-regularization parameter (β) was set to 800 (Tragardh, Minarik, et al., 2020). PET images were decay corrected to the start of each scan. The PET/CT system has a 128-slice CT. An adaptive statistical iterative reconstruction technique was used for the CT images.

2.4 | PET-CT image acquisition

Eight knee-to-head PET-CT scans were acquired. The first started 3 min after injection, followed by scans at 10, 20, 30, 60, 120, 210, and 330 min postinjection. Patients levelled their arms at their sides except for the 60- and 120-min scans, which were performed hands up to achieve diagnostic quality (imaging at 120 min is our clinical routine, a planned study will compare 60 and 120 min uptake time). The hands were not included in these scans. In 5 out of the total of 96 scans the top of the skull, part of the brain, and, in two cases, the lacrimal glands were accidentally not included. Figure 1 summarizes the PET and CT protocols.

2.5 | Blood and urine sampling

Venous blood samples were drawn before injection (to make sure activity in the blood = 0) of ^{18}F-PSMA-1007 and immediately after each PET scan. The activity concentration in 2-ml whole blood samples was determined using a gamma counter (HIDEX AMG; Hidex Oy).

Protocol Timing	Time (sec) per bed position (10 bed positions)										CT protocol
3 min	15	15	30	30	30	30	30	30	30	30	120 kV/30–160 mA
10 min	15	15	30	30	30	30	30	30	30	30	120 kV/30–160 mA
20 min	15	15	30	30	30	30	30	30	30	30	120 kV/30–160 mA
30 min	15	15	30	30	30	30	30	30	30	30	120 kV/30–160 mA
60 min	60	60	120	120	120	120	120	120	120	120	120 kV/30–160 mA
120 min	120	120	120	120	120	120	120	120	120	120	100 kV/80–480 mA
210 min	60	60	120	120	120	120	120	120	120	120	120 kV/30–160 mA
330 min	90	90	210	210	210	210	210	210	210	210	120 kV/30–160 mA

FIGURE 1 PET and CT protocol for a typical patient. The number of bed positions varied from 9 to 10, and the patient was scanned in a cranial direction. CT, computed tomography; PET, positron emission tomography.

All urine was collected until the morning after ^{18}F-PSMA-1007 administration. While at the clinic patients voided in sampling bottles that were labelled with a collection time. When going home, the patients were equipped with two bottles and instructed to switch bottles at bedtime. Bottles were collected the next morning. An average of 5.5 bottles per patient were collected (range 3–7 bottles) with a mean total collection time of 20 h and 12 min (range 19 h 02 min to 21 h 38 min). The net contents of the bottles were determined by weighing. The activity concentration of a 2-ml sample from each bottle was determined in the abovementioned gamma counter.

All measurements and analyses of blood and urine samples were performed in duplicate to identify inconsistencies. The calibration factor for the gamma counter was determined using an equal amount (2 ml) of the same ^{18}F-PSMA-1007 preparation as administered to the patient and measured in an identical geometry as the blood and urine samples (after the activity had decayed to a level suitable for measurements with the gamma counter, avoiding dead time effects).

2.6 | Image analysis

The Research Consortium for Medical Image Analysis (RECOMIA) platform (www.recomia.org; Trägårdh, Borrelli, et al., 2020) was used for the segmentation of volumes of interest (VOIs) in the eight image series for each patient. In this platform, VOIs are mapped onto the CT data; they are later resampled to match the voxel size of the PET data. The initial segmentation was done by RECOMIA's artificial intelligence with additional segmentation by a biomedical scientist. CT images were used for anatomical guidance. A physician with 5 years' clinical experience in PET/CT controlled all VOIs to ensure proper delineation. Extensive manual adjustment of the CT-based artificial intelligence segmentation was necessary, particularly in mobile organs. VOIs were created for the left adrenal gland, colon (left, right, rectosigmoid), gallbladder, heart, kidneys, lacrimal glands, liver, lungs, gluteal muscle, pancreas, prostate, salivary glands

(parotid, submandibular and sublingual), skeleton, small intestine, spleen, testes, thyroid, urinary bladder, and gastric ventricle. The right adrenal gland could not be delineated due to high activity in the liver, the same activity as the left gland was assumed.

The activity of the delineated organs was calculated by multiplying the mean activity concentration (Bq/ml) in the VOI with the VOI volume (ml). The normalized and decay-corrected activity as a percentage of injected activity (%IA DC) was then calculated:

$$\%IA \quad DC = 100 \cdot \left(\frac{A_{voi}(t)}{A_{inj}} \right) \cdot e^{\lambda t},$$

where A_{inj} is the injected activity at t_0, $A_{voi}(t)$ is the calculated VOI activity at time t, t is the PET scan start time relative to t_0, and $\lambda = \frac{\ln(2)}{T_{1/2}}$ is the decay constant for [18]F ($T_{1/2}$ =109.8 min).

2.7 | Biokinetics

Using MATLAB (MathWorks), a whole-body compartment model was constructed to model the biokinetics of ^{18}F-PSMA-1007. The model input data were the organ activities from PET image measurements (%IA DC), whole-blood activity concentration (%IA/ml DC), and the cumulated activity excreted to urine (%IA DC), all corrected for decay. Decay-correction simplified keeping track of activity over time (activity should add up to 1 when corrected). Also, without decay correction, late measurements would effectively be disregarded in the model due to decay and some other form of scaling to relative units would be necessary. At $t = 0$, all activity was assumed to be evenly distributed in the total blood volume. The start time for the PET scan was used as a time point for the organ activity measurements (neglecting scan duration). For blood, the activity concentration from each blood sample was entered with a time point corresponding to the time of drawing blood. For urine, activity for each collected bottle was entered with a time point corresponding to

bottle collection. Additional urine activity data was entered for each PET scan performed before the first voiding of urine for each patient. For this, the total activity in the VOI of the bladder was assumed to be in the urine. The activity from the gluteal muscle VOI was extrapolated into total muscle activity using mass values from International Commission on Radiological Protection (ICRP) Publication 133 (Bolch et al., 2016). Decay-corrected activity data for "rest-of-body" at the time points for PET imaging was calculated assuming biological elimination by urinary bladder voiding only. This was supported by the calculation of the combined activity in PET images at 5.5 h and activity in urine bottles collected at the clinic, the mean was 101%IA DC (range 96%–105%).

For most organs, a two-tissue compartment model was assumed with a bidirectional flow of activity between blood and the first tissue compartment, and an irreversible uptake from the first to the second tissue compartment. All organs were, thus, indirectly linked through the blood volume. The small and large intestines had additional compartments for content representing bile transfer from the liver and gallbladder to the small intestine and from the small intestine to the colon. Voiding of urine was assumed every 1.9 h (the average voiding interval during the stay at our clinic). This will give a lower dose, mainly to the bladder, than the 3.5-h interval recommended by ICRP Publication 128 (Mattsson et al., 2015) but we considered this value truer for our population. Figure 2 summarizes the compartment model.

The unknown variables of the system were the transfer rate constants between compartments, the total blood volume (for converting blood activity concentration to total blood activity), and blood volume in each organ. The model activity in each organ as a function of time was the sum of the activity contributions from organ blood, tissue, and content compartments. A single global fit of the kinetic model was performed by iteratively solving the differential equations of the system to minimize the sum of squared deviations between measured and calculated data (i.e., one datum for each organ at each time point in each patient). Thus, there was no need to calculate average activity concentrations per patient or per organ. This was particularly useful for urine data where there was a considerable variation in the time points for urine collection, and, therefore, no obvious approach on how to average data. The model, thus, rendered time-activity data for each compartment and values for total and organ blood volumes. For reader replication, a biexponential fitting of the blood curve was derived in Matlab.

Activity in both the urinary and gallbladder walls was assumed to be negligible and not calculated (i.e., they were not assigned tissue compartments). The gallbladder wall was generally not possible to delineate due to concentrated activity in liver and gallbladder content. When visible it contained negligible activity. The urinary bladder wall was not visualized as a separate structure.

An estimation of activity excreted in bile was made using the compartment model. Excretion at specific time points was calculated by adding the activity in the contents of the gallbladder and large and small intestines as determined by the model. This value was assumed to represent total excreted activity in bile.
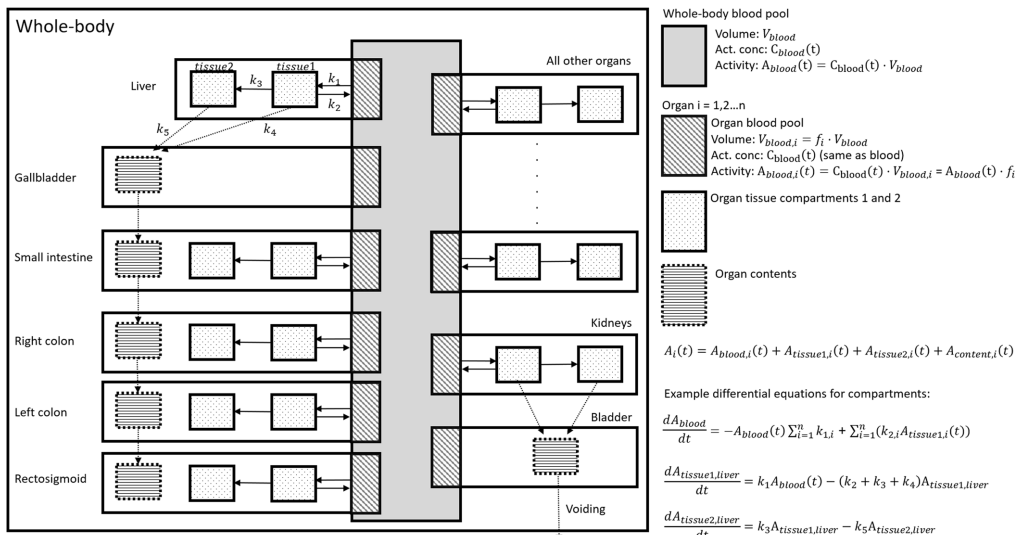
FIGURE 2 A whole-body compartment model for the biokinetics of ^{18}F-PSMA-1007. For activity $A(t)$ in each compartment, a differential equation was specified, exemplified in the figure by the equations for the compartment of the whole-body blood pool and tissue compartments of the liver. The system of equations was then solved iteratively as specified in the text. PSMA, prostate-specific membrane antigen.
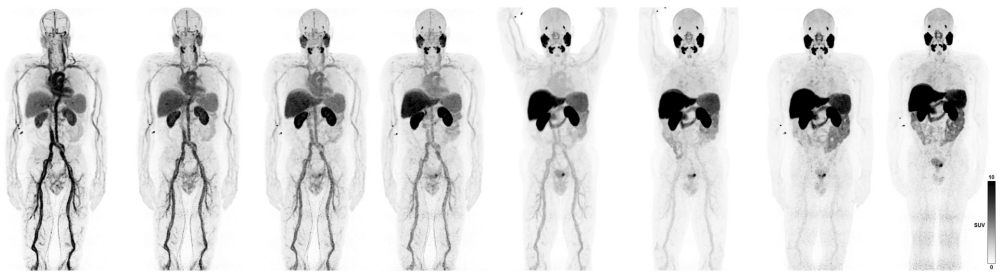
FIGURE 3   Maximum intensity projections of positron emission tomography scans 3, 10, 20, 30, 60, 120, 210, and 330 min post injection.
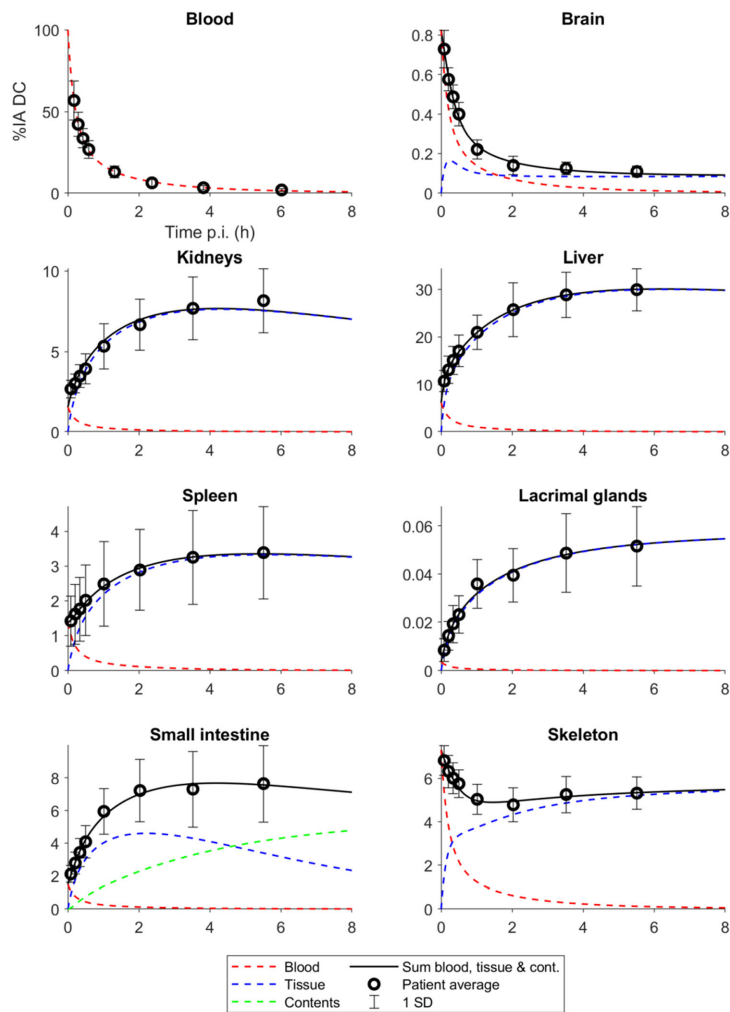

FIGURE 4   Time-activity curves (showing percentage of injected activity, corrected for physical decay) as determined by the compartment model (all segmented organs not displayed). Patient averages are included for comparison.

2.8 | Dosimetry

Time-activity curves (TACs) and time-integrated activity coefficients (TIACs) were derived for each organ using the biokinetic model (separate curves for blood, tissue, and content). The TAC for skeletal tissue was assumed to represent bone marrow. Absorbed doses and effective doses according to ICRP Publication 103 (ICRP, 2007) were calculated using the software IDAC-Dose 2.1 (Andersson et al., 2017). The lacrimal glands are neither included as source organs in ICRP publication 110 nor as contributing to an effective dose in ICRP Publication 103 (ICRP, 2007; Menzel et al., 2009). The absorbed dose was calculated using the IDAC-Dose 2.1 spheres module assuming a volume of 0.7 ml (Bingham et al., 2013).

3 | RESULTS

3.1 | Patients

The indication was a primary staging of biopsy-verified high-risk prostate cancer ($n = 5$ with mean PSA 13 μg/L, range 3.7–27 μg/L) or biochemical recurrence radically treated prostate cancer ($n = 7$ with mean PSA 1.4 μg/L, range 0.16–5.4 μg/L). The mean age was 63 years (range 53–77 years), mean weight 81 kg (range 68–96 kg), and mean body mass index 25 (range 21–30). Visually, all patients had a low tumour burden, limited to the prostate/prostate bed, and at most 1–2 suspected lymph node metastases.

3.2 | Biokinetics

Figure 3 shows the activity distribution in the body, describing serial maximum intensity projection images of one patient. There is a high concentration of activity in the liver, kidneys, parts of the small intestine, spleen, salivary glands, and lacrimal glands. All these organs show an increasing concentration over time with decay-corrected TACs reaching or approaching a plateau at the final imaging session at 5.5 h (Figure 4). Figure 5 shows activity in the blood from 0 to 8 h as determined by the biokinetic model and the biexponential fit ($a(t) = 0.01131e^{-2.559t} + 0.002527e^{-0.3864t}$ where a is %IA DC/ml in blood t hours after injection).

The mean urinary excretion as measured in collected urine was 8.1% 20 h after injection (range 5.2%–10.1%). Excretion determined by the compartment model was 3.1% and 7.8% at 5.5 and 20 h, respectively. The excretion through bile was estimated to be 5.9% and 15.0% at the same time points.

3.3 | Radiation dosimetry

TIACs and blood volume fractions for segmented organs, derived from the biokinetic compartment model, are shown in Table 1.
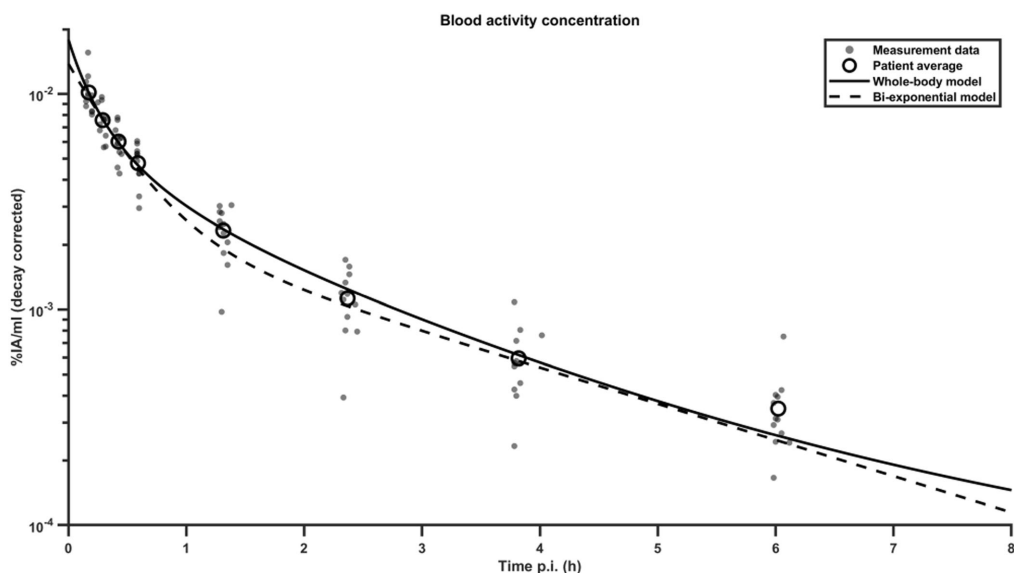

FIGURE 5 Time-activity curve data for blood. The equation for the bi-exponential model is given in the text.

TABLE 1 Time-integrated activity coefficient and blood volume (BV) fractions from the compartment model

Organ	Vascular	Tissue	Content	Total	BV%	BV%[a]
Blood	4.4E−01	[b]	[b]	4.4E−01	5.6 L[c]	5.3 L[c]
Heart	2.4E−02	1.4E−02	[b]	3.8E−02	5.5	10.0
Brain	3.7E−03	2.6E−03	[b]	6.3E−03	0.8	1.2
Lungs	3.3E−02	5.3E−02	[b]	8.6E−02	7.4	10.5
Liver	2.7E−02	5.9E−01	[b]	6.2E−01	6.1	10.0
Kidneys	6.8E−03	1.5E−01	[b]	1.6E−01	1.5	2.0
Spleen	6.1E−03	6.5E−02	[b]	7.1E−02	1.4	1.4
Small intestine	6.6E−03	9.3E−02	6.0E−02	1.6E−01	1.5	3.8
Colon right	2.1E−03	1.1E−02	9.8E−03	2.2E−02	0.5	
Colon left	1.7E−03	6.3E−03	3.7E−03	1.2E−02	0.4	
Colon rectosigmoid	1.3E−03	4.6E−03	4.0E−03	9.9E−03	0.3	2.2
Salivary glands	1.2E−03	4.6E−02	[b]	4.7E−02	0.3	[d]
Lacrimal glands	1.6E−05	9.7E−04	[b]	9.9E−04	<0.01	[d]
Adrenal glands	1.0E−04	3.6E−04	[b]	4.6E−04	0.02	0.1
Prostate	8.3E−04	5.5E−03	[b]	6.4E−03	0.2	[d]
Pancreas	4.9E−04	9.2E−03	[b]	9.7E−03	0.1	6.0
Ventricle	6.7E−04	1.3E−02	[b]	1.4E−02	0.2	1.0
Testis	1.1E−04	1.3E−03	[b]	1.4E−03	0.03	0.04
Thyroid	1.6E−04	4.7E−04	[b]	6.3E−04	0.04	0.1
Skeleton	3.2E−02	1.1E−01	[b]	1.4E−01	7.3	7.0
Skeletal muscle	9.3E−02	3.7E−01	[b]	4.6E−01	21.1	14.0
Gallbladder	0	[b]	9.6E−03	9.6E−03	<0.01	[d]
Urinary bladder	5.5E−04	[b]	1.5E−02	1.5E−02	0.1	0.02
Rest-of-body	2.0E−01	0.5E−01	[b]	7.2E−01	45.5	[d]

Abbreviation: ICRP, International Commission on Radiological Protection.
[a]Values from ICRP Publication 89 (ICRP, 2002).
[b]Not used in model.
[c]Total blood volume in litres.
[d]Not available.

Table 2 shows estimated absorbed and effective dose coefficients. Reported dose coefficients are from calculations made without the prostate as a source organ. When calculations were made with the prostate as a source organ the absorbed dose coefficient to the prostate was 55 μGy/MBq. Other dose coefficients, including effective dose, were unchanged to one decimal point. The highest absorbed dose coefficients are obtained for the lacrimal glands, kidneys, salivary glands, liver, and spleen (98–66 μGy/MBq). The effective dose coefficient determined using the tissue weighting factors of ICRP 103 is 25 μSv/MBq. This translates to 4.5–10 mSv for patients weighing 60–100 kg injected with 3–4 MBq/kg. The full output file from IDAC-Dose 2.1, which includes estimated doses for women, is available from the authors on request.

4 | DISCUSSION

In this paper, we present biokinetic and dosimetry data obtained from 12 patients with prostate cancer who underwent ^{18}F-PSMA-1007 PET-CT. The radiopharmaceutical ^{18}F-PSMA-1007 has the potential of becoming a widely used tracer and it is, therefore, important to confirm preliminary dosimetry results. The effective dose coefficient (25 μSv/MBq) is close to previous findings from three healthy subjects (Giesel et al., 2017) and to the dose coefficient for ^{68}Ga-PSMA of 20 μSv/MBq. While optimal injected activity has not been established for either radiopharmaceutical, published studies generally use a higher injected activity for ^{18}F-PSMA-1007 (3.0–4.0 vs. 1.8–2.2 MBq/kg). The main advantage of ^{18}F-PSMA-1007 is the

TABLE 2 Absorbed and effective dose (ED) coefficients

Organ	This study	Giesel et al. (2017)
Adrenals	37.7	19.4
Brain	3.40	7.20
Breast	10.6	8.06
Gallbladder wall	44.7	22.2
Heart wall	25.6	25.1
Kidneys	84.5	170
Lacrimal glands	97.6	[a]
Left colon	20.6	[a]
Liver	70.4	60.2
Lungs	23.3	11.1
Muscle	7.44	10.0
Pancreas	38.0	19.2
Prostate	9.09	[a]
Recto-sigmoid colon	17.1	[a]
Red marrow	21.6	13.3
Right colon	26.9	[a]
Salivary glands	82.9	[a]
Skin	6.50	7.30
Small intestine	31.8	15.6
Spleen	66.2	73.9
Stomach	29.1	14.2
Testes	9.42	8.37
Thymus	10.0	9.90
Thyroid	11.0	8.50
Urinary bladder wall	11.6	18.7
ED (ICRP 60)	22.0	22.0
ED (ICRP 103)	24.9	[a]

Note: The data are for men only.
Data are in μGy/MBq except for the ED which is in μSv/MBq.
Abbreviation: ICRP, International Commission on Radiological Protection.
[a]Comparison data are not available.

possibility of large-scale production in a cyclotron. Low excretion in urine compared to ^{68}Ga-PSMA is theoretically advantageous but clinical superiority has not been established, possibly due to a higher number of unspecific findings (primarily in bone) (Awenat et al., 2021; Fendler et al., 2017; Ferrari & Treglia, 2021).

When comparing organ absorbed doses between this study and the findings of Giesel et al., the variations are larger (up to a factor of 2, Table 2). The differences cannot be readily explained on a per organ basis, but our study has some advantages: higher number of patients included (12 vs. 3), more organs segmented for dosimetry (19 vs. 7), and our use of updated software for dosimetry calculations

(IDAC-Dose 2.1 vs OLINDA 1.1). IDAC-Dose 2.1 uses more realistic voxel phantoms and more recent data for specific absorbed fractions and tissue weighting factors (Andersson et al., 2017).

Determining the dose for the radiation-sensitive red bone marrow can be difficult. A commonly used method through venous blood sampling assumes that no binding to red bone marrow occurs (Sgouros, 1993). The rising TAC of skeletal tissue (Figure 4) and the concentration of skeletal activity to bone marrow-containing spaces in PET images show that this method is not valid for ^{18}F-PSMA-1007. An alternative method is assuming all skeletal activity is in the bone marrow and extrapolating from parts of the spine (Shen et al., 2002). Having segmented the entire skeleton, we instead assumed the TAC for skeletal tissue to represent bone marrow to avoid extrapolation. We deemed this the most correct method, even if it entails a slight overestimation of the red marrow activity (since a small fraction [≈1%] of the injected activity is free ^{18}F, which accumulates in cortical bone).

We used a whole-body compartment model to derive TACs for organs. Organ TACs can, thus, interact, indirectly through the blood pool and directly through various routes of excretion/transport. The main advantage of this approach is the simultaneous derivation of all TACs, "keeping track" of all injected activity. This contrasts with the method of curve fitting to mean patient TACs where each organ is considered a separate entity. The model also obtains separate blood TACs for each organ. The derived TACs generally display an excellent fit to the mean activity of patients. Some slight deviations from patient data were seen at late time points, for example, in the kidneys (Figure 4). The downwards turn of the TAC, not seen in patient means, is due to the model allowing excretion of activity from the kidneys into the urine. The effect on dosimetry is small, however, due to physical decay. It should be noted that the purpose of the model is to obtain TACs by fitting time-activity data for multiple organs in a coherent system. Except for comparing blood fractions to reference values (Table 1), its physiological accuracy has not been evaluated.

Our estimation of the hepatobiliary excretion of ^{18}F-PSMA-1007 should, therefore, be considered a rough estimate. The data suggest that urine excretion is minor (8% after 20 h as measured in urine) but not negligible compared to that through bile (15% after 20 h according to the model). The latter value is likely an overestimation. The separation of intestinal activity into tissue uptake and content is highly theoretical. The TAC of tissue activity in the small intestine turns downward after 2 h unlike other tissue curves, which generally rise steadily before reaching a plateau (Figure 4). This suggests an overestimation of the activity in the content of the small intestine which was part of the basis for our estimation of bile elimination. Overall elimination is slow, and the biological half-time of PSMA-1007 would far exceed the nuclear half-life of ^{18}F.

The input into the biokinetic model represents activity at a specific time point. The activity is, however, measured during a time interval, between 4 and 4.5 min (depending on patient length) in the early scans and 27–31 min in the late scans. The activity decay during this time interval is corrected but the redistribution of activity is unknown. This introduces a slight uncertainty in the position of the

activity points on the time axis. Late scans have longer scan times but slower redistribution. The integral of the resulting TAC which the absorbed dose depends on should not be significantly affected.

^{18}F-PSMA-1007 PET/CT is used clinically only in prostate cancer which limits our material to this patient group. To perform a dosimetric study on patients with cancer introduces the risk of a "sink effect" with high tumour uptake affecting the biodistribution. Activity in the prostate peaked at 0.25% IA. The extraprostatic disease was not quantified but was limited to at most 1–2 lymph nodes. We believe this precludes any significant sink effect in these patients. The most common indication for ^{18}F-PSMA-1007 PET/CT is biochemical recurrence after prostatectomy (7/12 patients in this study). We, therefore, calculated dose coefficients without using the prostate as a source organ.

Feet and (for two out of eight scans per patient) hands were not included in the scan protocols. In addition, the top of the skull was accidentally not included in a few scans. The expected activity in these regions is low and would not contribute significantly to the absorbed and effective doses.

To summarize, this study presents dosimetry data for the PET radiotracer ^{18}F-PSMA-1007. Previously available data was based on only three subjects. We confirm an acceptable radiation dose for patients using 12 subjects and updated dosimetric models.

CONFLICT OF INTEREST

The authors declare no conflict of interest.

DATA AVAILABILITY STATEMENT

The data that support the findings of this study are available from the corresponding author, Erland Hvittfeldt, upon reasonable request.

ORCID

Erland Hvittfeldt https://orcid.org/0000-0002-9606-2921
Mimmi Bjöersdorff https://orcid.org/0000-0001-8715-507X
Elin Trägårdh https://orcid.org/0000-0002-7116-303X

REFERENCES

Andersson, M., Johansson, L., Eckerman, K. & Mattsson, S. (2017) IDAC-Dose 2.1, an internal dosimetry program for diagnostic nuclear medicine based on the ICRP adult reference voxel phantoms. *EJNMMI Research*, 7, 88.

Awenat, S., Piccardo, A., Carvoeiras, P., Signore, G., Giovanella, L. & Prior, J.O. et al. (2021) Diagnostic role of ^{18}F-PSMA-1007 PET/CT in prostate cancer staging: a systematic review. *Diagnostics*, 11, 552.

Bingham, C.M., Castro, A., Realini, T., Nguyen, J., Hogg, J.P. & Sivak-Callcott, J.A. (2013) Calculated CT volumes of lacrimal glands in normal Caucasian orbits. *Ophthalmic Plastic & Reconstructive Surgery*, 29, 157–159.

Bolch, W.E., Jokisch, D., Zankl, M., Eckerman, K.F., Fell, T., Manger, R. et al. (2016) ICRP Publication 133: the ICRP computational framework for internal dose assessment for reference adults: specific absorbed fractions. *Annals of the ICRP*, 45, 5–73.

Fendler, W.P., Calais, J., Eiber, M., Flavell, R.R., Mishoe, A. & Feng, F.Y. et al. (2019) Assessment of 68Ga-PSMA-11 PET accuracy in localizing recurrent prostate cancer: a prospective single-arm clinical trial. *JAMA Oncology*, 5, 856–863.

Fendler, W.P., Eiber, M., Beheshti, M., Bomanji, J., Ceci, F. & Cho, S. et al. (2017) (68)Ga-PSMA PET/CT: Joint EANM and SNMMI procedure guideline for prostate cancer imaging: version 1.0, *European Journal of Nuclear Medicine and Molecular Imaging*, 44, pp. 1014–1024.

Ferrari, M. & Treglia, G. (2021) ^{18}F-PSMA-1007 PET in biochemical recurrent prostate cancer: an updated meta-analysis. *Contrast Media & Molecular Imaging*, 2021, 3502389.

Giesel, F.L., Hadaschik, B., Cardinale, J., Radtke, J., Vinsensia, M., Lehnert, W. et al. (2017) F-18 labelled PSMA-1007: biodistribution, radiation dosimetry and histopathological validation of tumor lesions in prostate cancer patients. *European Journal of Nuclear Medicine and Molecular Imaging*, 44, 678–688.

Giesel, F.L., Knorr, K., Spohn, F., Will, L., Maurer, T., Flechsig, P. et al. (2019) Detection efficacy of ^{18}F-PSMA-1007 PET/CT in 251 patients with biochemical recurrence of prostate cancer after radical prostatectomy. *Journal of Nuclear Medicine*, 60, 362–368.

Herlemann, A., Wenter, V., Kretschmer, A., Thierfelder, K.M., Bartenstein, P., Faber, C. et al. (2016) ^{68}Ga-PSMA positron emission tomography/computed tomography provides accurate staging of lymph node regions prior to lymph node dissection in patients with prostate cancer. *European Urology*, 70, 553–557.

Hofman, M.S., Lawrentschuk, N., Francis, R.J., Tang, C., Vela, I., Thomas, P. et al. (2020) Prostate-specific membrane antigen PET-CT in patients with high-risk prostate cancer before curative-intent surgery or radiotherapy (proPSMA): a prospective, randomised, multicentre study. *Lancet*, 395, 1208–1216.

ICRP. (2002) Basic anatomical and physiological data for use in radiological protection: reference values. A report of age- and gender-related differences in the anatomical and physiological characteristics of reference individuals. ICRP Publication 89. *Annals of the ICRP*, 32, 5–265.

ICRP. (2007) The 2007 recommendations of the International Commission on Radiological Protection. ICRP Publication 103. *Annals of the ICRP*, 37, 1–332.

Leek, J., Lench, N., Maraj, B., Bailey, A., Carr, I.M., Andersen, S. et al. (1995) Prostate-specific membrane antigen: evidence for the existence of a second related human gene. *British Journal of Cancer*, 72, 583–588.

Liu, A., Zhang, M., Huang, H., Zhang, C., Ruan, X. & Lin, W. et al. (2020) Clinical utility of ^{18}F-PSMA-1007 positron emission tomography/magnetic resonance imaging in prostate cancer: a single-center experience. *Frontiers in Oncology*, 10, 612701.

Mattsson, S., Johansson, L., Leide Svegborn, S., Liniecki, J., Noßke, D., Riklund, K.Å. et al. (2015) Radiation dose to patients from radiopharmaceuticals: a compendium of current information related to frequently used substances. *Annals of the ICRP*, 44, 7–321.

Maurer, T., Gschwend, J.E., Rauscher, I., Souvatzoglou, M., Haller, B., Weirich, G. et al. (2016) Diagnostic efficacy of (68)gallium-PSMA positron emission tomography compared to conventional imaging for lymph node staging of 130 consecutive patients with intermediate to high risk prostate cancer. *Journal of Urology*, 195, 1436–1443.

Menzel, H.G., Clement, C. & DeLuca, P. (2009) ICRP publication 110. realistic reference phantoms: an ICRP/ICRU joint effort. A report of

adult reference computational phantoms. *Annals of the ICRP*, 39, 1–164.

Perera, M., Papa, N., Christidis, D., Wetherell, D., Hofman, M.S., Murphy, D.G. et al. (2016) Sensitivity, specificity, and predictors of positive (68)Ga-prostate-specific membrane antigen positron emission tomography in advanced prostate cancer: a systematic review and meta-analysis. *European Urology*, 70, 926–937.

Ross, S. (2014) *Q.Clear white paper*. Waukesha: GE Healthcare.

Sgouros, G. (1993) Bone marrow dosimetry for radioimmunotherapy: theoretical considerations. *Journal of Nuclear Medicine*, 34, 689–694.

Shen, S., Meredith, R.F., Duan, J., Macey, D.J., Khazaeli, M.B., Robert, F. et al. (2002) Improved prediction of myelotoxicity using a patient-specific imaging dose estimate for non-marrow-targeting (90)Y-antibody therapy. *Journal of Nuclear Medicine*, 43, 1245–1253.

Sprute, K., Kramer, V., Koerber, S.A., Meneses, M., Fernandez, R., Soza-Ried, C. et al. (2021) Diagnostic accuracy of ^{18}F-PSMA-1007 PET/CT imaging for lymph node staging of prostate carcinoma in primary and biochemical recurrence. *Journal of Nuclear Medicine*, 62, 208–213.

Sung, H., Ferlay, J., Siegel, R.L., Laversanne, M., Soerjomataram, I., Jemal, A. et al. (2021) Global cancer statistics 2020: GLOBOCAN estimates of incidence and mortality worldwide for 36 cancers in 185 countries. *CA: A Cancer Journal for Clinicians*, 71, 209–249.

Trägårdh, E., Borrelli, P., Kaboteh, R., Gillberg, T., Ulén, J., Enqvist, O. et al. (2020) RECOMIA—a cloud-based platform for artificial intelligence research in nuclear medicine and radiology. *EJNMMI Physics*, 7, 51.

Trägårdh, E., Minarik, D., Brolin, G., Bitzen, U., Olsson, B. & Oddstig, J. (2020) Optimization of [^{18}F]PSMA-1007 PET-CT using regularized reconstruction in patients with prostate cancer. *EJNMMI Physics*, 7, 31.

Trägårdh, E., Simoulis, A., Bjartell, A. & Jogi, J. (2021) Tumor detection of ^{18}F-PSMA-1007 in the prostate gland in patients with prostate cancer using prostatectomy specimens as reference method. *Journal of Nuclear Medicine*, 62, 1735–1740.

Watabe, T., Uemura, M., Soeda, F., Naka, S., Ujike, T., Hatano, K. et al. (2021) High detection rate in [^{18}F]PSMA-1007 PET: interim results focusing on biochemical recurrence in prostate cancer patients. *Annals of Nuclear Medicine*, 35, 523–528.

Paper II

ORIGINAL ARTICLE

Open Access

PET/CT imaging 2 h after injection of [^{18}F] PSMA-1007 can lead to higher staging of prostate cancer than imaging after 1 h

Erland Hvittfeldt[1,2]* , Ulrika Bitzén[3], David Minarik[1,4], Jenny Oddstig[1,5], Berit Olsson[1,2] and Elin Trägårdh[1,2]

*Correspondence:
erland.hvittfeldt@med.lu.se

[1] Department of Translational
Medicine, Wallenberg Centre
for Molecular Medicine, Lund
University, Carl Bertil Laurells gata
9, 205 02 Malmö, Sweden
[2] Department of Clinical
Physiology and Nuclear
Medicine, Skåne University
Hospital, Malmö, Sweden
[3] Department of Clinical
Physiology and Nuclear
Medicine, Skåne University
Hospital, Lund, Sweden
[4] Department of Medical Physics,
Skåne University Hospital,
Malmö, Sweden
[5] Department of Medical Physics,
Skåne University Hospital, Lund,
Sweden

Abstract

Background: [^{18}F]PSMA-1007 is a prostate specific membrane antigen (PSMA) ligand for positron emission tomography (PET) imaging of prostate cancer. Current guidelines recommend imaging 90–120 min after injection but strong data about optimal timing is lacking. Our aim was to study whether imaging after 1 h and 2 h leads to a different number of detected lesions, with a specific focus on lesions that might lead to a change in treatment.

Methods: 195 patients underwent PET with computed tomography imaging 1 and 2 h after injection of [^{18}F]PSMA-1007. Three readers assessed the status of the prostate or prostate bed and suspected metastases. We analyzed the location and number of found metastases to determine N- and M-stage of patients. We also analyzed standardized uptake values (SUV) in lesions and in normal tissue.

Results: Significantly more pelvic lymph nodes and bone metastases were found and higher N- and M-stages were seen after 2 h. In twelve patients (6.1%) two or three readers agreed on a higher N- or M-stage after 2 h. Conversely, in two patients (1.0%), two readers agreed on a higher stage at 1 h. SUVs in suspected malignant lesions and in normal tissues were higher at 2 h, but lower in the blood pool and urinary bladder.

Conclusions: Imaging at 2 h after injection of [^{18}F]PSMA-1007 leads to more suspected metastases found than after 1 h, with higher staging in some patients and possible effect on patient treatment.

Keywords: [^{18}F]PSMA-1007, Prostate cancer, Uptake time, PET/CT, PSMA

Background

[^{18}F]PSMA-1007 is one of several ^{18}F-labeled prostate specific membrane antigen (PSMA) ligands available as a radiotracer for use in positron emission tomography/computed tomography (PET/CT) imaging of prostate cancer (Czarniecki et al. 2018). One of its advantages is hepatobiliary (rather than urinary) excretion, leading to lower activity in the urinary bladder which may increase visibility of lesions in this area (Giesel et al. 2017). A disadvantage with this compound is a relatively high number of unspecific lesions, especially problematic in bone (Grunig et al. 2021; Rauscher et al. 2020).

Hvittfeldt *et al. European Journal of Hybrid Imaging*   (2023) 7:9

Page 2 of 10

Optimal uptake time of [18F]PSMA-1007 before imaging has not been established. A study of 40 patients comparing 1 and 2 h uptake time reported increased activity in suspected malignant lesions, and lower background activity, but only one additional possible lymph node metastasis at 2 h compared with 1 h (Rahbar et al. 2018). Clinical studies of [18F]PSMA-1007 have generally used an uptake time of 90–120 min, and this interval is recommended in the recently published EANM/SNMMI guideline for prostate cancer imaging (Giesel et al. 2019; Ingvar et al. 2022; Sprute et al. 2021; Fendler et al. 2023). Imaging after 1 h would allow increased production and higher patient comfort compared to a longer interval.

Our primary aim was to study whether imaging after 1 h and 2 h leads to a different number of suspected metastases, with a specific focus on metastases that might lead to a change in treatment.

Methods

Subjects

Data were collected between May 2020 and June 2021. All patients referred to the two nuclear medicine units of Skåne University Hospital (located in Malmö and Lund, respectively) for [18F]PSMA-1007 PET/CT were eligible for inclusion. Unless deemed unsuitable for multiple scans (e.g., because of infirmity), patients were offered participation when the clinical schedule allowed for additional scanning. Our departments mainly accept the indications of biochemical recurrence (BCR) after curative treatment and primary staging (PS) of high-risk prostate cancer (modified D'Amico criteria from Swedish guidelines–stage T3–T4 *or* Gleason score 8–10 or 4+3 in targeted biopsy of PI-RADS 5 or > 50% of systematic biopsies *or* PSA > 20).

Imaging

Subjects were injected with 4.0 MBq/kg of [18F]PSMA-1007. Four GE Discovery MI PET-CT systems (GE Healthcare) were used for the examinations. PET/CT scans were performed 1 and 2 h after injection. Images were acquired from the base of the skull to the mid-thighs with an acquisition time of 120 s per bed position at both scan times. At 1 h a low dose CT (120 kV/30–160 Ma, mean DTP 233 mGy*cm) was performed and at 2 h a diagnostic CT (100 kV/80–480 mA, mean DTP 1710 mGy*cm), with intravenous contrast unless contraindicated. A block-sequential regularization expectation maximization algorithm (Q.Clear; GE Healthcare, Milwaukee, WI, USA) was used for reconstruction of PET data, with the noise-regularization parameter β set to 800 (Tragardh et al. 2020). Time-of-flight, point spread function modelling, and a 256×256 matrix (with a pixel size of 2.7×2.7 mm^2 and a slice thickness of 2.8 mm) were used.

Image review

Images were reviewed blinded and independently by two nuclear medicine specialists (ET and UB) and one nuclear medicine resident (EH) with > 3 years' experience of interpreting PSMA PET/CT scans. The readers judged whether pathologic uptake in the prostate suggestive of cancer was present and if seminal vesicle (SV) involvement was suspected or, alternatively, if local recurrence in the prostate bed was suspected. Readers counted the number of suspected metastases in seven anatomical regions—pelvic lymph

nodes (LNs) below the aortic bifurcation, abdominal LNs, LNs cranial to the diaphragm, inguinal LNs and lesions in bone, liver, or lungs. Suspected metastases in other sites and other findings deemed significant were also noted. A maximum of 5 metastases in any region were counted, to save time and to avoid incorrect reporting due to a high number of metastases.

The readers mainly used their clinical experience and judgement to interpret the images. In general, this meant that low-grade (clearly below spleen) symmetrical uptake in lymph nodes in the inguinal regions, axilla, mediastinum or along the distal external iliac arteries was not considered metastases. To minimize the problem of unspecific uptake in bone, readers were instructed to only classify distinct high-grade (at least above spleen) uptake as metastases, and lower uptake only in the presence of possibly malignant sclerotic lesions on CT.

Patients were then classified as N1, M1a, M1b and M1c (for regional lymph nodes, extra-pelvic lymph nodes, bone metastases and other sites, respectively) positive according to the PROMISE criteria (Eiber et al. 2018).

SUV measurements

A nuclear medicine technologist (BO) placed volumes of interest (VOIs) in the parotid gland, liver, spleen, aorta, and urinary bladder for measurement of SUVmean. SUVmax was measured in lesions which at least one reader judged pathological. For this purpose, EH placed VOIs around the highest uptake in the prostate or prostate bed and a maximum of 2 suspected metastases per anatomical region.

Statistics

Comparisons were made between findings at 1 and 2 h. Binary outcomes (visibility of primary tumor, SV involvement, local recurrence, and N/M-stages) were compared with McNemar's test. SUVs and number of suspected metastases found were compared with the Wilcoxon signed-rank test. To compensate for multiple analyses Bonferroni correction was applied. The significance level was set to $p < 0.005$ both for reader findings (11 comparisons) and SUVs (10 comparisons). Analyses were made with IBM® SPSS® Statistics 28.0.0.0.

Results

Subjects

197 patients were recruited. Two patients were excluded: one due to unsuitable indication (follow-up of ^{177}Lu therapy in widespread metastatic disease) and one due to technical problems with images at 1 h. Thus, a total of 195 patients were included, all with histopathologically verified prostate cancer. Patient data are reported in Table 1.

Image review

We analyzed the difference between findings at 1 and 2 h in 585 separate readings (3 readers and 195 subjects). The main findings are summarized in Table 2. More suspected metastases were found at 2 h as compared to 1 h in all lymph node regions and in bone. In primary staging, pathological uptake in the prostate was more often seen and SV involvement was more often suspected at 2 h. In BCR, local recurrence was more often

Hvittfeldt *et al. European Journal of Hybrid Imaging*   (2023) 7:9

Page 4 of 10

Table 1 Patient data

	All subjects ($n = 195$)					
Age*	70 (53–83)					
Injected dose (MBq/kg)**	4.0 ± 0.2 (2.7–6.0)					
ISUP grade	1	2	3	4	5	?
(*n*)	4	39	46	38	59	9
Scan time after injection (min)**	Scan 1	59.8 ± 1.8 (55–69)		Scan 2	120.2 ± 3.6 (115–142)	
Indication	Primary staging ($n = 128$)			BCR ($n = 67$)		
PSA at scanning (µg/l)*	11 (0.85–579)			4.1 (0.17–62)		
Previous prostatectomy (*n*)	–			56		
Previous external radiation (*n*)	–			8		
Previous brachy-/cryotherapy (*n*)	–			3		
Hormone treatment at scan (*n*)	–			10		

*Median (range) **mean ± SD (range)

Table 2 Findings by individual readers

	Any metastases found		Change in number of found metastases		
	At 1 h	At 2 h	More at 1 h	More at 2 h	p^c
Pelvic LNs *n* (%)	110 (18.8%)	130 (22.2%)	7 (1.2%)	51 (8.7%)	<0.001*
Abdominal LNs	23 (3.9%)	29 (5.0%)	1 (0.2%)	10 (1.7%)	0.008
Supradiafragmal LNs	19 (3.2%)	20 (3.4%)	0	5 (0.9%)	0.039
Inguinal LNs	7 (1.2%)	11 (1.8%)	0	5 (0.9%)	0.039
Bone	66 (11.3%)	84 (14.4%)	10 (1.7%)	30 (5.1%)	0.003*

	Status of prostate/prostate bed				
	At 1 h	At 2 h	Only at 1 h	Only at 2 h	p^d
Primary tumor detected[a]	342 (89.1%)	354 (92.2%)	7 (1.8%)	19 (4.9%)	0.031
SV involvement suspected[a]	67 (17.4%)	83 (21.6%)	4 (1.0%)	20 (5.2%)	0.002*
Local recurrence suspected[b]	48 (23.9%)	56 (27.9%)	1 (0.5%)	9 (4.5%)	0.021

	N- or M-stage				
	At 1 h	At 2 h	Higher at 1 h	Higher at 2 h	p^d
N1 disease	110 (18.8%)	130 (22.2%)	4 (0.7%)	24 (4.1%)	<0.001*
M1a disease	31 (5.3%)	41 (7.0%)	0	10 (1.7%)	0.002*
M1b disease	66 (11.3%)	84 (14.4%)	4 (0.7%)	22 (3.8%)	<0.001*

$n = 585$ (3 readings of 195 patients). *n* indicates number of readings, not number of suspected metastases

[a] Primary staging only ($n = 3 \times 128 = 384$)

[b] BCR only ($n = 3 \times 67 = 201$)

[c] Using Wilcoxon signed rank test to test for difference in number of found metastases at 1 and 2 h

[d] Using McNemar's test to test for difference in status/stage at 1 and 2 h

*$p < 0.005$

suspected at 2 h. N and M stages were higher at 2 h. Statistical significance was seen for pelvic LNs, bone metastases, SV involvement and all N/M-stages (except M1c which was not analyzed, see below). Distribution of number of suspected metastases found at 1 and 2 h for pelvic LNs, abdominal LNs and in bone are shown in Fig. 1.
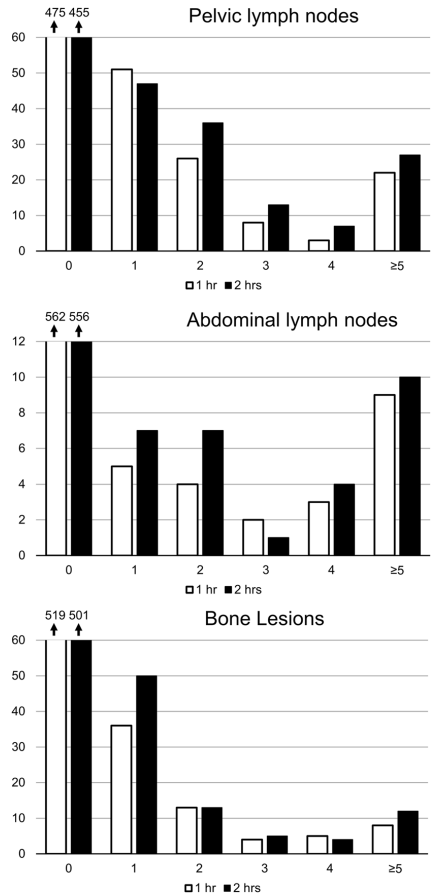
Fig. 1 Distribution of number of found suspected metastases (*x*-axis) at 1 and 2 h in three anatomical regions, in 3 readings of 195 patients ($n = 3 \times 195 = 585$)

M1c disease was uncommon, and no statistics were performed. Suspected lung metastases were found in one patient, with > 5 metastases reported by all readers at both scan times. In one patient, suspected metastases to the abdominal wall was detected by all readers at both time points. In ten patients, uptakes deemed unrelated to prostate cancer were found. These findings are reported in Additional file 1: Table S1. Two of these were focal uptakes in liver, both in the primary staging setting with no other metastases reported, so liver metastases were considered unlikely.

In two cases (1.0% of all cases) all three readers agreed on a higher N- or M-stage at 2 h (Fig. 2), while in ten cases (5.1%) two readers agreed on higher N- or M-stage
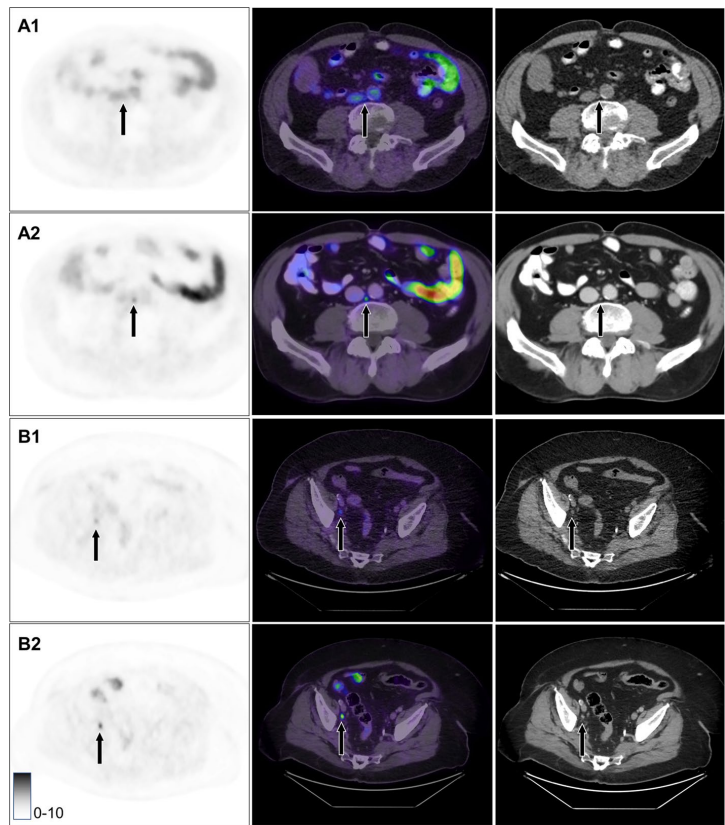
Fig. 2 Suspected metastases which were not found by any reader after 1 h but by all readers after 2 h. **A1** Paraaortic lymph node, imaging at 1 h. **A2** Same lymph node at 2 h. One more paraaortic lymph node was found in the same patient only at 2 h. **B1** Pelvic lymph node at 1 h. **B2** Same lymph node at 2 h

Table 3 Patients where at least two readers agreed on a different assessment at 1 and 2 h

Reader agreement	Higher stage at 1 h		Higher stage at 2 h	
	2 readers	3 readers	2 readers	3 readers
Primary tumor visible*	0	1	4	1
Vesicular involvement*	0	0	3	0
Local recurrence**	0	0	3	0
N1 disease	1	0	7	1
M1a disease	0	0	1	1
M1b disease	1	0	2	0

($n = 195$)

*Primary staging only ($n = 128$). **BCR only ($n = 67$)

at 2 h. Conversely, in two cases (1.0%) two readers agreed on a higher N- or M-stage at 1 h. Cases of agreement between two or three readers are listed in Table 3.

SUV measurements

Measured SUV was higher after 2 h in suspected malignant lesions and in normal tissues with statistical significance except for lesions in the prostate bed. Measured SUV was significantly lower after 2 h in the aorta and the urinary bladder. See Table 4.

Discussion

In this study, we compared PET/CT imaging of 195 prostate cancer patients 1 and 2 h after injection of [18F]PSMA-1007 and compared the number of suspected malignant lesions found and whether this changed the N- and M-stage of the disease. In general, more lesions were found after 2 h, with higher N- and M-stages as a result. There was inter-reader variability (which we did not analyze statistically) but in twelve patients (6.1%) two or three of our readers agreed on a higher N- or M-stage (most often due to additional lymph nodes found), with likely effect on patient treatment.

Our results are in line with the previous study by Rahbar et al., which compared imaging at 1 and 2 h after injection [18F]PSMA-1007 in 40 patients. They reported higher uptake in suspected malignant lesions at 2 h, but only one possible additional lymph node detected (Rahbar et al. 2018). The main advantage of our study is the higher number of patients and reviewers, and the focus on staging. Giesel et al. reported higher uptake in suspected malignant lesions at 3 h compared to 1 h, but no difference in the number of lesions, in 12 patients with BCR (Giesel et al. 2018). Lau et al. reported no difference in the number of found extra-prostatic lesions in 68 patients scanned at a mean 94 and 144 min after injection (Lau et al. 2022). The focus of their study was delineation of lesions, so the results cannot readily be used for determining optimal uptake time.

There are some limitations of this study to address. We did not seek histopathological verification of any of the metastases detected on PET/CT. Several studies with histopathological verification have shown high specificity of PSMA ligands for lymph node metastases, including one from our own center performed with [18F]PSMA-1007 (Ingvar

Table 4 SUV at 1 and 2 h in suspected malignant lesions and normal organs

Suspected malignant lesions	SUVmax at 1 h	SUVmax at 2 h	*p*
Bone (*n* = 177)	5.1 (4.0–8.6)	7.5 (5.6–12.0)	< 0.001*
Prostate (*n* = 118)	13.3 (8.5–23.0)	17.2 (11.2–34.1)	< 0.001*
Prostate bed (*n* = 18)	8.4 (4.6–14.2)	12.3(5.8–17.9)	0.021
Lymph nodes (*n* = 116)	5.7 (3.3–12.9)	9.5 (5.4–20.8)	< 0.001*
Normal organs (*n* = 195)	**SUVmean at 1 h**	**SUVmean at 2 h**	
Aorta	2.1 (1.7–2.4)	1.0 (0.8–1.3)	< 0.001*
Bladder	3.2 (1.7–4.8)	1.2 (0.7–2.1)	< 0.001*
Liver	10.5 (8.8–12.8)	12.9 (10.9–15.3)	< 0.001*
Parotid	3.6 (3.0–4.4)	4.0 (3.2–4.8)	< 0.001*
Spleen	9.6 (7.7–12.0)	11.5 (8.7–14.8)	< 0.001*

SUVs are Median (interquartile range)

*p < 0.005

et al. 2022; Baas et al. 2022; Hope et al. 2021; Pienta et al. 2021). Accuracy of PSMA PET for bone lesions with histopathological verification is less studied and considering the known problem of unspecific bone uptakes with [^{18}F]PSMA-1007, extrapolating from studies with other PSMA ligands could be misleading. It is likely that some number of the increase in suspected bone metastases is due to unspecific bone uptake. Research regarding PSMA PET accuracy for SV involvement is also limited with varied results (Prive et al. 2021; Sonni et al. 2022; Chen et al. 2020). We believe that as the main findings in our study concern lymph nodes (ten of twelve cases where at least two readers agreed on a higher stage were due to additional lymph nodes found), where specificity is high, our conclusions should not be greatly affected by the lack of verification.

We used two different CT protocols—a diagnostic CT at our standard imaging time of 2 h and a low dose CT at 1 h to limit radiation dose to the patient—which leads to two problems. First, blinding is affected as reviewers can deduct the time after injection from the CT images. This increases the risk of bias, but the magnitude and direction of this possible bias is hard to evaluate. Second, the interpretation of the PET scan can be affected by CT findings. For example, the morphology of lymph nodes, the visibility of subtle bone lesions and the delineation of the seminal vesicles could differ with different protocols. Again, the effect is hard to evaluate but is likely small. A diagnostic CT is not considered obligatory in PSMA PET imaging (Fendler et al. 2023).

A possible point of contention is our use of the aortic bifurcation as the classifier for M1a disease, in line with the PROMISE criteria and E-PSMA guidelines but contrary to the 8th edition of the TNM criteria which uses the iliac bifurcation (Fendler et al. 2023; Brierley et al. 2017; Ceci et al. 2021). There is ongoing debate about which is the clinically relevant M1a classifier (Arnfield et al. 2022; Oprea-Lager et al. 2022). In a 2020 Dutch multidisciplinary consensus meeting 39% of panelists chose the iliac bifurcation while 22% chose the aortic bifurcation (Mason et al. 2022). We chose the aortic bifurcation because it is used by our colleagues in the local urology department. Our use of classifier might affect the precise number of reclassified patients but not the fact that more lymph nodes were found at the different time points.

In summary, our data suggests that 2 h uptake time is preferable to 1 h, at least in primary staging and BCR. However, the results are not immediately generalizable to all clinical scenarios—for example we scanned no patients with castration resistant metastatic prostate cancer. There may be other situations when 1 h uptake time is acceptable, for example when it is not important to find additional small lesions (such as follow-up of patients with known high tumor burden).

Conclusions

This study demonstrates that [^{18}F]PSMA-1007 PET scans at different time points after injection lead to a difference in the number of found suspected prostate cancer lesions, with generally more lesions being found after 2 h as compared to 1 h. In some patients this can lead to a change in staging with possible consequences for treatment and patient outcome.

Abbreviations
BCR   Biochemical recurrence

CT	Computed tomography
LN	Lymph node
PET	Position emission tomography
PS	Primary staging
PSMA	Prostate specific membrane antigen
SUV	Standardized uptake value
SV	Seminal vesicles
VOI	Volume of interest

Supplementary Information

The online version contains supplementary material available at https://doi.org/10.1186/s41824-023-00167-4.

> **Additional file 1**. List of patients with reported findings likely unrelated to prostate cancer — site and number of findings.

Declarations

Ethics approval and consent to participate
The study was performed in accordance with the ethical standards as laid down in the 1964 Declaration of Helsinki and its later amendments or comparable ethical standards and approved by the Swedish Ethical Review Authority (#2020-00689). All participants provided written informed consent regarding participation in the study.

Consent for publication
All participants provided written informed consent to publish their anonymized PET/CT images.

Competing interests
The authors have no relevant financial or non-financial interests to disclose.

References
Arnfield EG, Roberts MJ, Pattison DA (2022) Lymph node classification in E-PSMA reporting guidelines for PSMA-PET. Eur J Nucl Med Mol Imaging 50:8–9. https://doi.org/10.1007/s00259-022-05943-1

Baas DJH, Schilham M, Hermsen R, de Baaij JMS, Vrijhof H, Hoekstra RJ et al (2022) Preoperative PSMA-PET/CT as a predictor of biochemical persistence and early recurrence following radical prostatectomy with lymph node dissection. Prostate Cancer Prostatic Dis 25:65–70. https://doi.org/10.1038/s41391-021-00452-y

Brierley J, Gospodarowicz MK, Wittekind C (2017) TNM classification of malignant tumours. Eighth edition. In: West Sussex C (ed) Wiley, Hoboken

Ceci F, Oprea-Lager DE, Emmett L, Adam JA, Bomanji J, Czernin J et al (2021) E-PSMA: the EANM standardized reporting guidelines v1.0 for PSMA-PET. Eur J Nucl Med Mol Imaging 48:1626–1638. https://doi.org/10.1007/s00259-021-05245-y

Chen M, Zhang Q, Zhang C, Zhou YH, Zhao X, Fu Y et al (2020) Comparison of ^{68}Ga-prostate-specific membrane antigen (PSMA) positron emission tomography/computed tomography (PET/CT) and multi-parametric magnetic resonance imaging (MRI) in the evaluation of tumor extension of primary prostate cancer. Transl Androl Urol 9:382–390. https://doi.org/10.21037/tau.2020.03.06

Czarniecki M, Mena E, Lindenberg L, Cacko M, Harmon S, Radtke JP et al (2018) Keeping up with the prostate-specific membrane antigens (PSMAs): an introduction to a new class of positron emission tomography (PET) imaging agents. Transl Androl Urol 7:831–843. https://doi.org/10.21037/tau.2018.08.03

Eiber M, Herrmann K, Calais J, Hadaschik B, Giesel FL, Hartenbach M et al (2018) Prostate cancer molecular imaging standardized evaluation (PROMISE): proposed miTNM classification for the interpretation of PSMA-Ligand PET/CT. J Nucl Med 59:469–478. https://doi.org/10.2967/jnumed.117.198119

Fendler WP, Eiber M, Beheshti M, Bomanji J, Calais J, Ceci F et al (2023) PSMA PET/CT: joint EANM procedure guideline/SNMMI procedure standard for prostate cancer imaging 2.0. Eur J Nucl Med Mol Imaging. https://doi.org/10.1007/s00259-022-06089-w

Giesel FL, Hadaschik B, Cardinale J, Radtke J, Vinsensia M, Lehnert W et al (2017) F-18 labelled PSMA-1007: biodistribution, radiation dosimetry and histopathological validation of tumor lesions in prostate cancer patients. Eur J Nucl Med Mol Imaging 44:678–688. https://doi.org/10.1007/s00259-016-3573-4

Giesel FL, Will L, Kesch C, Freitag M, Kremer C, Merkle J et al (2018) Biochemical recurrence of prostate cancer: initial results with [18F]PSMA-1007 PET/CT. J Nucl Med 59:632–635. https://doi.org/10.2967/jnumed.117.196329

Giesel FL, Knorr K, Spohn F, Will L, Maurer T, Flechsig P et al (2019) Detection efficacy of 18F-PSMA-1007 PET/CT in 251 patients with biochemical recurrence of prostate cancer after radical prostatectomy. J Nucl Med 60:362–368. https://doi.org/10.2967/jnumed.118.212233

Grunig H, Maurer A, Thali Y, Kovacs Z, Strobel K, Burger IA et al (2021) Focal unspecific bone uptake on [18F]-PSMA-1007 PET: a multicenter retrospective evaluation of the distribution, frequency, and quantitative parameters of a potential pitfall in prostate cancer imaging. Eur J Nucl Med Mol Imaging 48:4483–4494. https://doi.org/10.1007/s00259-021-05424-x

Hope TA, Eiber M, Armstrong WR, Juarez R, Murthy V, Lawhn-Heath C et al (2021) Diagnostic accuracy of 68Ga-PSMA-11 PET for pelvic nodal metastasis detection prior to radical prostatectomy and pelvic lymph node dissection: a multicenter prospective phase 3 imaging trial. JAMA Oncol 7:1635–1642. https://doi.org/10.1001/jamaoncol.2021.3771

Ingvar J, Hvittfeldt E, Tragardh E, Simoulis A, Bjartell A (2022) Assessing the accuracy of [18F]PSMA-1007 PET/CT for primary staging of lymph node metastases in intermediate- and high-risk prostate cancer patients. EJNMMI Res 12:48. https://doi.org/10.1186/s13550-022-00918-7

Lau YC, Chen S, Ho CL, Cai J (2022) Reliability of gradient-based segmentation for measuring metabolic parameters influenced by uptake time on 18F-PSMA-1007 PET/CT for prostate cancer. Front Oncol 12:897700. https://doi.org/10.3389/fonc.2022.897700

Mason MD, van der Kwast TH, Mottet N, Oprea-Lager DE, Rouviere O (2022) Modern imaging in prostate cancer: do we treat patients, or their scans? Eur Urol 81:319–322. https://doi.org/10.1016/j.eururo.2022.01.002

Oprea-Lager DE, Ceci F, Eiber M, Fanti S, Herrmann K (2022) Lymph node classification in E-PSMA reporting guidelines for PSMA-PET. Eur J Nucl Med Mol Imaging 50:10–11. https://doi.org/10.1007/s00259-022-06007-0

Pienta KJ, Gorin MA, Rowe SP, Carroll PR, Pouliot F, Probst S et al (2021) A phase 2/3 prospective multicenter study of the diagnostic accuracy of prostate specific membrane antigen PET/CT with 18F-DCFPyL in prostate cancer patients (OSPREY). J Urol 206:52–61. https://doi.org/10.1097/JU.0000000000001698

Prive BM, Israel B, Schilham MGM, Muselaers CHJ, Zamecnik P, Mulders PFA et al (2021) Evaluating F-18-PSMA-1007-PET in primary prostate cancer and comparing it to multi-parametric MRI and histopathology. Prostate Cancer Prostatic Dis 24:423–430. https://doi.org/10.1038/s41391-020-00292-2

Rahbar K, Afshar-Oromieh A, Bogemann M, Wagner S, Schafers M, Stegger L et al (2018) 18F-PSMA-1007 PET/CT at 60 and 120 minutes in patients with prostate cancer: biodistribution, tumour detection and activity kinetics. Eur J Nucl Med Mol Imaging 45:1329–1334. https://doi.org/10.1007/s00259-018-3989-0

Rauscher I, Kronke M, Konig M, Gafita A, Maurer T, Horn T et al (2020) Matched-pair comparison of 68Ga-PSMA-11 PET/CT and 18F-PSMA-1007 PET/CT: frequency of pitfalls and detection efficacy in biochemical recurrence after radical prostatectomy. J Nucl Med 61:51–57. https://doi.org/10.2967/jnumed.119.229187

Sonni I, Felker ER, Lenis AT, Sisk AE, Bahri S, Allen-Auerbach M et al (2022) Head-to-head comparison of 68Ga-PSMA-11 PET/CT and mpMRI with a histopathology gold standard in the detection, intraprostatic localization, and determination of local extension of primary prostate cancer: results from a prospective single-center imaging trial. J Nucl Med 63:847–854. https://doi.org/10.2967/jnumed.121.262398

Sprute K, Kramer V, Koerber SA, Meneses M, Fernandez R, Soza-Ried C et al (2021) Diagnostic accuracy of 18F-PSMA-1007 PET/CT imaging for lymph node staging of prostate carcinoma in primary and biochemical recurrence. J Nucl Med 62:208–213. https://doi.org/10.2967/jnumed.120.246363

Tragardh E, Minarik D, Brolin G, Bitzen U, Olsson B, Oddstig J (2020) Optimization of [18F]PSMA-1007 PET-CT using regularized reconstruction in patients with prostate cancer. EJNMMI Phys 7:31. https://doi.org/10.1186/s40658-020-00298-8

Publisher's Note

Paper III

ORIGINAL RESEARCH

Check for updates

Assessing the accuracy of [^{18}F]PSMA-1007 PET/CT for primary staging of lymph node metastases in intermediate- and high-risk prostate cancer patients

Jacob Ingvar[1,2*] , Erland Hvittfeldt[2,3,4], Elin Trägårdh[2,3,4], Athanasios Simoulis[2,5] and Anders Bjartell[1,2]

Abstract

Background: [^{18}F]PSMA-1007 is a promising tracer for integrated positron emission tomography and computed tomography (PET/CT).

Objective: Our aim was to assess the diagnostic accuracy of [^{18}F]PSMA-1007 PET/CT for primary staging of lymph node metastasis before robotic-assisted laparoscopy (RALP) with extended lymph node dissection (ePLND).

Design, Setting and Participants: The study was a retrospective cohort in a tertiary referral center. Men with prostate cancer that underwent surgical treatment for intermediate- or high-risk prostate cancer between May 2019 and August 2021 were included.

Interventions: [^{18}F]PSMA-1007 PET/CT for initial staging followed by RALP and ePLND.

Outcome measurements and statistical analyses: Sensitivity and specificity were calculated both for the entire cohort and for patients with lymph node metastasis ≥ 3 mm. Positive (PPV) and negative (NPV) predictive values were calculated.

Results and limitations: Among 104 patients included in the analyses, 26 patients had lymph node metastasis based on pathology reporting and metastases were ≥ 3 mm in size in 13 of the cases (50%). In the entire cohort, the sensitivity and specificity of [^{18}F]PSMA-1007 were 26.9% (95% confidence interval (CI); 11.6–47.8) and 96.2% (95% CI; 89.2–99.2), respectively. The sensitivity and specificity of [^{18}F]PSMA-1007 to detect a lymph node metastasis ≥ 3 mm on PET/CT were 53.8% (95% CI; 25.1–80.8) and 96.7% (95% CI; 90.7–99.3), respectively. PPV was 70% and NPV 93.6%.

Conclusions: In primary staging of intermediate- and high-risk prostate cancer, [^{18}F]PSMA-1007 PET/CT is highly specific for prediction of lymph node metastases, but the sensitivity for detection of metastases smaller than 3 mm is limited. Based on our results, [^{18}F]PSMA-1007 PET/CT cannot completely replace ePLND.

Patient summary: This study investigated the use of an imaging method based on a prostate antigen-specific radiopharmaceutical tracer to detect lymph node prostate cancer metastasis. We found that it is unreliable to discover small metastasis.

Keywords: Lymph node dissection, Metastases, PET/CT, Prostate cancer, Robotic surgery, Staging

---

*Correspondence: Jacob.ingvar@skane.se

[2] Department of Translational Medicine, Faculty of Medicine, Lund University, Jan Waldenströmsgata 5, 205 02 Malmö, Sweden
Full list of author information is available at the end of the article

Introduction

Prostate cancer is the most common cancer form in developed countries, and the incidence is increasing [1]. A significant proportion of patients diagnosed with

Ingvar *et al. EJNMMI Research*   (2022) 12:48

Page 2 of 8

localized prostate cancer is successfully managed with radical prostatectomy or radiotherapy. Accurate assessment of tumor stage, regional lymph node involvement and distant metastasis are essential to recommend proper treatment.

Conventional imaging, such as computed tomography (CT), magnetic resonance imaging (MRI), and bone scintigraphy (BS), have shown limited sensitivity to detect prostate cancer metastasis [2, 3]. Molecular imaging, using different radiopharmaceuticals, has shown promising results in visualizing the presence and extent of prostate cancer lesions [4, 5]. Radiolabeled choline positron emission tomography/computed tomography (choline PET/CT) was previously used to identify lymph node metastasis, but studies have shown a poor accuracy [5–7]. Ligands targeting prostate-specific membrane antigen (PSMA) have been introduced in PET/CT for localization of recurrent disease and more recently for primary staging of high-risk tumors. Several tracers have been developed for PSMA PET/CT. Studies have shown promising results with [^{68}Ga]Ga-PSMA-11 for both staging and disease recurrence [4, 8, 9]. In a recent study by Fendler et al. [10], a [^{68}Ga]Ga-PSMA-11 PET/CT scan changed management in more than 50% of cases with biochemical recurrence (BCR). Similar results were shown in another study by Sonni et al. in 2020 [11]. [^{18}F]PSMA-1007 is a radiopharmaceutical which has not been evaluated to the same degree as [^{68}Ga]Ga-PSMA-11. It has the advantage of a longer half-life and offers a low urinary clearance compared to [^{68}Ga]Ga-PSMA-11 PET/CT. However, a previous study by Vollnberg et al. showed that [^{18}F]PSMA-1007 PET/CT scans often present focal unspecific bone uptake, that should be interpreted carefully to avoid over-staging [12].

A head-to-head comparison by Kuten et al. [13] showed that both [^{18}F]PSMA-1007 and [^{68}Ga]Ga-PSMA-11 identified all lesions in the prostate in intermediate- or high-risk prostate cancer patients at staging. Similarly, Hoberück et al. [14] found no difference in staging accuracy between the two tracers.

The aim of this study was to evaluate the accuracy of [^{18}F]PSMA-1007 in lymph node staging in intermediate- and high-risk prostate cancer, using histopathology after extended pelvic lymph node dissection (ePLND) as reference method. We investigated a consecutive, retrospective cohort in a tertiary referral center.

Material and methods
All patients who underwent primary staging of intermediate- or high-risk prostate cancer with [^{18}F]PSMA-1007 PET/CT followed by robotic-assisted laparoscopic prostatectomy (RALP), with extended pelvic lymph node dissection (ePLND) from May 2019 until August 2021, were eligible to be included in the study. The study was approved by the Regional Ethics Committee in Lund (nr 2016/417, 2018/753), and all patients signed an informed consent. Data extracted from medical records included age, date of diagnosis, treatment modality, PSA, Gleason score, results of PSMA PET/CT and details from pathology reports. Patients were classified as intermediate- or high risk based on the EAU guidelines risk groups. Surgery was performed by experienced surgeons at Skåne University Hospital in Malmö using a detailed template. Bilateral ePLND was defined as removal of the tissue from the bifurcation of the common iliac artery and distally along the external iliac vessels, above the internal iliac artery and deep in the obturator fossa. Tissue from the left and right side was sent separately for histopathological examination. ePLND was performed in conjunction with RALP in every case.

PET/CT imaging
Patients were administered 4 MBq/kg [^{18}F]PSMA-1007 (median 4.0, range 3.7–6.7) through intravenous bolus injection. A head-to-knee PET/CT scan was performed using GE Discovery MI PET-CT systems (Discovery MI; GE Healthcare, Milwaukee, WI, USA) 120 min (median 120, range 115–130) after administration of the radiopharmaceutical [15]. No forced diuresis was applied as [^{18}F]PSMA-1007 is mainly eliminated through bile. Acquisition time was 2 min/bed position (3 min when BMI > 40). The PET/CT-system has a 128-slice CT. The Q.Clear reconstruction algorithm was used, including time-of-flight, point spread function and CT-based attenuation correction with a 256×256 matrix (pixel size, 2.7×2.7 mm^2, slice thickness, 2.8 mm [16]. The noise-regularization parameter (β) was set to 800 [17]. An adaptive statistical iterative reconstruction technique was used for the CT images.

PET/CT images were evaluated for lymph node metastases by a nuclear medicine physician with > 5 years' experience of whole-body PET/CT. Evaluation was done blinded and compared with a previous evaluation done for clinical purposes. If there was disagreement between the evaluations or if the clinical evaluation was inconclusive a third evaluation was performed by a nuclear medicine specialist with > 10 years' experience of PET/CT. Lymph nodes were graded 1–5 according to the E-PSMA reader confidence scale [18]. Grade 1–2 lymph nodes were considered non-pathological, while grade 4–5 were considered pathological. Grade 3 includes "faint uptake in a site typical for prostate cancer." We considered lymph node uptake clearly visible (with standardized uptake value threshold 0–10) but clearly below spleen as faint. Grade 3 was considered pathological when deviating from known patterns of unspecific uptake (mainly faint

symmetric uptake along the external iliac vessels or intense uptake in thorax or axilla). Maximum standardized uptake value (SUVmax) calculated by body weight was measured in the prostate.

Histopathology

Lymph node specimens from the left and right side were examined in a blinded fashion by experienced pathologists at Skåne University Hospital using routine methods. According to standard of practice in Sweden, the presence and size of metastases and the total number of lymph nodes extracted from each side were reported in detail.

Statistical analysis

Statistical analysis was performed using STATA (Stata-Corp. 2015. Stata Statistical Software: Release 14. College Station, TX: StataCorp LP). Sensitivity, specificity, positive predictive value (PPV) and negative predictive value (NPV) including 95% confidence intervals (CI) were calculated for [18F]PSMA-1007 PET/CT scan using the histology results after ePLND as gold standard. Two patient-based scenarios were analyzed: firstly, the ability of [18F]PSMA-1007 PET/CT scanning to detect the presence of lymph node metastasis of any size in a patient, and secondly the ability to detect lymph node metastasis ≥ 3 mm in diameter. The size of the metastasis and not the lymph node itself was reported. Considering all lymph nodes obtained at ePLND as separate observations, the ability of [18F]PSMA-1007 PET/CT scan to detect the presence of metastasis of any size in lymph nodes was analyzed (lesion-based analyses). The Mann–Whitney U-test was used for comparison of SUVmax in the prostate. A *p* value less than 0.05 was considered statistically significant.

Results

We evaluated a consecutive series of 106 intermediate- or high-risk prostate cancer patients who were evaluated with [18F]PSMA-1007 PET/CT prior to RALP with ePLND between May 2019 and August 2021. Two patients were excluded since a follow-up [18F]PSMA-1007 PET/CT was positive for lymph nodes on the exact location of the initial [18F]PSMA-1007 PET/CT, suggesting these lymph nodes were not removed during ePLND. After exclusions, 104 patients remained for final analysis. Patient characteristics are summarized in Table 1. In total, 2519 lymph nodes were removed by ePLND and prostate cancer metastases were found by histopathological examination in 41 lymph nodes from 26 patients (Table 2).

Lymph node metastasis was detected pre-operatively by [18F]PSMA-1007 in 7 of these 26 patients resulting

Table 1 Characteristics of patients in final analyses

Patient and tumor characteristics	N (%)
Total number of patients	104
Age (mean, range)	66.0 (42–76)
PSA at diagnosis ng/mL	
Mean	12.6 (2.2–86)
< 10	58 (55)
10–19.9	28 (27)
> 20	19 (18)
Clinical tumor stage	
T1	48 (46)
T2	47 (45)
T3	10 (9)
EAU risk group, *n* (%)	
Low	0 (0)
Intermediate	24 (23)
High	80 (77)
ISUP grade at biopsy	
1	1 (1)
2	11 (10)
3	30 (29)
4	28 (27)
5	35 (33)

in a sensitivity of 26.9% (95% CI; 11.6–47.8) and a specificity of 96.2% (95% CI; 89.2–99.2) (Table 3). PPV and NPV were 70% and 79.8%, respectively (Table 3).

For lymph nodes metastases ≥ 3 mm in diameter, [18F]PSMA-1007 PET/CT detected 7 out of 13 metastases, resulting in a sensitivity and specificity of 53.8% (95% CI; 25.1–80.8) and 96.7% (95% CI; 90.7–99.3), respectively. PPV and NPV for detecting lymph nodes ≥ 3 mm were 70% and 93.6%, respectively (Table 3). The area under curve (AUC) in receiver operating characteristics (ROC) analysis for [18F]PSMA-1007 PET/CT to detect lymph node metastases larger than 3 mm in size was 0.75 (95% CI; 0.61–0.89) compared to 0.62 (95% CI; 0.53–0.71) for metastases of any size.

In high-risk prostate cancers, the sensitivity to detect lymph node metastasis of any size with [18F]PSMA-1007 PET/CT pre-operatively was 35% (95% CI; 15.4–59.2) (Tables 4 and 5). Only one patient had a positive [18F]PSMA-1007 PET/CT in the intermediate risk group. The specificity was high in both groups; 96.7% (95% CI; 88.5–99.6) for high-risk and 94.4% (95% CI; 72.7–99.9) for intermediate prostate cancers. In the high-risk group, PPV and NPV for detecting lymph nodes were 77.8% and 81.7%, respectively, and AUC ROC was 0.66 (95% CI; 0.55–0.77).

Ingvar *et al. EJNMMI Research*   (2022) 12:48

Page 4 of 8

Table 2 Histopathology reported lymph nodes removed at ePLND

Total number of lymph nodes removed from 104 patients	$n = 2519$
Total number of lymph nodes with histologically confirmed metastasis (%)	$n = 41$ (1.6%)
Mean number of lymph nodes removed per patient (range)	24.2(6–48)
Median number of lymph nodes removed	23
Lymph node metastasis ≥ 3 mm that were positive on [^{18}F]PSMA-1007 PET/CT	7
Lymph node metastasis < 3 mm that were positive on [^{18}F]PSMA-1007 PET/CT	0

Table 3 Lymph node status from histopathology report (PAD) and by [^{18}F]PSMA-1007 PET/CT for all patients and if gold standard was lymph node ≥ 3 mm (number of patients)

	PAD positive	PAD negative	Total
All patients			
PSMA PET/CT positive	7	3	10
PSMA PET/CT negative	19	75	94
Total	26	78	104
Lymph nodes ≥ 3 mm			
PSMA PET/CT positive	7	3	10
PSMA PET/CT negative	6	88	94
Total	13	91	104

Table 4 Lymph node status by PSMA and by histology report (PAD) for intermediate and high risk

	PAD positive	PAD negative	Total
Intermediate risk			
PSMA positive	0	1	1
PSMA negative	6	17	23
High risk			
PSMA positive	7	2	9
PSMA negative	13	58	71
Total	26	78	104

Table 5 Sensitivity, specificity, positive predictive value (PPV) and negative predictive value (NPV) for prediction of lymph node metastases by PET/CT (95% confidence interval) with histopathology report as reference method based on risk groups

	Intermediate risk	High risk
Sensitivity	0 (0–45.9)	35 (15.4–59.2)
Specificity	94.4 (72.7–99.9)	96.7 (88.5–99.6)
PPV	0	77.8
NPV	73.9	81.7

Quantification of tracer uptake in lymph nodes and in the prostate

Three lymph nodes were classified as false positives on [^{18}F]PSMA-1007 PET/CT using histopathology as gold standard. They all displayed faint uptake in non-enlarged lymph nodes asymmetrically distributed along the external iliac vessels. All true positives showed moderate (close to or above spleen) or higher uptake on [^{18}F]PSMA-1007 PET/CT along the external iliac vessels or faint or higher uptake along the internal iliac vessels (Fig. 1).

There was no significant difference in SUVmax in the prostate between true positives (median 20.2, range 8.0–53.9, $n = 7$) and false negatives (median 17.0, range 5.2–47.5, $n = 19$), $p = 0.59$.

A sensitivity analysis was performed to investigate if sensitivity and specificity were affected if all grade 3 lymph nodes were either regarded as pathological or non-pathological. Regarding all grade 3 lymph nodes as pathological gave a sensitivity of 31%, specificity of 78% and AUC of 0.55, compared to a sensitivity of 17%, specificity of 100% and AUC of 0.56 when all grade 3 lymph nodes were classified as non-pathological.
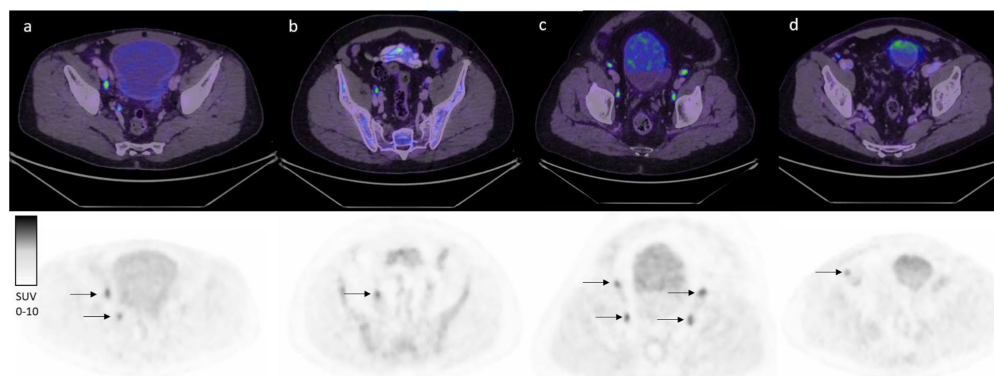
Discussion

In this study of intermediate- and high-risk prostate cancer patients evaluated with [^{18}F]PSMA-1007 PET/CT pre-operatively it was found that the sensitivity for detection of lymph node metastasis of any size was 26.9% and 53.8% for lymph node metastasis > 3 mm in size. However, [^{18}F]PSMA-1007 PET/CT was found to be highly specific, ruling out metastasis in 96.2% of patient with no metastases on histopathological examination.

Correct staging of prostate cancer is essential to select the most appropriate treatment for every patient. Conventional imaging such as CT, MRI, ^{18}F-choline PET/CT and BS has shown poor accuracy in both detecting and ruling out metastases in the lymph nodes [2, 7]. In the EAU guidelines for prostate cancer, lymph node dissection is recommended for staging of prostate cancer in some patients based on risk prediction by nomograms; however, the procedure is associated with significant side effects, and no survival benefit has been demonstrated [19–21].

Ingvar *et al. EJNMMI Research*   (2022) 12:48

Page 5 of 8

a) True positive [18F]PSMA-1007 PET/CT with low grade uptake in two lymph nodes

along the right external and internal iliac vessels. PAD showed one 5 mm metastasis

from the right side (presumably from the internal iliac since the lymph node along

the external vessels measured 12 mm and was PSMA+ in its entirety) and one 1,5

mm from the left (not detected by PET/CT).

b) False positive [18F]PSMA-1007 PET/CT with low grade uptake in one lymph node

along the right external iliac vessels.

c) True negative [18F]PSMA-1007 PET/CT with low grade uptake in several lymph nodes

along the external vessels bilaterally.

d) False negative [18F]PSMA-1007 PET/CT with faint uptake in three lymph nodes along

the external vessels bilaterally (only on shown in image).

Fig. 1 Examples of true and false positives and negatives with [18F]PSMA-1007 PET/CT. **a** True positive [18F]PSMA-1007 PET/CT with low grade uptake in two lymph nodes along the right external and internal iliac vessels. PAD showed one 5 mm metastasis from the right side (presumably from the internal iliac since the lymph node along the external vessels measured 12 mm and was PSMA + in its entirety) and one 1,5 mm from the left (not detected by PET/CT). **b** False positive [18F]PSMA-1007 PET/CT with low grade uptake in one lymph node along the right external iliac vessels. **c** True negative [18F]PSMA-1007 PET/CT with low grade uptake in several lymph nodes along the external vessels bilaterally. **d** False negative [.18F]PSMA-1007 PET/CT with faint uptake in three lymph nodes along the external vessels bilaterally (only on shown in image)

There is a need for improvement in prostate cancer staging, and different tracers used in PET/CT have been shown to provide additive value. [68 Ga]Ga-PSMA-11 has been investigated in several studies with promising results for both staging and recurrence detection [4, 8–10]. In a recent study by Moreira et al. [22], the sensitivity and specificity for lymph node metastases were 75% and 90%, respectively. Due to the longer half-life and lower urinary clearance, presumably causing less artifacts in PET/CT, [18F]PSMA-1007 PET/CT might further improve staging, but the method has not yet been sufficiently investigated. Prior studies evaluating the role of [18F]PSMA-1007 PET/CT in primary staging of prostate cancer have reported on limited patient

cohorts [23, 24]. Giesel et al. [23] found a high sensitivity of 94.7%, and however, their results were based on only eight patients. Similarly, Kesch et al. [24] analyzed ten patients and found a sensitivity and specificity of 71% and 81%, respectively. To the best of our knowledge, only three larger studies on prostate cancer staging using [18F]PSMA-1007 PET/CT have been published. In line with the results of our study, Meijer et al. [25] analyzed 757 patients and found a sensitivity of 38% and a specificity of 94%. However, they used three different tracers, [68Ga]Ga-PSMA-11, 18F-DCFPyL and 1[18F]PSMA-1007, which makes it difficult to compare with our present results. In a study by Hermsen et al. [26], 99 men were evaluated with a sensitivity of 53.3% and a specificity of 89.9% which is in line with our study. In the third study by Sprute et al. [27], the accuracy of [18F]PSMA-1007 PET/CT in lymph node staging was investigated in 96 prostate cancer patients. They found a significantly higher sensitivity of 73.5% and somewhat higher specificity of 99.4% than in our study. The differences between our results and those reported by Sprute et al. can to some extent be explained by patient selection. While our study included only patients that had been staged with [18F]PSMA-1007 PET/CT prior to ePLND performed simultaneously with RALP, Sprute et al. included [18F]PSMA-1007 PET/CT scannings performed both for staging and salvage ePLND. For patients with BCR, another tracer, [18F]-rhPSMA-7, has also been investigated [28–30] showing a high detection efficacy. In a study on 58 patients by Kroenke et al. [31] using this tracer, the sensitivity and specificity for detecting lymph node metastasis prior to salvage surgery were 72.2% and 92.5%, respectively. These results are difficult to compare to the results of our study due to the diverse patient base. On another note, a prior study analyzing pitfalls of PSMA-PET/CT found that PSMA-ligand uptake in benign lesions was considerably higher with [18F]PSMA-1007 compared to [68Ga]Ga-PSMA-11 [32]. Overall, due to the lack of head-to-head studies, it is still unclear if one PSMA-tracer offers significant advantages over the others in prostate cancer staging.

Our subanalysis of the metastasis size showed a significantly higher sensitivity and specificity with a larger metastasis size. This was also seen in Sprute et al. where the detection of nodes more than 3 mm in size the sensitivity and specificity was 85.9% and 99.5%, respectively. It is unclear if Sprute et al. measured the size of the metastasis or the size of the lymph node, which makes the results difficult to compare. Nevertheless, in line with the study by Sprute et al., as well as studies of [68Ga]Ga-PSMA-11, we found that [18F]PSMA-1007 PET/CT has a lower detection rate for small lymph node metastasis [27, 33]. In fact, no metastasis < 3 mm in size was identified on [18F]PSMA-1007 PET/CT in our study.

We attempted to analyze the benefit of [18F]PSMA-1007 PET/CT in different risk categories, according to the EAU risk groups for prostate cancer patients. Due to low numbers in the intermediate group, only one patient had a positive [18F]PSMA-1007 PET/CT, which makes it impossible to draw any conclusion. Regarding the interpretation of [18F]PSMA-1007 PET/CT scans we found that faint tracer uptake along the external iliac vessels is unspecific and should be interpreted cautiously. False negative findings were not associated with lower SUV-max in the prostate compared to true positives. Again, the low number of true positive cases makes our results uncertain.

Our study utilizes PET scanners with silicon photomultiplier technology and the Q.Clear reconstruction algorithm. Both these technologies can improve image quality and potentially lesion detection [34–36]. In prostate cancer, this has, to our knowledge, only been studied in BCR with promising results [37, 38]. It is possible that a lower sensitivity would have been found with conventional PET scanners.

The strengths of this study are the population-based design, the meticulous information collection, and the blinded assessment of [18F]PSMA-1007 PET/CT scans by one nuclear medicine physician. The main limitations are the retrospective design of the study and the limited number of patients.

Conclusion

We found [18F]PSMA-1007 PET/CT to be highly specific for prediction of lymph node metastases in patients with intermediate- or high-risk prostate cancer, but with low sensitivity for detection of metastatic lesions smaller than 3 mm in size. Currently, [18F]PSMA-1007 PET/CT cannot completely replace staging with ePLND in patients with no signs of distant metastases.

Ingvar *et al. EJNMMI Research*   (2022) 12:48

Page 7 of 8

Declarations

Ethics approval and consent to participate
The study was approved by the Regional Ethics. Committee in Lund (nr 2016/417, 2018/753) and all patients signed a written informed consent. All methods were carried out in accordance with the ethical standards as laid down in the 1964 Declaration of Helsinki and its later amendments or comparable ethical standards.

Consent for publication
Written informed consent was obtained from the patient for publication of this case report and accompanying images.

Competing interests
The authors declare that they have no competing interests.

Author details
[1]Department of Urology, Skåne University Hospital, Malmö, Sweden. [2]Department of Translational Medicine, Faculty of Medicine, Lund University, Jan Waldenströmsgata 5, 205 02 Malmö, Sweden. [3]Clinical Physiology and Nuclear Medicine, Skåne University Hospital, Malmö, Sweden. [4]Wallenberg Centre for Molecular Medicine, Lund University, Lund, Sweden. [5]Department of Pathology, Skåne University Hospital and Lund University, Malmö, Sweden.

References

1. Torre LA, Siegel RL, Ward EM, Jemal A. Global cancer incidence and mortality rates and trends–an update. Cancer Epidemiol Biomarkers Prev. 2016;25(1):16–27.
2. Hofman MS, Lawrentschuk N, Francis RJ, Tang C, Vela I, Thomas P, et al. Prostate-specific membrane antigen PET-CT in patients with high-risk prostate cancer before curative-intent surgery or radiotherapy (proPSMA): a prospective, randomised, multicentre study. Lancet. 2020;395(10231):1208–16.
3. Briganti A, Abdollah F, Nini A, Suardi N, Gallina A, Capitanio U, et al. Performance characteristics of computed tomography in detecting lymph node metastases in contemporary patients with prostate cancer treated with extended pelvic lymph node dissection. Eur Urol. 2012;61(6):1132–8.
4. Perera M, Papa N, Roberts M, Williams M, Udovicich C, Vela I, et al. Gallium-68 prostate-specific membrane antigen positron emission tomography in advanced prostate cancer-updated diagnostic utility, sensitivity, specificity, and distribution of prostate-specific membrane antigen-avid lesions: a systematic review and meta-analysis. Eur Urol. 2020;77(4):403–17.
5. Umbehr MH, Muntener M, Hany T, Sulser T, Bachmann LM. The role of 11C-choline and 18F-fluorocholine positron emission tomography (PET) and PET/CT in prostate cancer: a systematic review and meta-analysis. Eur Urol. 2013;64(1):106–17.
6. Kjolhede H, Ahlgren G, Almquist H, Liedberg F, Lyttkens K, Ohlsson T, et al. Combined 18F-fluorocholine and 18F-fluoride positron emission tomography/computed tomography imaging for staging of high-risk prostate cancer. BJU Int. 2012;110(10):1501–6.
7. Puterman C, Bjoersdorff M, Amidi J, Anand A, Soller W, Jiborn T, et al. A retrospective study assessing the accuracy of [18F]-fluorocholine PET/CT for primary staging of lymph node metastases in intermediate and high-risk prostate cancer patients undergoing robotic-assisted laparoscopic prostatectomy with extended lymph node dissection. Scand J Urol. 2021;55(4):293–7.
8. Hope TA, Eiber M, Armstrong WR, Juarez R, Murthy V, Lawhn-Heath C, et al. Diagnostic accuracy of 68Ga-PSMA-11 PET for pelvic nodal metastasis detection prior to radical prostatectomy and pelvic lymph node dissection: a multicenter prospective phase 3 imaging trial. JAMA Oncol. 2021;7(11):1635–42.
9. Esen T, Falay O, Tarim K, Armutlu A, Koseoglu E, Kilic M, et al. (68)Ga-PSMA-11 positron emission tomography/computed tomography for primary lymph node staging before radical prostatectomy: central review of imaging and comparison with histopathology of extended lymphadenectomy. Eur Urol Focus. 2021;7(2):288–93.
10. Fendler WP, Calais J, Eiber M, Flavell RR, Mishoe A, Feng FY, et al. Assessment of 68Ga-PSMA-11 PET accuracy in localizing recurrent prostate cancer: a prospective single-arm clinical trial. JAMA Oncol. 2019;5(6):856–63.
11. Sonni I, Eiber M, Fendler WP, Alano RM, Vangala SS, Kishan AU, et al. Impact of (68)Ga-PSMA-11 PET/CT on staging and management of prostate cancer patients in various clinical settings: a prospective single-center study. J Nucl Med. 2020;61(8):1153–60.
12. Vollnberg B, Alberts I, Genitsch V, Rominger A, Afshar-Oromieh A. Assessment of malignancy and PSMA expression of uncertain bone foci in [(18)F]PSMA-1007 PET/CT for prostate cancer-a single-centre experience of PET-guided biopsies. Eur J Nucl Med Mol Imaging. 2022. https://doi.org/10.1007/s00259-022-05745-5.
13. Kuten J, Fahoum I, Savin Z, Shamni O, Gitstein G, Hershkovitz D, et al. Head-to-head comparison of (68)Ga-PSMA-11 with (18)F-PSMA-1007 PET/CT in staging prostate cancer using histopathology and immunohistochemical analysis as a reference standard. J Nucl Med. 2020;61(4):527–32.
14. Hoberuck S, Lock S, Borkowetz A, Sommer U, Winzer R, Zophel K, et al. Intraindividual comparison of [(68) Ga]-Ga-PSMA-11 and [(18)F]-F-PSMA-1007 in prostate cancer patients: a retrospective single-center analysis. EJNMMI Res. 2021;11(1):109.
15. Rahbar K, Afshar-Oromieh A, Bogemann M, Wagner S, Schafers M, Stegger L, et al. (18)F-PSMA-1007 PET/CT at 60 and 120 minutes in patients with prostate cancer: biodistribution, tumour detection and activity kinetics. Eur J Nucl Med Mol Imaging. 2018;45(8):1329–34.
16. Ross S. Q.Clear White paper. GE Healthcare; 2014.
17. Tragardh E, Minarik D, Brolin G, Bitzen U, Olsson B, Oddstig J. Optimization of [(18)F]PSMA-1007 PET-CT using regularized reconstruction in patients with prostate cancer. EJNMMI Phys. 2020;7(1):31.
18. Ceci F, Oprea-Lager DE, Emmett L, Adam JA, Bomanji J, Czernin J, et al. E-PSMA: the EANM standardized reporting guidelines v.10 for PSMA-PET. Eur J Nucl Med Mol Imaging. 2021;48(5):1626–38.
19. Mottet N, van den Bergh RCN, Briers E, Van den Broeck T, Cumberbatch MG, De Santis M, et al. EAU-EANM-ESTRO-ESUR-SIOG guidelines on prostate cancer-2020 update. Part 1: screening, diagnosis, and local treatment with curative intent. Eur Urol. 2021;79(2):243–62.
20. Briganti A, Larcher A, Abdollah F, Capitanio U, Gallina A, Suardi N, et al. Updated nomogram predicting lymph node invasion in patients with prostate cancer undergoing extended pelvic lymph node dissection: the essential importance of percentage of positive cores. Eur Urol. 2012;61(3):480–7.
21. Preisser F, van den Bergh RCN, Gandaglia G, Ost P, Surcel CI, Sooriakumaran P, et al. Effect of extended pelvic lymph node dissection on oncologic outcomes in patients with d'amico intermediate and high risk prostate cancer treated with radical prostatectomy: a multi-institutional study. J Urol. 2020;203(2):338–43.
22. Moreira LF, Mussi TC, Cunha MLD, Filippi RZ, Baroni RH. Accuracy of (68)Ga-PSMA PET/CT for lymph node and bone primary staging in prostate cancer. Urol Oncol. 2022;40(3):104.e17-104.e21.
23. Giesel FL, Hadaschik B, Cardinale J, Radtke J, Vinsensia M, Lehnert W, et al. F-18 labelled PSMA-1007: biodistribution, radiation dosimetry and histopathological validation of tumor lesions in prostate cancer patients. Eur J Nucl Med Mol Imaging. 2017;44(4):678–88.
24. Kesch C, Vinsensia M, Radtke JP, Schlemmer HP, Heller M, Ellert E, et al. Intraindividual comparison of (18)F-PSMA-1007 PET/CT, multiparametric MRI, and radical prostatectomy specimens in patients with primary prostate cancer: a retrospective. Proof Concept Study J Nucl Med. 2017;58(11):1805–10.
25. Meijer D, van Leeuwen PJ, Roberts MJ, Siriwardana AR, Morton A, Yaxley JW, et al. External validation and addition of prostate-specific membrane antigen positron emission tomography to the most frequently used nomograms for the prediction of pelvic lymph-node metastases: an international multicenter study. Eur Urol. 2021;80(2):234–42.
26. Hermsen R, Wedick EBC, Vinken MJM, van Kalmthout LWM, Kusters-Vandevelde HVN, Wijers CHW, et al. Lymph node staging with fluorine-18 prostate specific membrane antigen 1007-positron emission tomography/computed tomography in newly diagnosed intermediate- to high-risk prostate cancer using histopathological evaluation of extended

Ingvar *et al. EJNMMI Research*   (2022) 12:48

Page 8 of 8

pelvic node dissection as reference. Eur J Nucl Med Mol Imaging. 2022. https://doi.org/10.1007/s00259-022-05827-4.

27. Sprute K, Kramer V, Koerber SA, Meneses M, Fernandez R, Soza-Ried C, et al. Diagnostic accuracy of (18)F-PSMA-1007 PET/CT imaging for lymph node staging of prostate carcinoma in primary and biochemical recurrence. J Nucl Med. 2021;62(2):208–13.

28. Eiber M, Kroenke M, Wurzer A, Ulbrich L, Jooss L, Maurer T, et al. (18)F-rhPSMA-7 PET for the detection of biochemical recurrence of prostate cancer after radical prostatectomy. J Nucl Med. 2020;61(5):696–701.

29. Wurzer A, Di Carlo D, Schmidt A, Beck R, Eiber M, Schwaiger M, et al. Radiohybrid ligands: a novel tracer concept exemplified by (18)F-or (68)Ga-labeled rhPSMA inhibitors. J Nucl Med. 2020;61(5):735–42.

30. Rauscher I, Karimzadeh A, Schiller K, Horn T, D'Alessandria C, Franz C et al. Detection efficacy of (18)F-rhPSMA-7.3 PET/CT and impact on patient management in patients with biochemical recurrence of prostate cancer after radical prostatectomy and prior to potential salvage treatment. J Nucl Med; 2021.

31. Kroenke M, Schweiger L, Horn T, Haller B, Schwamborn K, Wurzer A, et al. Validation of (18)F-rhPSMA-7 and (18)F-rhPSMA-7.3 PET imaging results with histopathology from salvage surgery in patients with biochemical recurrence of prostate cancer. J Nucl Med. 2022. https://doi.org/10.2967/jnumed.121.263707.

32. Rauscher I, Kronke M, Konig M, Gafita A, Maurer T, Horn T, et al. Matched-pair comparison of (68)Ga-PSMA-11 PET/CT and (18)F-PSMA-1007 PET/CT: frequency of pitfalls and detection efficacy in biochemical recurrence after radical prostatectomy. J Nucl Med. 2020;61(1):51–7.

33. Maurer T, Gschwend JE, Rauscher I, Souvatzoglou M, Haller B, Weirich G, et al. Diagnostic efficacy of (68)Gallium-PSMA positron emission tomography compared to conventional imaging for lymph node staging of 130 consecutive patients with intermediate to high risk prostate cancer. J Urol. 2016;195(5):1436–43.

34. Oddstig J, Leide Svegborn S, Almquist H, Bitzen U, Garpered S, Hedeer F, et al. Comparison of conventional and Si-photomultiplier-based PET systems for image quality and diagnostic performance. BMC Med Imaging. 2019;19(1):81.

35. Parvizi N, Franklin JM, McGowan DR, Teoh EJ, Bradley KM, Gleeson FV. Does a novel penalized likelihood reconstruction of 18F-FDG PET-CT improve signal-to-background in colorectal liver metastases? Eur J Radiol. 2015;84(10):1873–8.

36. Wagatsuma K, Miwa K, Sakata M, Oda K, Ono H, Kameyama M, et al. Comparison between new-generation SiPM-based and conventional PMT-based TOF-PET/CT. Phys Med. 2017;42:203–10.

37. Alberts I, Hunermund JN, Sachpekidis C, Mingels C, Fech V, Bohn KP, et al. The influence of digital PET/CT on diagnostic certainty and interrater reliability in [(68)Ga]Ga-PSMA-11 PET/CT for recurrent prostate cancer. Eur Radiol. 2021;31(10):8030–9.

38. Duan H, Baratto L, Hatami N, Liang T, Mari Aparici C, Davidzon GA, et al. (68)Ga-PSMA11 PET/CT for biochemically recurrent prostate cancer: Influence of dual-time and PMT- vs SiPM-based detectors. Transl Oncol. 2022;15(1): 101293.

Publisher's Note

Paper IV

ORIGINAL ARTICLE   **Open Access**

Semi-standardized evaluation of extraprostatic extension and seminal vesicle invasion with [18F]PSMA-1007 PET/CT: a comparison to MRI using histopathology as reference

Erland Hvittfeldt[1,2,3*] , Fredrik Hedeer[1,2], Erik Thimansson[1,4], Kevin Sandeman[5], David Minarik[1,3,6], Jacob Ingvar[1,7], Anders Bjartell[1,7] and Elin Trägårdh[1,2,3]

*Correspondence:
erland.hvittfeldt@med.lu.se

[1] Department of Translational Medicine, Lund University, Lund, Sweden
[2] Department of Clinical Physiology and Nuclear Medicine, Skåne University Hospital, Malmö, Lund, Sweden
[3] Wallenberg Centre of Molecular Medicine, Lund University, Lund, Sweden
[4] Department of Radiology, Helsingborg Hospital, Helsingborg, Sweden
[5] Department of Pathology, Region Skåne, Malmö, Sweden
[6] Department of Urology, Skåne University Hospital, Malmö, Sweden
[7] Radiation Physics, Skåne University Hospital, Malmö, Sweden

Abstract

Background: Positron emission tomography/computed tomography (PET/CT) with prostate specific membrane antigen ligands (PSMA) is established for use in primary staging of prostate cancer to screen for metastases. It has also shown promise in local tumor staging, including detection of extraprostatic extension (EPE) and seminal vesicle invasion (SVI). Previous studies have shown high heterogeneity in methods and results. Our aim was to compare [18F]PSMA-1007 PET/CT to magnetic resonance imaging (MRI) in evaluation of EPE and SVI, building on a previously described method for standardized evaluation. We retrospectively included 124 patients who had undergone MRI, PSMA PET/CT and prostatectomy. PSMA PET/CT images were evaluated by two nuclear medicine physicians. Using a standardized method, they measured length of capsular contact (LCC) and assessed EPE and SVI visually with the use of 5-point Likert scales. A radiologist evaluated MRI images using criteria based on Prostate Imaging–Reporting and Data System version and incorporating LCC measurement and Likert scales. We evaluated diagnostic performance with histopathology as reference, and the interrater reliability of the PET evaluations.

Results: The sensitivity and specificity for detecting EPE with the quantitative LCC method for PSMA PET/CT was 0.46/0.91, for the visual method 0.28/0.82 and for the combination of the two 0.54/0.76. AUC in ROC analysis for the LCC method was 0.70. For MRI the sensitivity and specificity were 0.80/0.64. For SVI, PET/CT and MRI had sensitivity and specificity of 0.14/1.0 and 0.50/0.92 respectively. The intraclass correlation coefficient for the PET LCC measurement was 0.68, the kappa values for the visual Likert scales for PET were 0.53 for EPE and 0.63 for SVI.

Conclusions: In this study, we attempted to standardize quantitative and qualitative PSMA PET/CT evaluation of EPE and SVI and compare the method with MRI. MRI had a higher sensitivity for EPE while PSMA had a higher specificity. For SVI, both methods

had high specificity. The interrater reliability for the PSMA PET/CT evaluations was moderate to substantial.

Keywords: PSMA PET/CT, MRI, Prostate cancer, T staging

Introduction

Prostate cancer (PC) is the second most common form of cancer worldwide (Bray et al. 2024). When classifying (PC), the distinction between organ-confined disease and cancer with an extraprostatic component is an important prognostic factor (Mottet et al. 2021). In the TNM (tumour, node, metastasis) classification this corresponds to T1–T2 and T3–T4 stages, respectively. T3 is subdivided into T3a (extraprostatic extension, EPE) and T3b (seminal vesicle invasion, SVI) while T4 represents tumor invading adjacent structures, such as the rectum or urinary bladder (Buyyounouski et al. 2017). Identifying patients with EPE or SVI influences risk stratification and treatment planning, notably the choice between radical surgery or radiation therapy and the selection of patients suitable for nerve-sparing surgery (Mottet et al. 2021; Eastham et al. 2022).

The role of imaging in T3 staging is unclear. The TNM classification states that clinical T-stage should be based on digital rectal exam only, and this is reflected in both European and American guidelines (Mottet et al. 2021; Buyyounouski et al. 2017; Eastham et al. 2022). However, all three materials acknowledge that magnetic resonance imaging (MRI) evaluated by an experienced radiologist can provide additional information on the extent of local disease. This information may be used in treatment planning, especially in high-risk disease. Prostate-specific membrane antigen positron emission tomography (PSMA/PET) with computed tomography (PET/CT) or MRI (PET/MRI) has become an important modality for imaging of PC, but mainly for N- and M-staging (local lymph nodes and distant metastases) in high-risk disease and in biochemical recurrence after curative treatment. Current guidelines do not recommend it for T-staging (Mottet et al. 2021; Eastham et al. 2022; Lowrance et al. 2023).

Several studies have evaluated T-staging using PSMA PET. A 2020 meta-analysis of 12 studies assessing T-staging with PSMA PET (in combination with CT or MRI) reported a pooled sensitivity and specificity of 0.72/0.87 for EPE and 0.68/0.94 for SVI (Woo et al. 2020). A more recent meta-analysis focusing only on head-to-head studies comparing PSMA PET to MRI (9 studies) found pooled sensitivity and specificity for PSMA PET of 0.59/0.79 for EPE and 0.51/0.93 for SVI, compared to MRI values of 0.66/0.76 for EPE and 0.60/0.96 for SVI (Ma et al. 2024). For all modalities the individual studies showed highly variable performance. This variability was underscored in a 2020 review which emphasized the need for standardized imaging techniques and reporting, particularly for PSMA PET (Abrams-Pompe et al. 2021). While MRI evaluation and reporting have been standardized with PI-RADS, reporting standards for PSMA PET are less detailed, especially for T-staging (Ceci et al. 2021; Turkbey et al. 2019). The measurement of the length of capsular contact as an indirect indication of the risk of T3a has been studied for MRI, showing diagnostic performance comparable to, and interrater reliability surpassing, that of subjective analysis (Rosenkrantz et al. 2016; Kim et al. 2020). Few studies have explored LCC for PSMA PET, but Brauchli et al. introduced a semi-standardized method for measuring LCC, providing a potential framework for further research (Brauchli et al. 2020).

Hvittfeldt *et al. EJNMMI Reports*   (2025) 9:1

Page 3 of 13

Our primary aim in this study was to evaluate the diagnostic performance of [^{18}F] PSMA-1007 PET/CT in T3 staging and compare it to MRI, using histopathology as reference method. In addition to the semi-standardized measurement of LCC from Brauchli et al., we used 5-point Likert scales for visual evaluation of EPE and SVI. We also evaluated the interrater reliability of the PSMA PET/CT evaluations.

Methods

Subjects

We retrospectively included patients with newly diagnosed, biopsy-verified prostate cancer who underwent radical prostatectomy at Skåne University hospital between September 2019 and March 2023, and who had performed both PSMA PET/CT and MRI before surgery. A maximum of 180 days between the first imaging procedure and surgery was accepted. From September 2019 to February 2021 intermediate- and high-risk prostate cancer patients according to D'Amico (PSA ≥ 10 or Gleason score ≥ 7 or clinical T stage ≥ T2b (D'Amico et al. 1998)) were accepted for PSMA PET/CT. From February 2021 to March 2023 only high-risk patients were accepted (PSA ≥ 20 or Gleason score ≥ 8 or clinical T stage ≥ T2c).

Imaging

PSMA PET/CT imaging

Patients were injected with 4.0 MBq/kg of [^{18}F]PSMA-1007 and imaging was performed after 120 min. Head to knee PET scans were performed on one of four GE Discovery MI PET/CT systems (GE Healthcare, Milwaukee, USA) at two nuclear medicine sites (Skåne University hospital, Lund and Malmö, Sweden), all using the same protocol. The acquisition time was 2 min/bed position (3 min for BMI > 40). The Q.-Clear reconstruction algorithm (GE Healthcare, Milwaukee, USA) was used, including time-of-flight, point spread function and CT-based attenuation correction with a 256 × 256 matrix (pixel size 2.7 × 2.7 mm2, slice thickness 2.8 mm). The noise regularization parameter was set to 800. The CT was of diagnostic quality (100 kV/80–480 mA), and intravenous and oral iodine contrast agents were administered unless contraindicated (in two patients). An adaptive statistical iterative reconstruction technique was used to reconstruct the CT images in a 512 × 512 matrix, slice thickness 5 mm. The fused images were viewed with Hermes Hybrid Viewer 6.1.3 (HERMES medical solutions, Stockholm, Sweden).

MRI imaging

MRI scans were performed at eight different radiology sites in the Swedish county Region Skåne. Seven varieties of MRI scanner with field strengths of 1.5 and 3 T were used. Local protocols varied but all included transversal, coronal, and sagittal T2-weighted (T2w) turbo spin-echo images and diffusion weighted transversal images, in compliance with the Prostate Imaging–Reporting and Data System (PI-RADS) version 2 (Weinreb et al. 2016).

Image analysis

All analyses were performed independently and blinded to patient data. The prostate was divided into 12 segments along left/right, ventral/dorsal, and base/mid/apex

lines. In the initial analyses all lesions in contact with the prostate capsule were noted and analyzed as described below. When comparing modalities, lesions were considered matching when they included the same or directly neighboring sections. For SVI only the side was noted. See also supplementary material Fig. 1.

PSMA PET/CT analysis

One nuclear medicine specialist (FH, 15 years' experience with PET, 6 years with PSMA) and one nuclear medicine resident (EH, 6 years' experience with PET, 4 years with PSMA) analyzed the images. For each lesion visually deemed as probable PC the LCC was measured using the method described by Brauchli et al., and with the same color look up table (LUT) (NEMA hot metal blue) (Brauchli et al. 2020). To summarize the method, the upper SUV window level was set to the SUVmax of the lesion in question. In heterogenous lesions where the lesion SUVmax was distant from the prostate capsule, the reviewer measured SUVmax closer to the capsule (Figs. 1 and 2). The length of the capsular contact (LCC) was measured as the longest straight line between two points on the tumor-capsule interface in the axial, sagittal or coronal orientation. In addition to the LCC measurement, the lesion was visually assessed (with the same window levels) for EPE and SVI using 5-point Likert scales (Table 1). For synchronization between raters ten patients not included in the study were jointly analyzed.

A composite PET evaluation was created for all lesions considered probable PC by both readers. The composite LCC was the mean of the readers' measurements. A composite visual evaluation of EPE or SVI was created from the 5-point Likert scale. Likert scores of 1–2 were considered negative, 3 equivocal, and 4–5 positive. When both readers were positive, negative or equivocal this was used as the composite. If one reader was equivocal and the other positive or negative the composite was set to the positive or negative. If one reader was positive and the other negative an agreement was reached through a mutual second look at the images.
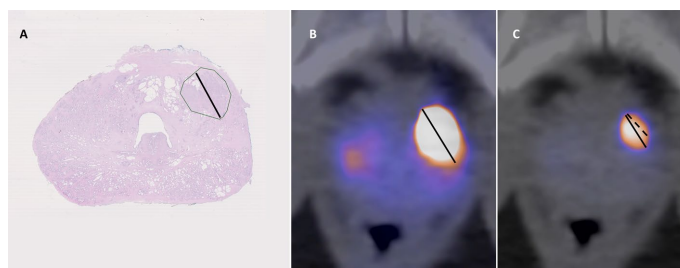
Fig. 1 A Histopathology shows prostate cancer (green outline) with Gleason 4 + 4 = 8 in the left ventral apical peripheral zone, largest diameter 10 mm (black line). No EPE was recorded. **B** PSMA PET/CT shows intense uptake with a SUVmax of 56. The diameter is measured to 17 mm with max window level set to 10. **C** With window level set to 56 the diameter is measured to 11 mm. Both reviewers measured LCC to 10 mm (dashed line)
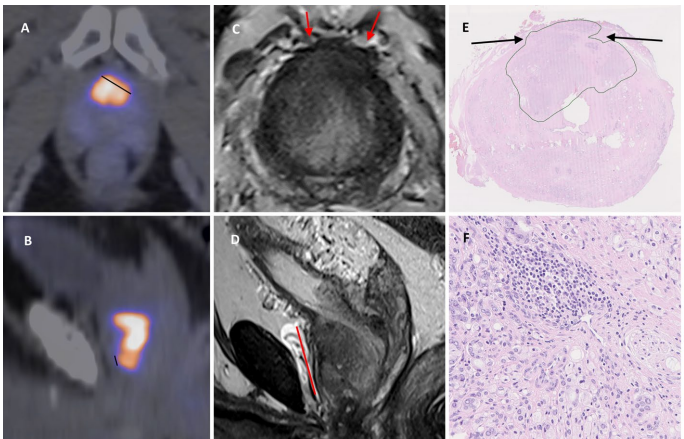
Fig. 2 **A**, **B** PSMA PET/CT shows intense heterogenous uptake ventrally in the prostate. SUVmax was 47.5 but measurements were also made with max window level 39.7 due to heterogeneity. Reviewer 1 measured maximum LCC to 16 mm in the axial plane (**A**, black line), reviewer 2 to 5 mm in the sagittal plane (**B**). Both reviewers set visual Likert to 2. **C**, **D** MRI shows a ventral PI-RADS 5 lesion with indirect signs of EPE (bulging contour; red arrows in axial plane T2W in **C**). LCC 30 mm in sagittal T2w images in **D**. **E**, **F** Histopathology shows a ventral Gleason 4 + 5 lesion (**F**) in the mid prostate (**E**, green outline) with EPE up to 14 mm in length and 1.5 mm in depth (**E**, arrows). EPE extends ventrally in a sagittal direction approximately 20 mm towards the prostate base

Table 1 Instructions for Likert scale for PSMA PET

Likert	EPE	SVI
1. EPE/SVI highly unlikely	No capsular contact	No vesicle contact
2. EPE/SVI unlikely	Capsular contact but no uptake outside the prostate	Vesicle contact but no uptake in the vesicle
3. EPE/SVI possible	Equivocal–capsular contact but no definite suspicion of uptake outside the prostate	Equivocal–vesicle contact but no definite suspicion of uptake in the vesicle
4. Suspected EPE/SVI	Suspicion of pathological uptake outside of the prostate	Suspicion of pathological uptake in the vesicle
5. EPE/SVI highly likely	Strong suspicion of pathological uptake outside of the prostate	Strong suspicion of pathological uptake in the vesicle

MRI analysis

A specialist in radiology (ETh) with 8 years' experience of prostate MRI reviewed the images using Sectra IDS7 PACS (Sectra Medical, Linköping, Sweden). 5 point Likert scales recommended by the Swedish national clinical cancer care guidelines were used for assessing EPE and SVI (Regionala cancercentrum 2024). The EPE Likert scales for MRI incorporate an LCC measurement with a cut-off of 12 mm (Table 2).

Histopathological evaluation

In addition to the routine clinical evaluation of prostatectomy specimens, a second evaluation was performed by a pathology specialist with 10 years' experience of prostate cancer pathology. All slides from the prostatectomy specimens were annotated and

Table 2 Instructions for Likert scales for MRI

Likert	EPE	SVI
1. EPE/SVI highly unlikely	No capsular contact	Not defined
2. EPE/SVI unlikely	Capsular contact < 12 mm, no signs of EPE	Not defined
3. EPE/SVI possible	Capsular contact ≥ 12 mm, no signs of EPE *or* capsular contact < 12 mm with indirect signs*	Tumor has contact with SV entry point in the prostate
4. Suspected EPE/SVI	Capsular contact ≥ 12 mm with indirect signs of EPE	Thickening of lower SV wall with restricted diffusion
5. EPE/SVI highly likely	Measurable radial extraprostatic component	Low signal, restricted diffusion tumor in the SV base

*Bulging prostatic contour, irregular or spiculated margin, thickened or broken capsular line

evaluated using the digital pathology system Sectra Digital Pathology solution (Sectra Medical, Linköping, Sweden). The length, depth, and location of EPE was noted for all T3a lesions. For T3b lesions the side of SVI was noted.

Statistical analysis

Diagnostic performance

We calculated the sensitivity, specificity, accuracy ([TP + TN]/n), positive predictive value (PPV) and negative predictive value (NPV) for MRI and PSMA PET/CT with histopathology as gold standard. For these diagnostic performance indices < 0.70 was considered low, 0.70–0.90 moderate and > 0.90 high. The calculations were made both on a per patient and per lesion level, and excluding patients where no pathological lesions were identified. Calculations were made with equivocal cases (Likert 3) counted as positive and as negative. In addition to the 10 mm LCC cut-off suggested by Brauchli et al. we determined the optimal cut-off in our material by calculating Youden's index (sensitivy + specificity-1).

Interrater reliability

For interrater reliability (IRR) calculations for the PSMA PET/CT Likert scales, we used Cohen's weighted kappa (k) with linear weights. For the LCC measurements, we used Intraclass correlation coefficient (ICC) (2-way random, absolute agreement, single measures). Agreement was considered poor for values < 0.20, fair for 0.21–0.40, moderate for 0.41–0.60, substantial for 0.61–0.80 and near perfect for > 0.80.

The statistical analyses were made with IBM SPSS Statistics 29 and Epitools (for exact calculation of CI:s when any performance measurement was zero) (Sergeant 2018).

Results

Subjects

We identified 965 patients who performed PSMA PET/CT and MRI in the chosen time period. Prostatectomy had been performed on 172 of these patients. In 145 of these patients less than 180 days had passed between first imaging and surgery. 124 of these patients signed informed consent for inclusion. Subject characteristics are in Table 3.

Hvittfeldt *et al. EJNMMI Reports*   (2025) 9:1

Page 7 of 13

Table 3 Subject characteristics

Age (years)	64 (42–78)
PSA (µg/L)	12.2 (1.2–96)
Clinical T-stage from digital rectal exam (n)	
cT1	34
cT2	70
cT3	20
Time between MRI and PET (days)	52 (1–150)
Time between imaging and surgery (days)	58 (1–126)
ISUP grade from needle-core biopsy (n)	
1	2
2	18
3	27
4	40
5	37
D'Amico risk classification (n)	
High	94
Intermediate	30

Values are mean (range)

Table 4 Diagnostic performance indices

	Sensitivity	Specificity	Accuracy
EPE PET combined	0.68 (0.54–0.80)	0.54 (0.32–0.65)	0.60 (0.51–0.68)
EPE PET combined*	0.54 (0.40–0.67)	0.76 (0.65–0.85)	0.67 (0.59–0.75)
EPE PET visual	0.28 (0.17–0.41)	0.82 (0.73–0.90)	0.60 (0.52–0.69)
EPE PET LCC	0.64 (0.50–0.76)	0.60 (0.48–0.70)	0.61 (0.53–0.70)
EPE PET LCC*	0.46 (0.33–0.60)	0.91 (0.83–0.96)	0.73 (0.65–0.80)
EPE MRI	0.80 (0.68–0.89)	0.64 (0.52–0.74)	0.70 (0.62–0.78)
SVI PET	0.14 (0.03–0.38)	1.0 (.97–1.0)	0.90 (0.85–0.96)
SVI MRI	0.50 (0.26–0.75)	0.92 (0.86–0.96)	0.87 (0.81–0.93)

All analyses are on a patient basis (n = 124). Equivocal (Likert 3) counts as negative. LCC ≥ 10 positive for PET except* where LCC ≥ 14 positive. Combined PET result positive if either visual or LCC result positive. 95% CI in parenthesis

Imaging and histopathology

PSMA PET/CT identified 186 tumor lesions, MRI 123 and pathology 169. For 6 PET lesions a mutual second look was needed for agreement on EPE. All these lesions were decided on as equivocal. When comparisons of EPE with histology were made on a per lesion basis, 169 comparisons were made for PET and 168 for MRI (see also supplementary material Fig. 1B). The prevalence in patients of histopathology-verified EPE and SVI was 40% (n = 50) and 11% (n = 14).

Diagnostic performance

Sensitivity, specificity, accuracy and contingency tables for PSMA PET/CT and MRI are presented in Tables 4 and 5. These analyses are on a per patient basis, consider Likert 1–3 negative and 4–5 positive, and with a PET LCC cut-off of 10 mm unless otherwise noted. ROC curve for the PET LCC parameter is presented in Fig. 3, AUC was 0.70 (95%

Hvittfeldt *et al. EJNMMI Reports*   (2025) 9:1

Page 8 of 13

Table 5 Contingency tables

	EPE histology positive	EPE histology negative	Totals for PET or MRI
EPE PET combined			
Positive	34	34	68
Negative	16	40	56
EPE PET visual			
Positive	14	13	27
Negative	36	61	97
EPE PET LCC			
Positive	32	30	62
Negative	18	44	62
MRI EPE			
Positive	40	27	67
Negative	10	47	57
Totals for EPE histology	50 (prevalence 40%)	74	
	SVI histology positive	**SVI histology negative**	
PET SVI			
Positive	2	0	2
Negative	12	110	122
MRI SVI			
Positive	7	9	16
Negative	7	101	108
Totals for SVI histology	14 (prevalence 11%)	120	

All analyses are on a patient basis (n = 124). Equivocal (Likert 3) counts as negative. LCC ≥ 10 positive. Combined PET result positive if either visual or LCC result positive

CI 0.61–0.79). Maximum Youden's index (0.37–0.38) was for a 13–14 mm cut-off. Additional analyses, including PPV, NPV and all contingency tables, are available in supplementary Table 1.
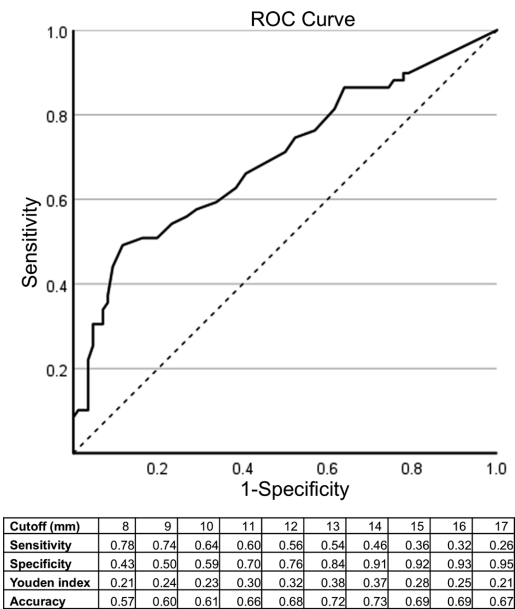
Interrater reliability

The ICC for the LCC measurement was 0.68 (95% CI 0.41–0.82). The weighted k for the visual Likert scale for EPE was 0.53 (0.43–0.63) and for SVI 0.63 (0.46–0.80).

Discussion

Diagnostic performance and comparisons with literature

In the present study we evaluated the diagnostic performance of PSMA PET/CT and MRI in T3 staging of prostate cancer. For EPE with PSMA PET/CT, on a patient basis, a moderate accuracy of 0.73 was achieved using only the LCC evaluation with a cut-off of 14 mm, with a high specificity of 0.91 but low sensitivity of 0.46. The visual and combined visual and LCC methods had lower accuracies between 0.60–0.70. The visual evaluation had moderate (0.82) specificity but very low (0.28) sensitivity. MRI had moderate accuracy (0.70), with moderate sensitivity (0.80) and low specificity (0.64). For SVI both PSMA PET/CT and MRI had high specificity (> 0.90) with low sensitivity. The low prevalence (11%) of SVI makes these numbers uncertain. Note

Cutoff (mm)	8	9	10	11	12	13	14	15	16	17
Sensitivity	0.78	0.74	0.64	0.60	0.56	0.54	0.46	0.36	0.32	0.26
Specificity	0.43	0.50	0.59	0.70	0.76	0.84	0.91	0.92	0.93	0.95
Youden index	0.21	0.24	0.23	0.30	0.32	0.38	0.37	0.28	0.25	0.21
Accuracy	0.57	0.60	0.61	0.66	0.68	0.72	0.73	0.69	0.69	0.67

Fig. 3 ROC curve for the PSMA PET/CT LCC parameter, with table showing diagnostic indices for different LCC cut-offs. Area under the curve is 0.70 (95% CI 0.61–0.79)

that accuracy, while convenient for comparisons, should be interpreted with care—it is highly dependent on prevalence. Depending on the clinical situation a lower accuracy may be acceptable to achieve higher sensitivity or specificity. On a lesion basis both PSMA PET/CT and MRI showed similar sensitivities but higher specificities, mainly due to more true negatives which make little difference clinically (Supplementary Table 1).

Previous studies have shown highly variable results for T3 staging with PSMA PET/CT. For example, a recent meta-analysis reported ranges of accuracy to 0.53–0.90 for EPE (7 studies) and 0.61–0.98 for SVI (9 studies), with pooled accuracies of 0.73 and 0.87 respectively (Gossili et al. 2023). Among these in total 9 studies, 6 did not report how EPE or SVI was evaluated other than "visually". Two studies used the MRI criteria "angulated contour of the prostate gland or obliteration of the rectoprostatic angle" for EPE. One study used the similar "irregular prostate outline or involvement of extraprostatic structure". These may not be applicable to PET images which do not directly visualize the contour or outline of the prostate. A recent large (n = 600) multicenter study (Donswijk et al.) with different PSMA tracers found sensitivity/specificity for EPE and SVI to be 0.58/0.59 and 0.30/0.97 respectively (Donswijk et al. 2024). ROC curve AUC was 0.59 for EPE. The study used a 3-point Likert scale with consensus-based criteria focused on tracer uptake outside the prostate and morphological CT findings. None of the studies in the meta-analysis discussed LUTs or window levels.

In this study LCC performed better than the visual evaluation but cases with evident EPE on imaging likely have not been included (see below under Limitations). This may lead to an underestimation of the performance of the visual method compared to the LCC method. Therefore, we believe that visual evaluation should form part of T3 staging with PSMA PET/CT unless prospective studies show otherwise.

Brauchli et al. achieved sensitivity and specificity of 0.74 and 0.86 for EPE with PSMA PET/CT using the same LCC method as in our study, compared to ours of 0.64 and 0.60 with their suggested cut-off of 10 mm (Brauchli et al. 2020). Their study used [18F] DCFPyL which, like most PSMA tracers, is excreted in urine as opposed to the mainly hepatobiliary excretion of [18F]PSMA-1007. Theoretically this is an advantage for [18F] PSMA-1007 in T-staging since the prostate is adjacent to the urinary bladder. The lower performance in our study could be due to differences in patient selection, the difference in clinical experience and practice of readers and the low reliability of the measurement. A recent study by Tang et al. using [18F]PSMA-1007 evaluated, among other things, EPE and SVI in 130 patients. EPE criteria were "angulated contour of the prostate gland or obliteration of the rectoprostatic angle", SVI criteria were not defined. The results were sensitivities and specificities of 0.23/1.0 and 0.52/1.0 respectively (Tang et al. 2023). Most notably, the previously mentioned study with 600 patients by Donswijk et al. compared four tracers, including [18F]PSMA-1007, and found no differences in diagnostic performance in T-staging (Donswijk et al. 2024).

Interrater reliability and generalizability

To our knowledge, this is the first study using semi-standardized techniques for both quantitative (LCC) and qualitative (visual) aspects of T3 staging with PSMA PET/CT. The IRR for these techniques were moderate to substantial with ICC and k between 0.50 and 0.70, highest for LCC (ICC=0.68). Donswijk et al. found moderate IRR for their visual evaluation with k between 0.40 and 0.50 (Donswijk et al. 2024). Sonni et al. found poor IRR for a visual interpretation of EPE and SVI (ICC 0.20 and 0.08 respectively) (Sonni et al. 2022).

In PSMA PET/CT the indicators of EPE and SVI are the direct visualization of tracer uptake outside the prostate or in the vesicles and, for EPE, the indirect measure of LCC. Both these indicators are dependent on SUV window levels. The challenge is similar to that of tumor volume determination in radiotherapy. In that setting a fixed threshold of 42% of SUVmax is often used although no optimal threshold has been established. Thresholds of 30–70% have been proposed, mostly based on studies of FDG PET. With small lesions (such as in prostate cancer), low thresholds should be avoided (Tamal 2020). The standardized NEMA Hot metal blue LUT we used switches from deep blue to reddish in the range of about 47–55% which serves as the visual tumor delineation zone. The exact threshold used is likely somewhat arbitrary but a LUT with narrower visual threshold, or even a stepped color palette such as the NEMA PET 20 step, could improve the reliability of the test.

Another factor that could reduce reliability is the subjectivity involved in choosing when to measure SUVmax close to the capsule in heterogenous lesions (as described in Methods). Both in this choice and in the visual interpretations the subjective component might be reduced with training materials.

We used 5 mm axial CT slices which are not optimal for non-axial reconstructions and could affect measurements in sagittal and coronal planes. Many PSMA PET scans are performed with a low-dose CT. For eventual clinical implementation of LCC measurements, optimization of protocols and reconstructions should be pursued.

To further improve reliability and to overcome the heterogeneity of study data standardization of PET interpretation is required, such as has been accomplished for MRI with PI-RADS (Weinreb et al. 2016). The Swedish prostate cancer guidelines apply a Likert scale to EPE and SVI evaluation with MRI (Table 2). It is based on ESUR guidelines but with clearly defined criteria for the EPE scale, including LCC, and might serve as a model for PET standardization (Regionala cancercentrum 2024).

Limitations

The retrospective nature of this study introduces a selection bias. Patients with strong suspicion of T-stage 3 or higher are more likely to be selected for radiotherapy rather than prostatectomy, or may not be eligible for curative therapy. This bias could lower the diagnostic performance of PET and MRI, mainly the sensitivity.

For the MRI scans a variety of protocols and scanners were used, reflecting a real world setting but possibly making interpretation more difficult compared to the PET/CT scans where only one type of scanner was used.

Conclusion

In this retrospective study, we compared semi-standardized quantitative and qualitative aspects of [^{18}F]PSMA-1007 PET/CT to MRI in the evaluation of T3 (EPE and SVI) staging in prostate cancer. For EPE with PSMA PET/CT the quantitative length of capsule contact measurement performed best with high specificity, moderate accuracy, and substantial agreement between readers. The qualitative visual PSMA PET/CT evaluation of EPE performed relatively poorly with low accuracy and moderate agreement. MRI also achieved moderate accuracy with higher sensitivity than PET. For SVI both modalities had high specificity and low sensitivity, but the prevalence of SVI was low.

In this and other studies PSMA PET has shown promise in T3 staging of prostate cancer, but with low reproducibility between studies. To accurately assess the diagnostic performance of PSMA PET further standardization of interpretation is needed. The measurement of capsular contact may outperform the visual assessment of EPE in PSMA PET/CT and should be investigated further.

Abbreviations

ADC	Apparent diffusion coefficient
AUC	Area under the curve
CT	Computed tomography
EPE	Extraprostatic extension
ICC	Intraclass correlation coefficient
IRR	Interrater reliability
LCC	Length of capsular contact
LUT	Look up table
NEMA	National Electrical Manufacturers Association
PET	Positron emission tomography
PI-RADS	Prostate Imaging–Reporting and Data System
PSA	Prostate specific antigen
PSMA	Prostate Specific
ROC	Receiver operating characteristic

SV	Seminal vesicle
SVI	Seminal vesicle invasion
SUV	Standardized uptake value
TNM	Tumor node metastasis

Supplementary Information

The online version contains supplementary material available at https://doi.org/10.1186/s41824-024-00234-4.

Supplementary Material 1.

Supplementary Material 2.

Declarations

Ethics approval and consent to participate
The study was approved by the Swedish Ethical Review Authority (#2016/417, #2018/117, #2018/753). All patients signed an informed consent form.

Consent for publication
The informed consent form included consent for publication of anonymized image data.

Competing interests
The authors declare no competing interests.

References
Abrams-Pompe RS, Fanti S, Schoots IG, Moore CM, Turkbey B, Vickers AJ et al (2021) The role of magnetic resonance imaging and positron emission tomography/computed tomography in the primary staging of newly diagnosed prostate cancer: a systematic review of the literature. Eur Urol Oncol 4:370–395. https://doi.org/10.1016/j.euo.2020.11.002

Brauchli D, Singh D, Chabert C, Somasundaram A, Collie L (2020) Tumour-capsule interface measured on 18F-DCFPyL PSMA positron emission tomography/CT imaging comparable to multi-parametric MRI in predicting extra-prostatic extension of prostate cancer at initial staging. J Med Imaging Radiat Oncol 64:829–838. https://doi.org/10.1111/1754-9485.13084

Bray F, Laversanne M, Sung H, Ferlay J, Siegel RL, Soerjomataram I et al (2024) Global cancer statistics 2022: GLOBOCAN estimates of incidence and mortality worldwide for 36 cancers in 185 countries. CA Cancer J Clin 74:229–263. https://doi.org/10.3322/caac.21834

Buyyounouski MK, Choyke PL, McKenney JK, Sartor O, Sandler HM, Amin MB et al (2017) Prostate cancer—major changes in the American Joint Committee on cancer eighth edition cancer staging manual. CA Cancer J Clin 67:246–253. https://doi.org/10.3322/caac.21391

Ceci F, Oprea-Lager DE, Emmett L, Adam JA, Bomanji J, Czernin J et al (2021) E-PSMA: the EANM standardized reporting guidelines v1.0 for PSMA-PET. Eur J Nucl Med Mol Imaging 48:1626–1638. https://doi.org/10.1007/s00259-021-05245-y

D'Amico AV, Whittington R, Malkowicz SB, Schultz D, Blank K, Broderick GA et al (1998) Biochemical outcome after radical prostatectomy, external beam radiation therapy, or interstitial radiation therapy for clinically localized prostate cancer. JAMA 280:969–974. https://doi.org/10.1001/jama.280.11.969

Donswijk ML, Ettema RH, Meijer D, Wondergem M, Cheung Z, Bekers EM et al (2024) The accuracy and intra- and inter-observer variability of PSMA PET/CT for the local staging of primary prostate cancer. Eur J Nucl Med Mol Imaging 51:1741–1752. https://doi.org/10.1007/s00259-024-06594-0

Eastham JA, Boorjian SA, Kirkby E (2022) Clinically localized prostate cancer: AUA/ASTRO guideline. J Urol 208:505–507. https://doi.org/10.1097/Ju.0000000000002854

Gossili F, Mogensen AW, Konnerup TC, Bouchelouche K, Alberts I, Afshar-Oromieh A et al (2023) The diagnostic accuracy of radiolabeled PSMA-ligand PET for tumour staging in newly diagnosed prostate cancer patients compared to histopathology: a systematic review and meta-analysis. Eur J Nucl Med Mol Imaging 51:281–294. https://doi.org/10.1007/s00259-023-06392-0

Kim TH, Woo S, Han S, Suh CH, Ghafoor S, Hricak H et al (2020) The diagnostic performance of the length of tumor capsular contact on MRI for detecting prostate cancer extraprostatic extension: a systematic review and meta-analysis. Korean J Radiol 21:684–694. https://doi.org/10.3348/kjr.2019.0842

Lowrance W, Dreicer R, Jarrard DF, Scarpato KR, Kim SK, Kirkby E et al (2023) Updates to advanced prostate cancer: AUA/SUO guideline (2023). J Urol 209:1082–1090. https://doi.org/10.1097/Ju.0000000000003452

Ma J, Yang Q, Ye X, Xu W, Chang Y, Chen R et al (2024) Head-to-head comparison of prostate-specific membrane antigen PET and multiparametric MRI in the diagnosis of pretreatment patients with prostate cancer: a meta-analysis. Eur Radiol 34:4017–4037. https://doi.org/10.1007/s00330-023-10436-2

Mottet N, van den Bergh RCN, Briers E, Van den Broeck T, Cumberbatch MG, De Santis M et al (2021) EAU-EANM-ESTRO-ESUR-SIOG Guidelines on Prostate Cancer-2020 Update. Part 1: screening, diagnosis, and local treatment with curative intent. Eur Urol 79:243–262. https://doi.org/10.1016/j.eururo.2020.09.042

Regionala cancercentrum – Prostatacancer Nationellt vårdprogram 9.0 2024

Rosenkrantz AB, Shanbhogue AK, Wang A, Kong MX, Babb JS, Taneja SS (2016) Length of capsular contact for diagnosing extraprostatic extension on prostate MRI: assessment at an optimal threshold. J Magn Reson Imaging 43:990–997. https://doi.org/10.1002/jmri.25040

Sergeant E (2018) Epitools Epidemiological Calculators. Ausvet. Available at: http://epitools.ausvet.com.au

Sonni I, Felker ER, Lenis AT, Sisk AE, Bahri S, Allen-Auerbach M et al (2022) Head-to-head comparison of (68)Ga-PSMA-11 PET/CT and mpMRI with a histopathology gold standard in the detection, intraprostatic localization, and determination of local extension of primary prostate cancer: results from a prospective single-center imaging trial. J Nucl Med 63:847–854. https://doi.org/10.2967/jnumed.121.262398

Tamal M (2020) Intensity threshold based solid tumour segmentation method for positron emission tomography (PET) images: a review. Heliyon 6:e05267. https://doi.org/10.1016/j.heliyon.2020.e05267

Tang Y, Ji X, Lin Q, Huang H, Zhu H, Huang X et al (2023) Status of (18)F-PSMA-1007-PET/CT compared with multiparametric MRI in preoperative evaluation of prostate cancer. World J Urol 41:1017–1024. https://doi.org/10.1007/s00345-023-04345-8

Turkbey B, Rosenkrantz AB, Haider MA, Padhani AR, Villeirs G, Macura KJ et al (2019) Prostate imaging reporting and data system version 2.1: 2019 update of prostate imaging reporting and data system version 2. Eur Urol 2019(76):340–351. https://doi.org/10.1016/j.eururo.2019.02.033

Weinreb JC, Barentsz JO, Choyke PL, Cornud F, Haider MA, Macura KJ et al (2016) PI-RADS prostate imaging—reporting and data system: 2015, version 2. Eur Urol 69:16–40. https://doi.org/10.1016/j.eururo.2015.08.052

Woo S, Ghafoor S, Becker AS, Han S, Wibmer AG, Hricak H et al (2020) Prostate-specific membrane antigen positron emission tomography (PSMA-PET) for local staging of prostate cancer: a systematic review and meta-analysis. Eur J Hybrid Imaging 4:16. https://doi.org/10.1186/s41824-020-00085-9

Publisher's Note